

**Molecular Diversity and Physiological Contributions of Neuronal Trek
Channels**

A DISSERTATION
SUBMITTED TO THE FACULTY OF THE GRADUATE SCHOOL
OF THE UNIVERSITY OF MINNESOTA
BY

Kelsey R. Mirkovic

IN PARTIAL FULFILLMENT OF THE REQUIREMENTS
FOR THE DEGREE OF
DOCTOR OF PHILOSOPHY

Kevin D. Wickman, Advisor

October, 2012

Acknowledgements

I would like to acknowledge Tyler Rehbein for assistance with the cell-cycle project, Desirae Haluk, Lydia Kotecki, and Jaime Palmersheim for assistance with the conditioned place preference task, Daniel Bomsta and Benjamin Yun for assistance with the elevated plus maze, and Daniele Young for maintenance of the mouse colonies.

I would also like to thank Dr. Matt Hearing and Nicole Wydeven for assistance with manuscript preparation, experimental design, and helpful advice on analysis, which was provided throughout my tenure at the University of Minnesota.

I would like to give a special thanks to Dr. Kevin Wickman, who served as my thesis advisor and mentor. The completion of my PhD is a direct result of his patience and persistence during my training. I would also like to thank the other faculty members who served on my preliminary examination and thesis committees: Dr. Stan Thayer (chair), Dr. Paulo Kofuji, Dr. Kirill Martemyanov, and Dr. Colin Campbell.

I would also like to give thanks to my family for providing a seemingly endless amount of support, most especially my husband Dragoljub Mirkovic.

This work is supported by NIH grants RO1 MH061933 (KW), P50 DA011806 (KW), R21 DA029343 (KW), T32 DA07234 (KM), and a grant from the Fondation pour la Recherche Médicale (Equipe labellisée FRM 2007; FL).

Abstract

Two-pore domain K^+ (K_{2P}) channels underlie leak or background potassium conductances in many cells. The Trek subfamily consists of three members: *Trek1/Kcnk2*, *Trek2/Kcnk10*, and the more distantly-related family member *Traak/Kcnk4*. Trek family members exhibit complex regulation and can modulate cell excitability in response to a wide array of stimuli, and have been implicated in depression, nociception, and cognition. Furthermore, a number of studies support a role for the Trek family in neuroprotection during ischemia. Despite their identification more than one decade ago, they are still relatively understudied, which is especially true for *Trek2*.

To further our understanding of molecular diversity within the Trek family, we identified and characterized the murine alternative splice variants of *Trek2*. We identified two novel exons, which contribute to the production of six alternative splice variants; three N-terminal two-pore variants and three non-functional C-terminal one-pore variants. Of the N-terminal variants, the previously unreported isoform, *Trek2b*, displayed significantly greater whole-cell current amplitudes when expressed heterologously, a phenomenon ultimately attributable to greater surface expression.

While characterizing the *Trek2* splice variants, we observed significant cell-to-cell variability in current amplitudes in HEK293 cells heterologously expressing Trek channels. We hypothesized this was the result of changes in Trek channel expression during the cell cycle. Indeed, changes in current amplitudes and Trek protein expression correlated with cell cycle stage.

Ultimately, we concluded this was likely a non-Trek specific effect of cell cycle progression on the artificial CAG promoter used to drive heterologous Trek expression.

To further our understanding of the physiological contributions of Trek channels to animal behavior, specifically Trek2, we probed the effect of constitutive *Trek2* ablation, as well as the simultaneous constitutive ablation of all three *Trek* family genes, in paradigms that assess motor activity, coordination, anxiety-related behavior, learning and memory, and drug-induced reward-related behavior. Few behavioral differences were observed between *Trek2*^{-/-}, *Trek1/2/Traak*^{-/-} and wild-type mice, which argue that despite their broad distribution in the CNS, Trek channels exert a minimal influence on a wide-range of behaviors. Instead, we propose that Trek channel activity may be low under normal conditions, where they become impactful only under certain circumstances, such as during ischemia.

Table of Contents

Acknowledgments	i
Abstract	iii
Table of Contents	v
List of Tables	vii
List of Figures	viii
List of Abbreviations	x
Chapter 1 INTRODUCTION	1
Introduction to K ⁺ channels	2
Introduction to Trek channels	12
Regulation of Trek channels	23
Physiological roles for Trek channels	40
Summary	50
Chapter 2 IDENTIFICATION AND CHARACTERIZATION OF ALTERNATIVE SPLICE VARIANTS OF THE MOUSE <i>TREK2/KCNK10</i> GENE	53
Introduction	54
Experimental Procedures	55
Results	60
Discussion	78
Chapter 3 A ROLE FOR TREK CHANNELS DURING CELL CYCLE PROGRESSION	82
Introduction	83
Experimental Procedures	86

	Results	91
	Discussion	108
Chapter 4	BEHAVIORAL CHARACTERIZATION OF MICE LACKING TREK CHANNELS	111
	Introduction	112
	Experimental Procedures	113
	Results	119
	Discussion	141
Chapter 5	DISCUSSION	145
	Challenges in studying Trek channels	146
	Summary of major findings	151
	Future directions	156
Chapter 6	BIBLIOGRAPHY	160

List of Tables

Table 1.	Pharmacological agents that activate Trek channels.	37
Table 2.	Pharmacological agents that inhibit Trek channels.	39
Table 3.	Murine Trek2-related cDNAs identified in the GenBank© database.	64

List of Figures

Figure 1.	Two-pore domain K ⁺ channel family members.	11
Figure 2.	Regulation of Trek1 and Trek2.	22
Figure 3.	Structure and splicing of the mouse <i>Trek2</i> gene.	66
Figure 4.	Expression patterns of mouse <i>Trek2</i> splice variants.	70
Figure 5.	Functional characterization of Trek2 splice variants.	74
Figure 6.	Whole-cell and plasma membrane expression levels of Trek2 splice variants.	77
Figure 7.	Biochemical characterization of Trek1 and Trek2 stable cell lines.	94
Figure 8.	Electrophysiological characterization of Trek1 and Trek2 stable cell lines.	96
Figure 9.	Validation of cell-cycle synchronization.	100
Figure 10.	Effect of cell cycle synchronization on Trek whole-cell currents.	104
Figure 11.	Effect of cell cycle synchronization on Trek protein and mRNA expression.	107
Figure 12.	Motor activity and coordination in mice lacking Trek channels.	124
Figure 13.	Elevated plus maze performance in mice lacking Trek channels.	128
Figure 14.	Light/dark box behavior in mice lacking Trek channels .	130
Figure 15.	Contextual fear conditioning in mice lacking Trek	134

	channels.	
Figure 16.	Novel object recognition in mice lacking Trek channels.	136
Figure 17.	Opioid-induced motor activity and reward in mice lacking Trek channels.	140

List of Abbreviations

ANOVA	analysis of variance
Bp	base pair
cDNA	complementary deoxyribonucleic acid
CNS	central nervous system
DNA	deoxyribonucleic acid
dNTP	deoxyribonucleotide triphosphate
DTT	dithiothreitol
GABA	γ -aminobutyric acid
GAPDH	glyceraldehyde 3-phosphate dehydrogenase
IBMX	3-isobutyl-1-methylxanthine
mRNA	messenger ribonucleic acid
NHS-PEG4	<i>N</i> -hydroxysuccinimide ester polyethylene glycol 4
PBS	phosphate buffered saline
PCR	polymerase chain reaction
PMA	phorbol 12-myristate 13-acetate
qRT-PCR	quantitative reverse transcription polymerase chain reaction
RNAi	interfering ribonucleic acid
RT-PCR	reverse transcription polymerase chain reaction
SDS	sodium dodecyl sulfate
SEM	standard error of the mean
siRNA	short interfering ribonucleic acid

Task	Twik-related acid-sensitive K ⁺ channel
UTR	untranslated region

Chapter 1

INTRODUCTION

Introduction to K⁺ channels

Introduction to ion channels

The cell membrane is comprised of a thin lipid bilayer that separates the intracellular components from the extracellular fluid. Within the membrane are highly specific molecules that control the passage of information from one side to the other. Information can be transmitted in a number of ways, such as through activation of receptors, the passage of lipids across the membrane, and/or the passage of ions across the membrane through highly regulated ion channels.

Ion channels are pore-forming proteins that allow the flow of ions across a cell membrane, where they may then act to alter cellular processes in many ways. These could include the activation of downstream signaling pathways, activation of other ion channels, and/or alterations in charge distribution across the membrane. The four most abundant ions in the CNS are Na⁺, K⁺, Ca²⁺ and Cl⁻, which are most relevant to ion channels and cellular excitability [1].

Each ion channel opens in response to a specific and unique set of stimuli. These stimuli may include changes in the membrane potential, a neurotransmitter, or chemical stimulus [1]. The opening of an ion channel in response to a stimulus is referred to as gating, which involves a structural rearrangement, such that the pore region of the channel is opened and ions are able to flow through [1]. The specific set of stimuli involved in the channels gating, is often used to classify the ion channel.

Ion channels are also classified based on their selective permeability, which refers to the specific set of ions they allow to cross the membrane [2]. For example, some ion channels allow the passage of all positively charged ions, termed a non-selective cation channel. Whereas other ion channels preferentially allow the passage of a single ion type over others. For example, K^+ -selective ion channels are highly selective for K^+ over Na^+ and Ca^{2+} . An ion channels selective permeability and gating mechanisms are generally used to classify the ion channel.

There are many ion channels which are open in response to changes in the membrane potential [2]. These ion channels are referred to as voltage-gated ion channels. Voltage-gated ion channels include members which are selective for Na^+ , K^+ or Ca^{2+} [2]. Voltage-gated sodium channels are among the most well-known ion channels and play an important role in the generation and propagation of an action potential [2]. These channels are open rapidly in response to membrane depolarization, which results in an influx of Na^+ ions, followed by a rapid closure of the channel and a brief inactivation period [2].

Voltage-gated K^+ channels also play an important role in re-establishing the resting membrane potential after an action potential has been generated [2]. These channels are again opened in response to depolarization of the membrane, however display slower gating kinetics than voltage-gated Na^+ channels, therefore these channels open after voltage-gated Na^+ channels and allow K^+ ions to flow into the cell and re-establish the resting membrane potential [2].

Voltage-gated Ca^{2+} channels play an important role in neurotransmitter release [2]. These ion channels are located at nerve terminals. In response to membrane depolarization, voltage-gated Ca^{2+} channels will open, which results in the influx of Ca^{2+} . This local increase in Ca^{2+} leads to the fusion of neurotransmitter containing vesicles with the membrane, releasing neurotransmitter into the synaptic cleft [2]. The neurotransmitters will then transmit information to the post-synaptic neuron through activation of receptors or ligand-gated ion channels located on the post-synaptic neuron.

While voltage-gated ion channels are opened in response to changes in the membrane voltage, ligand gated ion channels are opened in response to binding of specific ligands [2]. There are two major classifications of ion channels, which include inotropic ion channels and metabotropic ion channels. Inotropic ion channels open in response to the direct binding of a ligand to the channel and display relatively faster gating kinetics than metabotropic ion channels [2]. In contrast, metabotropic ion channels are coupled to G-protein coupled receptors. Activation of a G-protein coupled receptor will result in a signaling cascade that will lead to the activation of a metabotropic ion channel, which will display relatively slower gating kinetics [2].

Ligand-gated ion channels that display selective permeability for Na^+ , K^+ , Ca^{2+} and Cl^- can all be found in CNS. For example, the nicotinic acetylcholine receptor contains two binding sites for the neurotransmitter acetylcholine [3]. When acetylcholine is bound, the ion channel opens and Na^+ ions are allowed to flow out of the cell [3]. The same neurotransmitter, acetylcholine, can also

activate the G-protein coupled muscarinic acetylcholine receptors and activate both K^+ -selective and Ca^{2+} -selective metabotropic ion channels under different conditions [3]. As my work focused on a member of the K^+ -selective ion channel family, this channel family will be discussed in greater detail.

Features of K^+ channels

K^+ -selective ion channels possess more members than any other ion channel family, and contribute greatly to a number of important biological functions [4]. Under physiological conditions, the K^+ concentration within the cell is significantly greater than the K^+ concentration in the extracellular solution [4]. Thus, opening of a K^+ -selective channel results in the outward flow of K^+ and a hyperpolarization of the cell membrane [4]. K^+ is the major ion responsible for setting the resting membrane potential, which is primarily due to the relatively high permeability of K^+ ions across the membrane compared with the other major ions. Other significant contributions of K^+ -selective channels include, reestablishing the membrane potential after an action potential, controlling the duration of cardiac output, and contributing to the release of hormones such as insulin [5]. Indeed, mutations in K^+ channels have been associated with numerous disease states including long-QT syndrome, epilepsy, episodic ataxia, neurodegenerative diseases, schizophrenia, hearing loss, Bartter's syndrome, dysregulation in insulin secretion and many others [5].

All K^+ channels share a number of common structural features most notably, a pore domain containing a K^+ selectivity filter [4]. Each K^+ channel subunit

contains a minimum of one pore domain, also called the pore-loop [4]. This region of the protein exists between two transmembrane segments on the extracellular side of the membrane. This region integrates into the plasma membrane and contains the K^+ selectivity filter [4]. The selectivity filter in K^+ channels is made up of the highly conserved sequence motif GYG [4]. A functional K^+ channel involves multiple K^+ channel subunits that may assemble to form homomeric or heteromeric channels. The pore region, which allows the passage of K^+ ions, displays four-fold symmetry, thus four pore loops are required to form a functional channel [4].

K^+ channel families

K^+ channels are classified into four major families based on their structural topology and gating mechanism. They are the voltage-gated K^+ channel family, the inwardly-rectifying K^+ channel family, the Ca^{2+} -activated K^+ channel family, and the two-pore domain K^+ channel family.

As their name suggests, voltage-gated K^+ channels (K_v) are activated by depolarization of the membrane [4]. Structurally, these channels are generated through the tetrameric assembly of four individual subunits, each of which contains six transmembrane segments and one pore domain. These channels are best known for their role in repolarizing the membrane after an action potential has fired [4].

The inwardly-rectifying K^+ channel (K_{ir}) family is classified based on similarity in structure and rectification profile [4]. Structurally, each subunit

contains two transmembrane domains and a single pore domain, thus they also assemble as tetramers to form a functional K^+ channel. Every K^+ channel is characterized by a unique set of intrinsic biophysical properties, which distinguish that channel from any other. One such property that is commonly reference is the rectification profile, which summarizes the relationship between membrane voltage and the ability to pass current [4]. Members of the inwardly-rectifying K^+ channel family conduct K^+ more effectively in the inward direction, due to intracellular positively charged molecules that cause a partial blockade of the outward K^+ flux [4]. Physiologically, K^+ always flows in the outward direction, thus this family makes smaller physiological contributions at highly depolarized membrane potentials, but important contributions at or near the resting membrane potential. As such, these channels are involved in regulating action potential duration and in maintaining the resting membrane potential.

As the name suggests, the classification of Ca^{2+} -activated K^+ channels (K_{Ca}) is based on their gating mechanism; they are activated by a rise in intracellular Ca^{2+} [4]. These channels are structurally similar, in that they possess 6 (or 7) transmembrane domains and one pore domain; thus, four subunits are required to form a functional K^+ channel. These channels are activated by increases in intracellular Ca^{2+} and are known to be involved in regulating arterial tone [4].

Two-pore domain K^+ channels (K_{2P}) are the most recently identified K^+ channel family (**Fig. 1**). As the name implies, all members of this channel family contain 2 pore-domains (**Fig. 2**), therefore functional K^+ channels are generated through the dimeric assembly of two subunits. This family is best

known for its role as contributors to the background or leak conductance that is important for setting the resting membrane potential [4]. My work has focused on a member of this family, which will be discussed in greater detail below.

Techniques used to study K⁺ channels

Many techniques have been used to study K⁺ channels, including patch clamp electrophysiology. As this technique is widely used in the study of ion channels, and was used to generate a significant amount of the data discussed in the introduction and coming chapters, a brief overview will be provided. Patch clamp electrophysiology is a very sensitive technique that allows an experimenter to measure ion flow across a membrane [6]. In this technique, a glass pipette containing a known solution and recording electrode is lowered onto a small portion of a cell membrane. Through this recording electrode the patch can be held at a specified potential (relative to the bath solution), and the flow of ions across the membrane can be measured [6].

There are multiple patch clamp configurations that can be utilized including cell-attached, inside-out, and whole-cell configurations. In the cell-attached configuration, the cell remains intact, and ion flux can be recorded from the single channel (or few channels) present in the small patch of membrane contained within the glass pipette [6]. By quickly withdrawing the pipette from the intact cell, the small patch of membrane can be removed from the surrounding membrane, resulting in the inside-out configuration. In this configuration, the cytosolic surface of the membrane is exposed to the bath

solution, which can be controlled by the experimenter. Whole-cell configuration was the most commonly employed for the collection of data described here.

After making contact with the intact cell, negative pressure (suction) is applied through the pipette to rupture the membrane of the cell [6]. In whole-cell configuration ion flow is measured across all channels present in the cell membrane and the intracellular and extracellular solutions can be controlled.

Figure 1. Two-pore domain K⁺ channel family members.

A dendrogram of the two-pore domain K⁺ channel (K_{2P}) family members. The conventional name is listed followed by the gene name in parenthesis. Sub-family groupings are indicated by brackets on the right, along with the sub-family name.

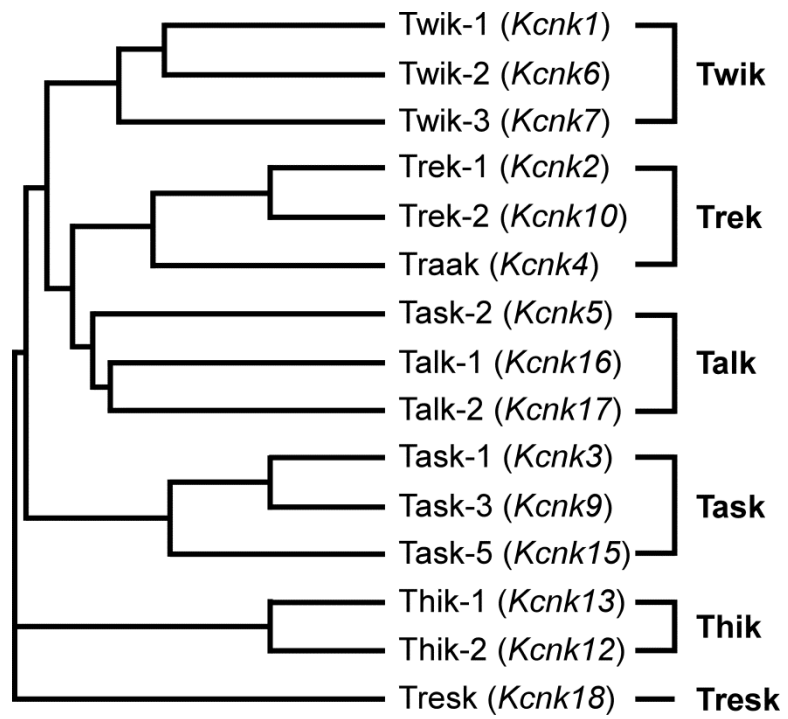


Figure 1

Introduction to Trek channels

Introduction to the two-pore domain K⁺ channel family

The resting K⁺ conductance of the plasma membrane is very high. This is best explained by the presence of potassium selective pores in the membrane that allows for the unregulated flow of K⁺ ions [7]. Such a background, or leak channel, should display no voltage-dependence, such that the membrane potential should have no influence on the open probability of the channel. It should display no time-dependence, such that the current instantaneously follows the membrane potential. The background channel should not rectify, but should be driven only by the unequal distribution of K⁺ across the membrane.

The two-pore domain K⁺ channel family (K_{2P}) is the most recently-identified family in the K⁺ channel superfamily and while its members do not fit the above criteria perfectly, they are now well-established as key contributors to the background (leak) conductance.

The first member, Tandem of P domains in a weak inwardly-rectifying K⁺ channel (Twik), was cloned in 1996 [8]. This channel was structurally distinct from any previously identified mammalian K⁺ channel, thus it represented a new class of K⁺ channels. Twik was proposed to contribute as a background leak channel based on its widespread tissue distribution and biophysical properties, which were open at all potentials and displayed time-independent gating [8]. The K_{2P} family rapidly gained an additional 14 members, which are further

divided into 6 sub-families based on sequence similarity and functional properties (**Fig. 1**).

All members of the K_{2P} family of K^+ channels contain two pore loops (**Fig. 2**), which differentiate this family from all other K^+ channels, which contain only one. In addition to the two pore loops, all channels contain four transmembrane segments, and intracellular N- and C- termini (**Fig. 2**). And, in contrast to all other K^+ channels, a functional channel is formed from the dimerization of two subunits. K_{2P} channels are also found in lower organisms, including *Caenorhabditis elegans* and yeast, as well as members of the plant kingdom [9-13].

Introduction to the Trek family

The Trek sub-family is comprised of three members (**Fig. 1**); Trek1 (Twik-related K^+ channel; *Kcnk2*), Trek2 (*Kcnk10*), and Traak (Twik-related arachidonic acid activated K^+ channel; *Kcnk4*). Trek1 and Trek2 are more closely related [14] and are regulated by an almost identical set of stimuli (**Fig. 1-2**). This includes activation by membrane stretch [14-16], increase in temperature [17, 18], arachidonic acid and other poly unsaturated fatty acids [14, 15], and intracellular acidification (**Fig. 2**) [14, 19, 20]. Trek1 and Trek2 are also inhibited by protein kinase A (PKA) phosphorylation and protein kinase C (PKC) phosphorylation [14, 15, 21-24], which couples these channels to G protein dependent signaling cascades involving G_s , $G_{i/o}$, and G_q G proteins (**Fig. 2**). Trek channels have also been implicated in a number of physiological

processes including pain sensing [25, 26], mediating the actions of inhaled anesthetics [27], depression [28], and neuroprotection during ischemia [27]. *Trek* channel regulation and physiological significance will be discussed in greater detail in the following sections.

Localization of *Trek1* and *Trek2*

Trek1 mRNA is widely distributed throughout the CNS in both rodents and humans, with highest levels observed in the caudate/putamen (striatum) and thalamus [14, 29-32]. Multiple groups have also noted high levels of *Trek1* expression in the spinal cord, olfactory bulb, amygdala, fetal brain, and hippocampus (notably the CA2 region) [21, 29-32].

There is considerably less consensus on *Trek2* mRNA localization, with the exception of very high levels detected by all in the cerebellum. Talley et al (2001) detected a limited distribution of *Trek2* mRNA in the rodent with notably high levels only in the cerebellum and slightly lower levels in the amygdala. In contrast, data from human CNS tissue suggest a broader distribution, with especially high levels in caudate/putamen and cerebellum [29]. The broad distribution of *Trek2* observed has been corroborated by others in human [14], rat [16] and, by our lab, in mouse tissue (**Fig. 4**) [33]. Thus widespread distribution of both *Trek1* and *Trek2* channels suggest they may make a broad and significant contribution to neurophysiology and behavior.

Overall, human and rodent localization display comparable levels for both *Trek1* and *Trek2*, with one exception. In human CNS tissue, *Trek2* levels were

found to be especially high in caudate and putamen [29] (also observed for *Trek1*), however studies from multiple groups, including ours, detect only low levels in the striatum/accumbens from rodent [16, 30, 33] indicating an interesting difference between species.

In addition to the widespread distribution of *Trek1* and *Trek2* in the CNS, both channels have also been detected in peripheral tissues. There is less consensus in the field with regards to peripheral *Trek1* localization, which may result from species-related differences. In human tissue, two groups reported high levels of *Trek1* mRNA in the stomach, with low or undetectable levels in all other peripheral regions investigated [29, 32]. In contrast, a wider distribution has been reported from rodent, where highest levels are reported in kidney, lung, heart, ovaries, and intestine, with detectable levels in most other tissues including testis, prostate skeletal muscle, and pancreas [14, 21]. A broad and consistent peripheral distribution of *Trek2* has been reported in both the human and rodent. Highest levels of *Trek2* mRNA were detected in pancreas, kidney, small intestine, testis, colon and spleen [14, 16]. This work is corroborated by work in our lab that indicate a broad distribution of *Trek2* in peripheral tissue from the mouse (**Fig. 4**) [33].

Biophysical properties and molecular diversity of Trek channels

Trek1 single channel recordings display bursting behavior [15, 21], where the single channel conductance is 95-130 pS [15, 34-36]. While whole-cell *Trek1* currents display outward rectification, single channel recordings from

symmetrical K^+ concentrations are linear or inwardly rectifying [14, 34]. This is explained by the actions of external divalent cations (Ca^{2+} or Mg^{2+}) on Trek1 channels. When these cations are present, the unitary conductance of Trek1 channels decreases at more negative potentials, and thus in physiological solutions, outward rectification is observed [15, 37]. The actions of divalent cations on Trek1 are unique among the Trek family, as neither Trek2 nor Traak display this effect [16].

The mouse *Kcnk2* gene is located on chromosome 1 and consists of 8 exons which can be alternatively spliced to generate three splice isoforms. Two alternative splice variants of Trek1 have been identified in cardiac myocytes, which differ only at the extreme N-terminus [38], and are the result of the differential inclusion of the first exon. These variants display different single channel conductances, which include the well-characterized ~135 pS conductance state and a novel ~40 pS conductance state [34]. Both exhibit similar biophysical and regulatory properties, and thus the second conductance state may result from the interaction with an unidentified intracellular accessory protein [34].

A third isoform of Trek1 has also been identified. This alternative splice variant is the product of the exclusion of exon 4, which results in an early stop codon within the first pore domain [39]. While this variant is not able to function as a potassium channel, it acts as a dominant negative regulator of Trek1 channel activity by limiting the surface expression of full length Trek1 [39].

The molecular diversity of Trek1 is further increased via alternative translation initiation. This occurs when the first AUG start site on an mRNA strand is skipped, and translation is initiated from another AUG start site downstream. In this way, multiple protein products can be generated from a single RNA strand. The first AUG start codon for Trek1 contains a naturally weak Kozak sequence. When the first AUG site is skipped, translation can initiate from a second AUG start codon located 57 amino acids downstream [40]. Single channel properties are again altered in the truncated variant. While the unitary conductance of the truncated variant was ~30% greater, the open-channel probability was 6-fold lower, which lead to a net reduction in current at the whole-cell level [40]. More striking was the shift in ion selectivity that was observed from the truncated channel. In addition to being permeable to K^+ , the truncated channel is also permeable to Na^+ [40]. Thus, the expression of the truncated channel may result in more depolarized membrane potentials in native cells.

At the single channel level, Trek2 also displays inward rectification, with a greater single channel conductance at hyperpolarized potentials (128 pS at -40 mV vs 100 pS at +40 mV) [14, 16]. However, the mean open time increases with membrane depolarization ($P_o = 0.26$ at -40 mV vs $P_o = 0.45$ at +40 mV), which results in a net linear or outwardly rectifying profile at the whole cell level [14, 16].

Alternative splice variants of Trek2 have also been identified in humans. Indeed, three N-terminal splice variants have been identified resulting from the

alternative use of exon1 [41]. While key functional and regulatory processes did not differ between these three isoforms, the expression patterns did [41]. *Trek2c* was deemed the dominant CNS isoform; however the presence of *Trek2a* could also be detected at low levels. In contrast, *Trek2b* expression was predominantly observed in kidney and pancreas, with no detectable levels in the brain [41]. At the start of my thesis work, nothing was known with regard to alternative splice variants that may exist in the mouse. The goal of chapter 2 was to identify murine *Trek2* splice variants, evaluate their expression patterns, and probe for isoform-dependent differences in channel function.

Alternative translation initiation has also been proposed to increase *Trek2* channel diversity. Indeed, the Kozak sequence that initiates translation of *Trek2* may also be less than optimal, as was the case for *Trek1* [40]. Furthermore, two conductance states have been identified in *Trek2* single channel recordings [42]. Together, this led to the hypothesis that *Trek2* may also be subjected to alternative translation initiation. *Trek2* possesses two alternative AUG start sites proximal to the first transmembrane segment, which are located at amino acids 55 and 67 [43]. As speculated, forced expression at these internal start sites produces channels with single channel properties consistent with only the large conductance state, whereas production of only full length *Trek2* results in single channel properties consistent with only the small conductance state [43].

A single alternative splice variant has also been reported for *Traak*, which contains a severely truncated C-terminus. This variant is only 67 amino acids in

length; the first 63 corresponding to full length Traak followed by four dissimilar amino acids that result from a frameshift [44]. This variant does not form a functional channel [38], and at present its physiological contribution is unknown.

Trek interaction partners

Three interaction partners have been identified for the Trek family, which interact with different family members to different degrees. A-kinase anchoring protein 150 (AKAP150) was the first identified interaction partner for Trek1 and Trek2 [45]. AKAP150 is a scaffolding protein, which interacts with cAMP-dependent protein kinase (PKA), Ca²⁺ dependent protein kinase (PKC), as well as a number of other ion channels and neuronal proteins [46]. Co-expression of Trek channels with AKAP150 dramatically increased whole-cell currents, rendering the channel insensitive to other stimulatory regulators [45]. Furthermore, Trek channel inhibition by G protein coupled receptor (GPCR) activation of G_s is faster, as one would predict from a scaffolding protein that may spatially organize such signaling components [45]. Interestingly, inhibition by G_q GPCR activation is reduced, supporting a role for AKAP150 in scaffolding Trek channels with specific GPCR's. AKAP150 binds within the proximal C-terminal domain, which is highly-conserved between Trek1 and Trek2, but less so in Traak. As such, Traak is likely not an interaction partner for AKAP150. Furthermore, Traak is not influenced by GPCR activity [44], thus there lacks a rational explanation as to why these proteins would be coupled.

Microtubule associated protein II (Map2) is the second verified binding partner for Trek1 and Trek2, and again does not interact with Traak [47]. Map2 is best known for its role in binding and stabilizing microtubules, but it also functions as an adaptor protein through secondary interactions with a variety of other cellular proteins [48]. While interaction with Map2 does not alter the regulatory or single channel properties of Trek proteins, it acts to alter channel activity by increasing the membrane delivery of Trek1 and Trek2 [47]. Importantly, Map2 has also been shown to interact with PKA [49], thus its interactions with Trek proteins may serve as a mechanism to arrange proper subcellular localization of channels with other important channel regulators.

In addition to Map2 increasing Trek surface expression, an interaction that accomplishes the same task has been identified between Trek1 and β -COP, a subunit of the coat protein complex I (COP1) [50]. This complex is involved in the vesicular transport of proteins between the golgi and endoplasmic reticulum. This interaction between β -COP and Trek1 was identified using a yeast two hybrid approach, and verified using immunoprecipitation in mammalian cells, and has not yet been validated *in vivo* [50]. This interaction has only been verified for Trek1, and involves the N-terminal region which displays less conservation between the other Trek family members, thus is likely specific for Trek1.

Figure 2. Regulation of Trek1 and Trek2.

A schematic depicting a single Trek subunit. Each subunit contains 4 transmembrane segments (TM), two pore-domains (P), and intracellular N- and C- termini. Regulators of Trek1 and Trek2 are depicted on the schematic. Trek channels are activated by membrane stretch via interactions with the cell membrane. Trek channels are activated by heat, intracellular acidosis, arachidonic acid and other PUFAs at the post-TM4 regulatory region depicted by the arrows. Trek channels couple to GPCRs via inhibition by PKC and PKA phosphorylation; disrupted arrows indicate indirect activation of PKA and PKC after GPCR activation through changes in intracellular cAMP and Ca²⁺ concentrations respectively.

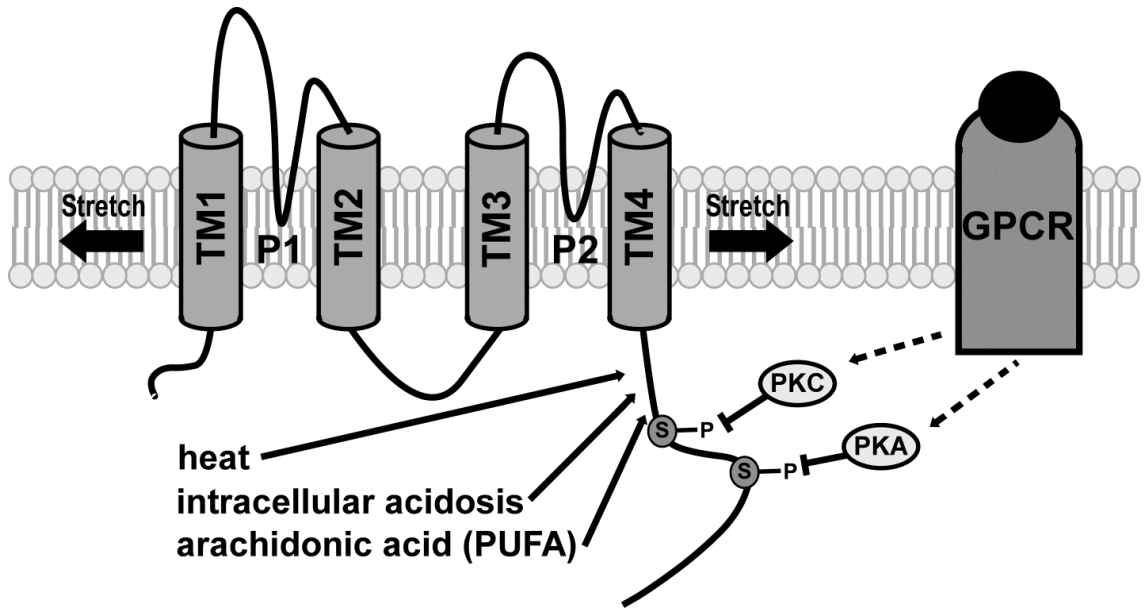


Figure 2

Regulation of Trek channels

Shortly after the cloning of Trek1 in 1996, a similarity was observed between Trek1 and the *Aplysia* S-type K⁺ channel. The *Aplysia* S-type K⁺ is the serotonin activated pre-synaptic K⁺ channel [51-53], which has been shown to underlie the gill withdrawal reflex [51, 54, 55]. As behavioral sensitization of the gill withdrawal reflex is considered a simple form of learning, the *Aplysia* S-type K⁺ channel was highly studied due to its potential relevance in learning and memory. The *Aplysia* S-type K⁺ channel is outwardly-rectifying and weakly-sensitive to voltage [51], is opened by both membrane stretch [56] and arachidonic acid (AA) [57], and displays a unique pharmacological profile. The *Aplysia* S-type channel is resistant to the classical K⁺ channel blockers tetraethylammonium (TEA) and 4-aminopyridine (4-AP), is resistant to external barium (Ba²⁺) [52], and is opened by volatile anesthetics [58]. These early observed similarities have formed a basis for the characterization of all Trek family members, and the biased approach used to characterizing this family has certainly influenced how it was studied. What follows is a summary of what is known with regards to Trek channel regulation.

Mechanosensitivity

Trek channels are regulated by a complex set of stimuli. All three family members are sensitive to tension changes within the lipid membrane, as all three family members are reversibly activated by membrane stretch (**Fig. 2**) [14, 15, 37, 59]. The mechanisms underlying Trek channel regulation likely involve

interactions between the channel and the lipid bilayer, as well as the cytoskeleton. The cytoskeleton exerts an inhibitory influence over channel activity, as pharmacological disruption of the cytoskeleton has been shown to increase channel activity [15, 59, 60]. However, Trek1 can be further activated by stretch after cytoskeletal disruption, indicating that the membrane alone is sufficient to modulate channel activity [15].

The concave conformation of the cell membrane has been shown to activate Trek channels using the anionic crenator trinitrophenol (TNP). TNPs are amphipathic molecules that preferentially insert into the outer membrane leaflet [15], thus creating a concave conformation of the membrane. The inclusion of TNP in the bath solution during whole-cell electrophysiological recordings from Trek1 transfected COS cells, an immortal fibroblast-like cell line derived from monkey kidney tissue, resulted in activation of Trek1, indicating that the concave conformation of the membrane triggered Trek channel activation. In contrast, bath application of the cationic amphipathic molecules, which preferentially insert into the inner membrane leaflet creating a cup-like conformation of the membrane, led to reduced Trek1 currents [15]. Consistent with a concave conformation of the membrane resulting in Trek channel activation, application of positive pressure to the pipette during whole-cell electrophysiology recording results in little or no change in channel activity, however application of negative pressure, while in cell-attached mode, leads to increased channel activity [14-16, 37, 59]. This effect is mimicked by changes in cell volume, as increasing extracellular osmolarity results in a reduction of

basal Trek1 currents, whereas reducing extracellular osmolarity results in increased Trek1 currents [15].

The C-terminal region of Trek1, Trek2 and Traak is involved in regulating Trek channel activity by a variety of stimuli, including mechanosensitivity (**Fig. 2**) [19, 20, 36, 37]. Progressive truncation of the C-terminus results in reduced mechanosensitivity of all Trek family members when heterologously expressed in oocytes or immortal cell lines, however complete abolishment was never achieved [19, 20, 36, 37]. Chimeric approaches have also been used to study the C-terminal contribution of Trek family members, through fusion with members of the Task family (**Fig. 1**), which display no mechanosensitivity. Substitution of the Trek1 C-terminus with that of Task1, results in a channel insensitive to mechanical stimuli [15]. While the Trek1/Task1 chimera did not display mechanosensitivity, replacement of the C-terminus of Trek2 with that of Task3, resulted in a channel that displayed mechanosensitivity in two separate studies [20, 37]. This was also true for the Traak/Task1 and Traak/Task3 chimeras [37]. While it is possible that different mechanisms underlie the mechanoregulation among Trek family members, the C-terminal region deemed responsible in Trek1 displays almost 100% sequence identity with Trek2. The most likely explanation for this discrepancy lies within the assays used in these studies. The study finding a significant role for the Trek1 C-terminus was testing shear stress, as opposed to the other studies, which measured the results of negative pressure directly applied to the membrane. Further studies are necessary to resolve this issue.

Thermosensitivity

All members of the Trek family are sensitive to the actions of temperature on channel activity. All members are reversibly activated by an increase in temperature (**Fig. 2**) [17, 18]. Moreover, they exhibit a broad range of temperature sensitivity, with activity levels increasing 18-20 fold between 24°C and 42°C [17, 18]. These studies suggest that at physiological temperatures there exists a basal level of Trek activity contributing to the background/leak conductance.

The mechanism underlying the temperature regulation of Trek family members is not well understood. It is clear that cellular integrity is required for thermoregulation, as increasing temperature has no effect in inside-out patches [17, 18]. This observation supports a role for cytosolic modulators in temperature regulation (**Fig. 2**). Chimeric studies involving the C-terminus of Trek1 have produced conflicting results, similar to that observed for Trek channel mechanoregulation. Truncation of the C-terminus of Trek1 abolishes most of the channels heat sensitivity, which cannot be rescued through replacement with the Task1 C-terminus [17]. This is in contrast to a Trek2/Task3 chimera, where the C-terminus of Task 3 has been fused to the Trek2 backbone, which retains its thermoregulatory properties, albeit to a lesser extent [18].

Arachidonic acid, lysphospho-, phosphor- and other lipids

All Trek family members are potently and reversibly activated by arachidonic acid (AA) [14-16, 32, 37, 44, 61]. Indeed the 'AA' in Traak is short for "arachidonic acid sensitive". AA is a polyunsaturated fatty acid important for many biological processes. It is one of the most abundant fatty acids in the brain, important for maintaining cell membrane fluidity, protecting the brain from oxidative stress, and involved in neuron growth and repair [62, 63]. Additionally, AA plays a role in cellular signaling as a second messenger involved in the regulation of signaling enzymes and inflammatory mediators [64, 65]. AA is able to activate all Trek family members independent of cell integrity from both extracellular and intracellular sides of the membrane (**Fig. 2**) [15, 16, 44]. Importantly, Trek family members are activated by a number of other polyunsaturated fatty acids (PUFAs), but insensitive to the actions of saturated fatty acids [14-16, 37, 44, 61].

Chimeric studies involving the C-terminus of Task family members, which are inhibited by AA, suggest that the highly-conserved C-terminal region proximal to the TM4 domain is critical for the AA-dependent activation of Trek1 and Trek2 channels (**Fig. 2**) [15, 20, 37]. Indeed, replacement of this region with that of a Task family member either abolished the effect of AA, or actively inhibited the channels' response to AA application [15, 20]. This region has been narrowed down to Trek1 residues V298-T322 [15], and Trek2 residues V324-T348 (**Fig. 2**) [20]. More specifically, a 6 amino acid cluster within this region is critical for the regulation of Trek2 by AA [20]. Chimeric substitution of

the C-terminus of Trek1 onto the Task1 channel was unable to activate Task by AA, thus the C-terminal region is necessary but not sufficient to confer AA sensitivity to Trek channels [15]. However, the post TM4 region is not critical for AA regulation of Traak, as C-terminal replacement with that of Task1 or Task3 retains AA activation of this channel [37]. Thus the regions involved in AA sensitivity appear conserved between Trek1 and Trek2, but represent another difference observed with respect to Traak.

Trek family members are also sensitive to the effects of some lysophospholipids, including lysophosphatidylcholine (LPC), lysophosphatidic acid (LPA), and lysophosphatidyl inositol (LPI), all of which can act as second messengers in cellular signaling cascades [14, 22, 61, 66]. All Trek family members are activated by extracellular application of LPC, which unlike AA, relies on cellular integrity for activation [22]. In the case of LPA, Trek channels are activated only from intracellular application [66]. Interestingly, the proximal C-terminal domain is not necessary for LPA modulation, as serial C-terminal deletions of Trek1 actually enhanced LPA-induced channel activity [66].

Trek1 and Traak have also been shown to be activated by increases in cytosolic phosphatidylinositol 4,5-bisphosphate (PIP₂) [67, 68]. Indeed a cluster of positively charged amino acids in the proximal C-terminus has been deemed responsible for this mode of regulation [67]. As G_q GPCR activation results in the depletion of PIP₂, and subsequent production of inositol triphosphate (IP₃) and diacyl glycerol (DAG), modulation by these second messengers has been postulated as a possible mechanism underlying Trek channel activation by G_q

GPCRs. The data surrounding this issue are somewhat contradictory. While application of PIP₂ results in Trek channel activation [67], depletion of PIP₂ has been shown to have no effect [69, 70]. Furthermore, one group has reported that application of intracellular DAG results in the inhibition of Trek channels [69], whereas others have observed no effect of DAG on Trek currents [70]. Further research is needed to understand how the PIP₂ sensitivity of Trek channels may contribute to regulation by G_q GPCRs.

Intracellular acidification

Trek1 and Trek2 are also activated by internal acidification (**Fig. 2**) [14, 19, 20]. Such pH sensing is important, as deviation from a cell's standard pH can signal many adverse cellular processes, most notably those related to metabolic stress. Trek1 and Trek2 are reversibly activated by a reduction in internal pH (pH 7.2-5.0), to a point where no further activation by the application of negative pressure can be achieved [14, 19, 20]. Interestingly, smaller alterations to intracellular pH, also appear to sensitize the channel to activation by other modulators, including membrane stretch and AA [19].

The C-terminal domain is also critical for intracellular pH sensing (**Fig. 2**). Serial deletions of both Trek1 and Trek2 result in a progressive reduction of sensitivity to internal acidification [19, 20]. Through chimeric studies with the pH-insensitive channel Task3, amino acids 334-348 of Trek2 have been deemed critical for this modulation [20]. Importantly, this region is highly conserved in Trek1. Interestingly, a separate study focused on Trek1 identified

E306 as the intracellular pH sensor, as mutation of this residue to alanine resulted in a constitutively active channel, which could not be further activated by other channel openers including pressure, arachidonic acid, or temperature [36]. This group cites the conserved glutamate at position 332 as the corresponding Trek2 proton sensor. While this amino acid was not found within the critical region identified for Trek2 (amino acids 334-348), it was located only two amino acids away from the Trek2/Task3 chimera boundary used to establish that region, thus it is possible that integrity within this region is important for intracellular pH sensing.

Extracellular pH has also been shown to modulate Trek channels. This represents one of the few regulatory differences recorded between Trek1 and Trek2. Trek1 is potently inhibited by extracellular acidification [71, 72]. In contrast, Trek2 was activated by extracellular acidification [71]. The relevant amino acid was found to be a histidine located in the extracellular loop between TM1 and TM2, preceding P1, which was conserved in both Trek1 and Trek2, but differentially interacted with positive or negatively charged residues in the extracellular region located between P2 and TM4 (**Fig. 2**) [71]. It is important to note that external acidification had no effect on Trek2 currents in a separate study [14]. As this represents one of the only differences between Trek1 and Trek2 modulation, this property may be used in future studies to better identify which Trek family member may be underlying a specific current *in vivo*.

In contrast to Trek1 and Trek2, intracellular acidification had no effect on Traak currents, whereas internal alkylation activates the channel [37]. The

regions responsible for pH sensing also appear to be different for Traak, as replacing the C-terminal domain with that of Task1 or Task3 had no effect on pH sensitivity, indicating the C-terminus is not critical for this effect [37].

Interestingly, increasing the internal pH has been shown to sensitize Traak to activation by other channel modulators such as membrane stretch and AA [37], which is also true for internal acidification with Trek1 [19].

Phosphoregulation of Trek1 and Trek2

In addition to the complex set of stimuli that exert regulatory control over the Trek family members, Trek channels are also regulated through phosphorylation by PKA, PKC and cGMP dependent protein kinase (PKG) (**Fig. 2**). These protein kinases couple Trek channel activity to GPCRs that work via G_s , $G_{i/o}$ and G_q subclasses of G-proteins. In contrast, Traak does not display regulation by phosphorylation [44].

Both Trek1 and Trek2 channels are inhibited by forskolin, IBMX, and other pharmacological agents that result in the downstream activation of PKA [14, 15, 21, 24, 35, 41, 73, 74]. Furthermore, activation of G_s GPCRs co-expressed with these channels, results in the reversible inhibition of Trek currents [14, 24]. In contrast, drugs that result in the downstream inhibition of PKA lead to activation of Trek currents. Moreover, co-expression of Trek channels with $G_{i/o}$ GPCRs (metabotropic glutamate receptor 2, mGluR2; GABA_B receptor) results in the activation of Trek currents [73-76]. Interestingly, current produced through activation of $G_{i/o}$ GPCRs is not reversible.

The C-terminus has been proposed as the regulatory region for PKA-dependent modulation of both Trek1 and Trek2. While there are many PKA consensus sites within the C-terminus, a conserved serine residue (S333 in Trek1 and S359 in Trek2) has been identified as the phosphorylation site that mediates the inhibitory effects of PKA phosphorylation (**Fig. 2**) [15, 24, 35, 41]. Indeed, mutation of this amino acid to aspartate (to mimic the phosphorylated state) resulted in a channel with low activity, insensitive to pharmacological agents that alter PKA signaling [15, 24, 41]. Conversely, mutation of this amino acid to alanine (to mimic the dephosphorylated state) resulted in a channel with high basal activity also insensitive to pharmacological modulations that alter PKA [15, 24, 41]. In addition to this well-established regulation via PKA phosphorylation, inhibition of Trek1 has also been shown in one cell type (bovine adrenal zona fasciculata cells) through cAMP-mediated activation of exchange protein directly activated by cAMP 2 (Epac2) [77]. Thus, multiple cAMP-dependent mechanisms may converge to ensure proper regulation of Trek currents.

Both Trek1 and Trek2 are inhibited by the PKC activator, PMA [14, 21, 41, 78], thus also sensitive to phosphorylation by PKC (**Fig. 2**). Indeed the C-terminus has been implicated in this regulatory pathway as well. Both Trek1 and Trek2 share a conserved PKC consensus site at S300 (Trek1)/S326 (Trek2), which in the phosphorylated state renders the channel inactive (**Fig. 2**) [24, 41, 70]. Importantly, activation of G_q GPCRs co-expressed with either Trek channel, results in the reversible inhibition of Trek currents [24, 70, 78, 79].

Trek1 has also been shown to display regulation by cGMP activated protein kinase (PKG). Guanylate cyclase produces the second messenger cGMP in response to activation by extracellular signaling molecules including peptide hormones and nitric oxide. Trek1 channel activity has been shown to increase after PKG activation. Indeed pharmacological application of 8-Br-cGMP, a stable form of cGMP, to COS cells heterologously expressing Trek1, resulted in the activation of Trek1 [35]. This was determined to result from the phosphorylation of S351 within the C-terminal regulatory domain [35]. Indeed mutation of this residue rendered the channel insensitive to 8-Br-cGMP [35]. While S351 is not conserved in Trek2, no studies have addressed the sensitivity of Trek2 to PKG.

AMP- activated protein kinase (AMPK) has also been shown to modulate Trek channel activity. This kinase is activated when the AMP:ATP ratio is increased, signaling an increase in ATP production and reduction in energy expenditure. Phosphorylation of both Trek1 and Trek2 by AMPK results in the reversible inhibition of Trek currents [80]. Interestingly, S300/S333 on Trek1 and S326/S359, those residues shown to modulate PKA and PKC activity, are also responsible for the inhibition by AMPK [80]. Thus, multiple signaling pathways converge on key residues for the phosphoregulation of channel activity.

Despite a large number of studies investigating GPCR-mediated activation of Trek channels in *Xenopus oocytes* or immortal cell lines, few studies have investigated GPCR activation of Trek channels using native cell systems. In

DRG neurons, a heat-activated current also activated by β adrenergic receptor stimulation, has been proposed to be Trek1 [78]. Additionally, Trek2 has been shown to be activated downstream of α_2 adrenergic receptor [74] and GABA_B receptor [73] in the entorhinal cortex. A recent study has also established that Trek1 carries ~30% of the GABA_B receptor-induced K⁺ current in hippocampal neurons [76]. Other than these few studies, the physiological contribution these channels make as downstream signaling targets of GPCR activation remains unknown.

Trek channel pharmacology

The K_{2P} family is well known for its insensitivity to classical K⁺ channel blockers, including TEA and 4-AP [81]. Varying sensitivities to external Ba²⁺ have been reported for the different K_{2P} members [81]. As for the Trek family, the general consensus is that these members are insensitive to low doses of extracellular Ba²⁺ (<1 mM), but will display partial blockade at higher doses (1-5 mM) [14-16, 79].

Numerous pharmacological compounds have been shown to activate (**Table 1**) or inhibit (**Table 2**) Trek channels. These lists contain a number of clinically relevant compounds including a number of volatile anesthetics, antipsychotics, antidepressants, and neuroprotective agents. The pharmacological modulation by such compounds has propelled a substantial amount of research into a role for Trek channels in many clinical conditions, and will be discussed further in the next section. It is important to note that Trek1 and Trek2 display similar

sensitivities to pharmacological manipulation, whereas significantly less consistency is observed with Traak (**Table 1,2**). Moreover, selective blockers do not exist for any of the Trek family members, which has made studying this family in endogenous systems very difficult.

Table 1. Pharmacological agents that activate Trek channels.

Pharmacological agents that activate Trek family members. Drug name, drug class, effect on Trek family members, EC_{50} , and relevant references are outlined in the table above. Empty cells in the Trek modulation column represent a lack of data for that family member. Empty cells in the EC_{50} column represent no specified value. Abbreviations: activate (A), insensitive (X), non-steroidal anti-inflammatory drug (NSAID)

Drug	Drug Class	Modulation			EC ₅₀	Ref
		Trek1	Trek2	Traak		
Baicalein	neuroprotective agent	A	A			104
Carbon monoxide	poisonous gas	A				196
Chloral hydrate	anesthetic	A		A		85
Chloroform	volatile anesthetic	A		X	0.79 mM	15
Cyclopropane	volatile anesthetic	A				84
Diethyl ether	volatile anesthetic	A		X	0.6 mM	15
Flufenamic acid	NSAID	A	A	A		197
Halothane	volatile anesthetic	A		X	0.21 mM	14, 15, 84
Isoflurane	volatile anesthetic	A		X	0.31 mM	14, 15
Mefenamic acid	NSAID	A	A	A		197
Niflumic acid	NSAID	A	A	A		197
Nitric oxide	free radical	A				84, 196
Riluzole	neuroprotective agent	A	A	A		14, 102, 103, 104
Trichloroethanol	anesthetic	A		A		85
Wogonin	neuroprotective agent	A	A			104
Xenon	volatile anesthetic	A				84
Zinc	divalent metal ion		A		87.1 μ M	138

Table 1

Table 2. Pharmacological agents that inhibit Trek channels.

Pharmacological agents that inhibit Trek family members. Drug name, drug class, effect on Trek family members, IC_{50} , and relevant references are outlined in the table above. Empty cells in the Trek modulation column represent a lack of data for that family member. Empty cells in the IC_{50} column represent no specified value. Abbreviations: inhibit (I), insensitive (X)

Drug	Drug Class	Modulation			IC ₅₀	Ref
		Trek1	Trek2	Traak		
2-nitrobenzoic acid	oxidizing agent	X	I	X		195
3-n-butylphthalide	neuroprotective agent	I			0.06 μmol/L	198
Amlodipine	Ca ²⁺ channel inhibitor	I			0.43 μM	77
Anandamide	cannabinoid	I			5.07 μM	77
Bupivacaine	anesthetic	I			370 μM	199
Caffeine	stimulant	I			377 μM, 2.44 mM	85, 200
Chlorpromazine	antipsychotics	I	I	X	2.7 μM	201
Cisplatin	antineoplastic	I				202
Citalopram	antidepressant	I			189 μM	87
Curcumin	phytochemical	I			0.93 μM	128
Cyclopiazonic acid	Ca ²⁺ store activator	I				203
Diltiazem	Ca ²⁺ channel inhibitor	I	I	X	T1: 0.18 mM T2: 0.33 mM	197
Doxepin	antidepressants	I			243 μM	87
Flunarizine	Ca ²⁺ channel inhibitor	I			2.48 μM	77
Fluoxetine	antidepressant	I			6.5 μM, 19 μM	28, 86, 87
Fluphenazine	antipsychotic	I	I	X	4.7 μM	201
Flupenthixol	antipsychotic	I	I	X	2.0 μM	201
Fluvoxamine	antidepressant	I			8.5 μM	85
Haloperidol	antipsychotic	I	I	X	5.5 μM	201
Lamotrigine	anticonvulsant	I		I		204
Lead	divalent metal ion		I		15.6 μM	138
Lidocaine	anesthetic	I			180 μM	205
Loxapine	antipsychotic	I	I	X	19.7 μM	201
Mirtazapine	antidepressant	I			129 μM	87
Nifedipine	Ca ²⁺ channel inhibitor	I			8.18 μM	77
Niguldipine	Ca ²⁺ channel inhibitor	I			0.75 μM	77
Norfluoxetine	antidepressant	I			9 μM	86
Paroxetine	antidepressant	I			5.5 μM	28
Pimozide	antipsychotic	I	I	X	1.8 μM	201
Quinine	antimalarial	I				15
Ryanodine	Ca ²⁺ store activator	I				203
Sertraline	antidepressant	I			3.2 μM	28
Sipatrigine	neuroprotective agent	I		I	T1: 4 μM T: 10 μM	204
Thapsigargin	Ca ²⁺ store activator	I				203
Theophylline	stimulant	I			486 μM	85, 203

Table 2

Physiological roles for Trek channels

The lack of highly selective pharmacological blockers has made the use of knockout mice an invaluable tool for studying the endogenous contributions of Trek channels. The generation of the *Trek1*^{-/-} mouse in 2004 [27] has confirmed a number of the physiologically relevant contributions of Trek1, which had been proposed based on studies from work in immortal cell lines. In many cases, the *Traak*^{-/-} mouse has been used for comparison, and many differences have been observed between these two knockout animals. Importantly, neither *Trek1*^{-/-} nor *Traak*^{-/-} mice display abnormal phenotypes related to appearance, body weight, reflexes, or object memory [27].

Trek1^{-/-} mice display an increased sensitivity to pain [25, 26], an increased sensitivity to ischemia and epilepsy [27], show lower sensitivity to the effects of inhaled anesthetics [27], and display a depression-resistant phenotype [28]. In contrast, little is known about the neurobiological relevance of Trek2. A single behavioral study has been conducted using siRNA knockdown of *Trek2* localized to the entorhinal cortex. This study demonstrated altered spatial learning to result from the knockdown of Trek2 [73]. The recent generation of a mouse constitutively lacking *Trek2* [82] will now make further behavioral testing possible, however as of yet these animals not been subjected to any behavioral characterization. The goal of Chapter 4 was to probe the consequences of constitutive *Trek* ablation in mice paradigms that assess motor activity, coordination, anxiety-related behavior, learning and memory, and drug-induced

reward-related behavior, utilizing the newly generated *Trek2^{-/-}* mouse, and a mouse lacking all three members of the Trek family (*Trek1/2/Traak^{-/-}*).

Pain

As Trek1 and Traak are both mechano- and temperature sensitive [15, 59], and highly expressed in dorsal root ganglion (DRG) neurons [17, 18, 29], a role for Trek channels in transmitting pain information has been proposed. Indeed *Trek1* mRNA is present in both small and medium sensory neurons, including those associated with peptidergic substance P-positive fibers and non-peptidergic IB4-positive C-fibers [17, 25], where they also co-localize with the transient receptor potential channel subfamily V member 1 (TRPV1) [25].

A physiological role for both Trek1 and Traak in pain has been further tested utilizing knockout mice. Indeed, both *Trek1^{-/-}* and *Traak^{-/-}* mice display increased sensitivity to painful stimuli in a number of pain-provoking behavioral tests [25, 26]. This includes a hypersensitivity to thermal pain, mechanical pain, pain induced by osmotic changes, and enhanced sensitivity to both hot and cold temperatures [25, 26]. Furthermore, *Trek1* mRNA is up-regulated during inflammation [25]. Thus, both Trek1 and Traak represent novel targets for analgesic drug development.

General anesthetics

Activation of Trek channels by volatile anesthetics was established early, as the *Aplysia* S-type K⁺ channel is also activated by volatile anesthetics [58, 83].

Indeed, both *Trek1* and *Trek2* are activated by a number of volatile anesthetics (**Table 1**) [14, 15, 84, 85]. Consistent with the *in vitro* pharmacological studies, *Trek1*^{-/-} mice display lower sensitivity to the effects of numerous volatile anesthetics used clinically, including chloroform, halothane, sevoflurane, desflurane and isoflurane [27].

Depression

A number of clinically relevant anti-depressants have been shown to inhibit *Trek* channel activity (**Table 2**), including members of the selective serotonin reuptake inhibitor (SSRI) drug family such as fluoxetine [28, 86, 87]. Thus, a possible role for *Trek* channels in mediating the therapeutically beneficial effects of these drugs was proposed.

Accordingly, *Trek1*^{-/-} and *Traak*^{-/-} mice have been subjected to behavioral tasks aimed at assessing their role in depression. *Trek1*^{-/-} mice displayed depression-resistant behavior in four commonly used behavioral assays including the forced swim test, the tail suspension test, the conditioned suppression of motility test, and the learned helplessness task [28].

Furthermore, administration of numerous anti-depressant drugs provided no further behavioral benefit to *Trek1*^{-/-} mice, whereas *Traak*^{-/-} and wild-type mice displayed a reduction in depression-related behaviors [28], suggesting that the therapeutic benefits of such drugs act, at least in part, through their actions on *Trek1* channels.

The behavioral evidence suggesting that pharmacological blockade of *Trek1* may provide therapeutic benefits in depression, has highlighted *Trek1* as a novel therapeutic target [88, 89]. Indeed, recent work has focused on a promising new candidate, spadin [88, 89]. This peptide is derived from the pro-peptide generated by the maturation of the neurotensin receptor 3 (NTSR3/Sortilin) [88]. Spadin has been shown to potently inhibit *Trek1*, with an IC_{50} = 70.7 nM [88]. Furthermore, preclinical studies display depression-resistant behaviors in wild-type mice treated with spadin, similar to that observed with chronic fluoxetine treatment, or constitutive *Trek1* ablation [88]. Traditionally used pharmaceutical treatments for depression require administrations for three or more weeks before a therapeutic benefit is observed. In contrast, the behavioral results obtained from mice chronically treated with fluoxetine, were achieved after only 4 days of spadin treatment [88], thus this drug may provide therapeutic benefit much earlier than traditional treatments. Concerns regarding severe side effects associated with *Trek1* blockade have also been addressed. No drug-induced differences were observed with regards to pain, epilepsy, cardiac function, or neural damage after focal ischemia [89]. Thus clinical trials utilizing this compound may be on the horizon.

Individual polymorphisms within the human *KCNK2* gene have also been associated with both frequency in major depressive disorders and treatment-related outcomes [90-92]. In humans, the rs6686529 single nucleotide polymorphism (SNP), located in the 3' UTR region on exon 7, was observed at

significantly higher frequency in individuals suffering from major depressive disorder [90]. Individuals carrying the heterozygote allele G/C or C/G displayed lower incidences of major depressive disorders [90]. Furthermore, homozygotes possessing the C/C allele displayed a greater likelihood of receiving therapeutic benefit from SSRI treatment than those possessing the G/G allele [90]. An association between *KNCK2* polymorphisms and therapeutic benefit was also observed in the Sequenced Treatment Alternatives to Relieve Depression (STAR*D) study [91]. Four *KCNK2* polymorphisms were associated with resistance to multiple anti-depressant drug classes, thus may identify individuals at risk for therapeutic-resistant depression [91].

As high levels of *Trek1* have been observed in many brain regions involved in reward-related activities, including the nucleus accumbens, caudate and putamen [29, 30], it has been proposed that the influence of *KCNK2* polymorphisms on depression may overlap with a role for *KCNK2* in reward-processing. To test this hypothesis, functional magnetic resonance imaging (fMRI) was conducted during a monetary incentive delay task. The analysis focused on the relationship between *KCNK2* polymorphisms and basal ganglia responses to reward-predicting cues and gains. As hypothesized, polymorphisms associated with better therapeutic responses in the STAR*D study [91] were also associated with stronger responses to gains in many reward-related regions of the brain, indicating variations in *Trek1* may influence hedonic responses to rewarding stimuli [92].

Neuroprotection during ischemia

Significant evidence supports a neuroprotective role for Trek channels. This work has originated from the early observations that Trek channels are activated by intracellular acidification [14, 19, 20], membrane stretch [14-16], and PUFAs [14, 15, 22], which are all triggered by ischemia [93]. Ischemia refers to a generalized condition where a shortage of oxygen is experienced either globally or locally within a tissue, usually a result of inadequate blood flow. Cardiac ischemia occurs when the heart receives insufficient blood flow, and represents one of the most common causes of death in western nations [94]. An ischemic stroke results in oxygen deprivation to the brain and may range in severity from temporary loss of neurological function to death.

There is substantial evidence suggesting that PUFAs may provide beneficial effects during periods of ischemia, which has been proposed to result through their reduction in cellular excitability [95, 96]. Indeed, administration of the PUFA, linolenic acid (LIN), has been shown to inhibit neuronal loss in an *in vivo* model of cerebral global ischemia [97, 98]. LIN has also been shown to prevent kainate-induced seizures and neuronal death associated with kainate-induced excitotoxicity [97, 98]. LIN will also protect against neuronal cell death and loss of motor neuron function after spinal cord ischemia [99] and protects against neuron death in an *in vivo* model of focal ischemia [100]. Furthermore, multiple lysophospholipids, which have been shown to activate Trek channels, also prevent neuronal cell death during both an *in vitro* model of glutamate toxicity and an *in vivo* model of global ischemia [101].

The clinically used neuroprotective agent, riluzole, has also been shown to activate Trek channels (**Table 1**) [14, 102-104]. Currently, this drug is used to treat patients with amyotrophic lateral sclerosis (ALS). Furthermore, riluzole has also been shown to provide neuroprotection and reduce cell death in an *in vivo* rodent model of focal ischemia [100], and reduce paraplegia and cell death in an *in vivo* model of spinal cord ischemia in the rabbit [105]. Other natural compounds, including the oriental flavonoids baicalein and wogonin, have been shown to activate Trek channels (**Table 1**) [104]. These flavonoids have also been shown to elicit neuroprotective benefits [106-108].

The induction of ischemia both *in vitro* and *in vivo* has been shown to increase Trek channel expression and enhance cellular protection as well [109-113]. Heterologous expression of Trek1 has been shown to protect cells against oxidative injury and prevent apoptosis in Chinese hamster ovary (CHO) cells [111]. Moreover, *in vivo* cerebral ischemia and focal ischemia have resulted in increased *Trek1* mRNA [109, 110] and protein [110, 112]. The increase in Trek1 protein correlated with an increase in astroglial proliferation (astrogliosis), and inhibition of Trek1 in cultured astrocytes inhibited their proliferation after exposure to hypoxia [112]. Trek2 protein levels were shown to increase in cultured astrocytes, ultimately resulting in the ability to continue to buffer cells against glutamate excitotoxicity, an *in vitro* model of cellular excitability. [113]. Furthermore, *Trek2* mRNA and protein levels have also been shown to increase in both the cortex and hippocampus after inducing cerebral ischemia *in vivo* [110]. Increased mRNA levels after *in vivo* cerebral ischemia

has also resulted in increased levels of *Traak* [109, 110], supporting a role for all Trek family members in hypoxia-related neuroprotection.

The availability of *Trek1*^{-/-} and *Traak*^{-/-} mice has further confirmed a protective role for this family during ischemia. *Trek1*^{-/-} mice were more susceptible to both kainic acid-induced and pentylenetetrazol-induced seizures, and displayed significantly greater mortality rates associated with the seizure activity [27]. As PUFAs have been shown to provide a neuroprotective effect during epileptic activity [97], the increased mortality rate observed in *Trek1*^{-/-} mice is likely the result of a complete or partial loss of sensitivity to such neuroprotective agents. Indeed, pre-injection of LPA or LPC before kainic acid-induced seizures failed to protect *Trek1*^{-/-} mice, however resulted in decreased seizure activity in wild-type mice [27].

Trek1^{-/-} mice also displayed increased sensitivity to both brain and spinal ischemia. Global ischemia resulted in seizure activity, followed by death in more than 70% of *Trek1*^{-/-} mice compared with a 34% mortality rate in wild-type mice [27]. Again, PUFAs display a neuroprotective effect during ischemia [97], and pre-injection of such agents again failed to protect *Trek1*^{-/-} mice against ischemia-induced death [27]. Interestingly, *Traak* channels are also sensitive to the actions of PUFAs [44], however, *Traak*^{-/-} mice displayed no difference from wild-type in seizure activity or ischemia-induced death [27].

Trek1^{-/-} mice have also been subjected to a model of decompression sickness. Decompression sickness arises when sudden decompression causes nitrogen bubbles to form in tissues, including the brain. It occurs most

commonly when a scuba diver ascends to the surface too quickly, and is associated with severe pain, cramps, paralysis and possible death. *Trek1^{-/-}* displayed lower resistance to decompression sickness, were more likely to develop neurological symptoms such as paraplegia, paraparesis, and convulsions, and had higher mortality rates, consistent with a neuroprotective role for Trek1 in this assay as well [114].

In contrast to the neuroprotective role proposed during epilepsy, ischemia, and decompression sickness, Trek1 appears to provide no protection in a model of traumatic brain injury [115]. Indeed, no differences were observed with respect to contusion volume or hippocampal cell count between *Trek1^{-/-}* and wild-type mice [115]. Further work is needed to better understand the exact mechanisms through which Trek channels may provide a neuroprotective effect, however the evidence supporting such a role is substantial.

Despite the evidence supporting a neuroprotective role for Trek channels, one research group has raised some concerns regarding the actual contribution Trek channels may actually have during conditions of low oxygen [116-118]. This group argues that during hypoxia, when O₂ levels are very low, Trek channel activity is substantially decreased, to a point where activity is negligible [116-118]. These experiments have been refuted by others, who were able to detect Trek channel activity at low O₂ levels [119]. This group demonstrates that heterologously expressed Trek1 can be further activated by AA and intracellular acidosis during simulated hypoxic conditions, mimicking the protective mechanism that has been proposed to occur *in vivo*. The numerous

in vitro studies, together with a number of studies utilizing *in vivo* models make a strong argument for this family in neuroprotection.

Trek channels in development

During embryogenesis, *Trek1*, *Trek2*, and *Task3* display the highest levels of mRNA expression among the K_{2P} superfamily, where *Trek1* and *Trek2* are broadly expressed in neuronal tissue [120]. This suggests a role for Trek channels during development. Indeed, highest levels of *Trek1* and *Trek2* are detected in the subventricular and ventricular zones [120], regions best known as a site for neurogenesis and a source for neuronal stem cells in the adult [121, 122]. Post-natal changes are most apparent with *Trek2*, where high embryonic levels of neuronal expression remain during early post-natal development, but fall rapidly in the first days after birth [120]. In contrast, *Trek1* levels remain more or less stable during postnatal development into adulthood [123]. Despite these proposed roles, no developmental abnormalities have been reported in any *Trek*^{-/-} mice, thus more work is needed to determine the extent of Trek involvement during development.

Non-neuronal roles for Trek channels

A role for Trek channels (most notably *Trek1*) has been proposed in a number of non-neuronal processes as well, however in most cases, Trek channels were suggested based on a generalized electrophysiological characterization and the identification of *Trek* mRNA in the relevant cell type.

The lack of specific pharmacological blockers makes such roles proposed for Trek family members difficult to validate. At present, the best tools available to study proposed physiological roles are the knockout mice, which have not been used in any of the studies mentioned below. Thus, more work is needed to validate that the proposed processes do in fact involve Trek channels.

In the heart, Trek1 may contribute to the regulation of atrial natriuretic peptide secretion [124], protect cardiac tissue during ischemia [125], and varying expression levels may differentiate mechanoelectric feedback [126, 127]. Other proposed roles include the control of cortisol secretion by adrenal cortical cells [128], to stabilize bladder excitability as urinary volume increases [129, 130], to mediate cytokine secretion in alveolar epithelial cells [131], to support uterine quiescence during pregnancy [132, 133], and unregulated cell growth in prostate cancer [134]. Few studies have focused on Trek2 outside of the CNS, however a possible role in regulating insulin release has been proposed [135]. Ultimately, there is significantly more work needed to fully understand how Trek channels, especially Trek2, contribute to whole animal physiology and how to capitalize on their contributions for therapeutic benefit.

Summary

Trek channels have been implicated in a number of physiological and neurobehavioral processes, where most research has focused on Trek1. Given the contribution of these channels to physiology and neuropharmacology, understanding the molecular diversity in this family is important. Alternative

translation initiation and alternative splicing both contribute to the structural and functional diversity of *Trek1*; however the impact of post-transcriptional modifications on the expression and function of *Trek2* is unclear. In chapter 2, two novel splice isoforms of the mouse *Trek2* gene are characterized, which provides new insights into the molecular diversity of *Trek2* channels and suggests a potential role for the *Trek2* amino terminus in channel trafficking and/or stability.

During the characterization of murine *Trek2* alternative splice variants, discussed in chapter 2, significant variability in whole-cell currents from HEK293 cells transiently transfected with *Trek2* were observed. Given the presence of all three *Trek* family members in neuronal stem cells and neuronal progenitor cells [136, 137], understanding a potential interaction between cell cycle regulation and *Trek* channels is critical. In chapter 3, the influence of cell cycle on the variability of whole-cell currents from cells heterologously expressing *Trek* channels was investigated.

Constitutive ablation of the *Trek1* gene in mice correlates with enhanced sensitivity to ischemia and epilepsy, decreased sensitivity to the effects of inhaled anesthetics, increased sensitivity to thermal and mechanical pain, and resistance to depression. While the distribution of *Trek2* mRNA in the CNS is broad, little is known about the relevance of this *Trek* family member to neurobiology and behavior. In chapter 4, the effect of constitutive *Trek2* ablation, as well as the simultaneous constitutive ablation of all three *Trek* family genes, is assessed in paradigms that assess motor activity, coordination,

anxiety-related behavior, learning and memory, and drug-induced reward-related behavior.

Chapter 2

IDENTIFICATION AND CHARACTERIZATION OF ALTERNATIVE SPLICE VARIANTS OF THE MOUSE *TREK2/KCNK10* GENE

Mirkovic K., and K. Wickman, Identification and characterization of alternative splice variants of the mouse *Trek2/Kcnk10* gene. *Neuroscience* 2011; 194:11-8.

Introduction

Trek channels have been implicated in a wide array of physiological and neurobehavioral processes. For example, genetic variation in the *TREK1* gene in humans was linked to individual differences in mood and responses to rewarding stimuli [92]. Mice lacking the *Trek1* gene are more sensitive to painful heat [25], are resistant to the sedative effects of volatile anesthetics [27], are more susceptible to ischemia and epilepsy [25], and exhibit a depression-resistant phenotype [28]. While less is known regarding physiological roles for *Trek2*, recent studies suggest that *Trek2* contributes to the resting membrane potential in mouse superior cervical ganglion neurons [102], and that *Trek2* mediates the postsynaptic inhibitory effects of GABA_B and α_2 adrenergic receptor activation in neurons of the entorhinal cortex [73, 74]. Moreover, knock-down of *Trek2* mRNA in the entorhinal cortex impaired spatial learning in mice [73].

Given the contribution of *Trek* channels to neurophysiology and neuropharmacology, understanding the molecular diversity within this K_{2P} subfamily, particularly within the CNS, is important. Previous studies have documented multiple post-transcriptional modifications that increase structural diversity in the *Trek* family, and in some instances, these modifications correlate with functional diversity. For example, alternative translation initiation was shown to yield both short and long variants of *Trek1* that differ with respect to Na⁺ permeability [40]. At present, the full scope and functional relevance of alternative splicing in the *Trek* family is unclear, particularly for the *Trek2* gene.

While some Trek2 splice variants harboring unique N-terminal domains have been characterized [41], rigorous comparative assessments of expression or function have not been undertaken. The goal of this study was to identify murine Trek2 splice variants, evaluate their expression patterns, and probe for isoform-dependent differences in channel function.

Experimental Procedures

RT-PCR and Trek isoform expression analysis. Total mouse brain RNA (500 ng, Clontech; Mountain View, CA) was reverse-transcribed using the iScript cDNA synthesis kit according to manufacturer's recommendations (BioRad; Hercules, CA). For subsequent PCR amplification, 2 μ L of reverse transcribed cDNA was combined with 0.1 μ L Hi-Fidelity Taq (Invitrogen Life Sciences; Carlsbad, CA), 10X Hi-Fidelity Taq buffer, 2.5 μ M oligonucleotide mixture, 0.5 μ M MgSO₄, and 2.5 μ M dNTPs in a final volume of 25 μ L. Sense oligonucleotides targeting the unique 5' UTR for Trek2a (5'-gcagagcgagaccaaccactcc-3'), Trek2b (5'-ggctgcaactccaccgagcacg-3'), and Trek2c (5'-ccgttggtctgtttaaccgacgag-3'), were paired with an antisense oligonucleotide targeting either the 3'UTR found in exon 5 (5'-ccaacatggtagcgcacagtcc-3') to amplify the truncated one-pore (1p) variants, or 3'UTR found in exon 8 (5'-gccactgtctgaaatgaagctcttgc-3') to amplify full-length Trek2 variants. The thermal cycling protocol consisted of a 2 min denaturation step at 94°C, followed by 25/35/45 cycles of 94°C/30 s, 58°C/30 s, and 68°C/3 min, and a 10 min final extension step at 68°C. Predicted amplicon sizes were

869 bp (Trek2c-1p), 1871 bp (Trek2a), 1822 bp (Trek2b), 1935 bp (Trek2c), Amplicons were extracted using a gel purification kit (Qiagen; Valencia, CA), inserted into pCR2.1-Topo (Invitrogen Life Sciences; Carlsbad, CA), and sequenced. Identical PCR conditions and isoform-specific oligonucleotides were used to evaluate regional differences in Trek2 variant expression in 8 mouse tissues (Clontech; Mountain View, CA) and 15 different brain regions (Zyagen; San Diego, CA). PCR samples were subject to DNA electrophoresis on 1% agarose gels containing ethidium bromide for band visualization.

Generation of Trek2 expression constructs. C-terminal myc-tagged Trek2-1p, Trek2a, Trek2b, and Trek2c expression constructs, were generated by PCR using Hi-Fidelity Taq. Trek2 cDNA (BC132487) was purchased from Open Biosystems (Huntsville, AL) and used as the PCR template. PCR fragments consisting of a Kozak sequence (5'-gccgccacc-3'), Trek2 variant open reading frame, and carboxyl-terminal myc tag sequence (5'-gagcagaaacttagcgaggaggacctg-3'), framed by Nhe1 and HindIII (Trek2a and Trek2c) or Not1 and HindIII (Trek2b) restriction enzyme sites, were then incorporated into the pCR2.1-Topo vector according to manufacturer's protocols (Invitrogen Life Science; Carlsbad, CA). Inserts were sequenced in both directions for accuracy. Amplified fragments were then subcloned into a modified pcDNA3.1- expression plasmid harboring the CAG promoter (pCAG3.1).

Immunoblotting. Human embryonic kidney (HEK) 293FT cells were purchased from Invitrogen Life Sciences (Carlsbad, CA) and cultured according to supplier recommendations. No tests were conducted to rule out the potential contamination of mycoplasma. Cells were plated at 60-70% confluence in 6-well plates, and transfected using the calcium phosphate method with the myc-tagged Trek2 expression constructs (2 $\mu\text{g}/\text{well}$). Two days after transfection, cells were collected in ice-cold PBS and centrifuged at 9200 x g for 1 min. Following centrifugation, the supernatant was aspirated and the pellet was resuspended in 250 μL 2x SDS sample buffer; samples were sonicated briefly. For immunoblotting, 2 μL 1M DTT was added to 10 μL of sample, and the mixture was incubated at 80°C for 10 min. Samples were then loaded onto 12% Bis-Tris gels, and run in a Tris-Glycine buffer under reducing conditions. Samples were transferred using a wet transfer system (Bio-Rad Laboratories; Hercules, CA) onto nitrocellulose membranes (Thermo Fisher Scientific Inc.; Rockford, IL), and probed with either a mouse anti-myc (1:500 dilution, Hoffman-La-Roche; Nutley, NJ) or mouse anti- β -actin (1:10000 dilution, Abcam, Cambridge, MA) antibodies. An IRDye 800CW donkey x mouse secondary antibody (LiCor Biosciences; Lincoln, NE) was used at a dilution of 1:7000. Visualization and quantification of band intensity was performed using the Odyssey Imaging System (LiCor Biosciences; Lincoln, NE). Integrated intensity values were recorded for all lanes and normalized to the intensity of the β -actin band.

Electrophysiology. HEK293 cells were cultured according to ATCC specifications, plated on 8-mm glass coverslips (30,000 cells/coverslip), and transfected using Lipofectamine LTX (Life Technologies Corporation; Carlsbad, CA) with an EGFP expression plasmid (0.02 $\mu\text{g}/\text{coverslip}$) and either a Trek2 splice variant or empty vector (0.09 $\mu\text{g}/\text{coverslip}$). One day after transfection, whole-cell currents were measured in EGFP-labeled cells with hardware (Axopatch-200B amplifier, Digidata 1320) and software (pCLAMP v. 9.0) from Molecular Devices, Inc. (Sunnyvale, CA). Borosilicate (3-6 M Ω) pipettes were filled with (in mM): 140 KCl, 2 MgCl₂, 1 EGTA, 5 HEPES, pH 7.2 with KOH. The bath solution consisted of (in mM): 136 NaCl, 4 KCl, 1.5 CaCl₂, 2 MgCl₂, 5 HEPES, pH 7.4 with NaOH. In some experiments, cells were switched from the normal bath solution to solutions containing 20 or 40 mM KCl (osmotically-balanced by equimolar reductions in NaCl) using an SF-77B Perfusion Fast-Step system (Warner Instrument Corp.; Hamden, CT). Upon achieving whole-cell access, cells were held at -70 mV and subjected to either a voltage-ramp (-100 mV to 60 mV in 1 s) or voltage-step (-100 mV to 60 mV in 20 mV increments; 0.5 s/step) protocol. Only experiments with low R_A (<20 M Ω) and low C_M (<50 pF) were included in the final data set. All measured currents were filtered at 2 kHz and stored directly on hard disk for subsequent analysis.

Surface biotinylation HEK 293FT cells were plated at 60-70% confluency in 6-well plates, and transfected using the calcium phosphate method with myc-tagged Trek2 expression constructs (2 $\mu\text{g}/\text{well}$). Two days after transfection,

cells were washed three times with ice-cold PBS (pH 8.0), and then incubated with 2 mM NHS-PEG₄ Biotin (Thermo Fisher Scientific Inc.; Rockford, IL) in ice-cold PBS, with slow shaking at 4°C for 30 min. Cells processed in parallel but not treated with biotin served as negative controls. Biotin was gently removed and cells were washed five times with ice-cold PBS. Cells were collected in PBS and centrifuged at 9200 x g for 1 min. Following centrifugation, supernatants were aspirated and pellets were resuspended in 250 µL Lysis Buffer consisting of PBS, 1% Triton, and a mixture of protease inhibitors (10 µg/ml Pepstatin A, 10 µg/ml Aprotinin, 10 µg/ml PMSF, and 1 µg/ml Leupeptin); Samples were sonicated briefly and incubated with rocking for 30 min at 4°C. Debris was pelleted in a microcentrifuge at 16800 x g at 4°C for 30 min and supernatants were retained. 25 µL of sample (“input”) was removed, and the rest of the sample was mixed by rotation for 30 min at 4°C with 60 µL of a 50% slurry of NeuroAvadin beads (Thermo Fisher Scientific Inc.; Rockford, IL). Beads were washed three times with Lysis Buffer and bound proteins were eluted in 100 µL of 2X SDS sample buffer plus 25 µL 1 M DTT by boiling for 10 min. Immunoblotting for myc-tagged proteins was performed as described above. Visualization and quantification of band intensity was performed using the Odyssey Imaging System (LiCor Biosciences; Lincoln, NE). Integrated intensity values were recorded for all lanes, and normalized to the intensity value of Trek2b.

Data analysis. Data are presented as the mean ± SEM. Statistical analyses

were done using Prism v. 11 (GraphPad Software Inc., USA). Whole-cell current amplitudes were analyzed using Kruskal-Wallis or Mann-Whitney tests, as appropriate. Protein levels were analyzed by ANOVA, followed by multiple comparisons with Newman-Keuls (NK) *post hoc* test when a significant interaction and/or main effect was found. Differences were considered significant if $P < 0.05$.

Results

Identification of *Trek2* splice variants

A BLAST search was used to identify all mouse cDNAs harboring sequence coding for the first pore domain in *Trek2* in the GenBank® database (www.ncbi.nlm.nih.gov/genbank/); **Table 3** lists the 8 entries identified using this approach. Five of the 8 entries correspond to a mouse *Trek2* variant that shares homology with a human and rat *Trek2* isoform termed *Trek2a* [41]. Another entry (DQ185134) corresponds to a previously-described mouse *Trek2* variant similar to the human and rat *Trek2c* variant [41]. In this study, we focused on the 2 remaining *Trek2* cDNAs (AK031904 and AK019376), which code for unique *Trek2* variants that have not been studied to date.

cDNA AK019376 codes for a C-terminal truncation of *Trek2*. The cDNA sequence was aligned with the mouse *Trek2/Kcnk10* gene (MGI:1919508), found on chromosome 12 (99672204-99816150: Mouse Genome Database). Five exons were identified in this splice variant (exons 1c, 2, 3, 4, 5), the first four of which were known previously (**Fig. 3A,B**). Exon 5 contains a short

stretch (60 bases) of coding sequence followed by an in-frame stop codon and 188 bp of 3' UTR. This variant generates a protein with only two transmembrane segments (M1 and M2) and one pore (P1) domain (**Fig. 3B**), for a total of 241 amino acids; we termed this a one-pore domain-containing Trek2 (Trek2-1p) variant.

cDNA AK031904 codes for an N-terminal Trek2 splice variant (**Fig. 3A,C,D**). Alignment of this cDNA with the mouse *Trek2/Kcnk10* gene revealed a previously-unrecognized exon that we termed exon 1b based on its location between exon 1a and 1c. In total, 7 exons contribute to this splice variant (exons 1b, 2, 3, 4, 6, 7, 8), which we termed Trek2b (**Fig. 3D**). It should be noted that the database sequence for AK031904 (Trek2b) is lacking a thymidine in exon 2 (between bases 181 and 182 of coding sequence) that is found in the mouse Trek2a and Trek2c variants, as well as the *Trek2* gene. Absence of this thymidine introduces a frame shift leading to premature termination of Trek2 translation. To determine whether the database sequence was in error, we designed intron-spanning oligonucleotides targeting the unique 5'UTR in exon 1b along with the 3'UTR from exon 8 for use in RT-PCR experiments in whole brain total RNA (**Fig. 4**). We were able to amplify a product of the predicted size, and DNA sequencing demonstrated that the amplicon did contain the missing thymidine.

The translation initiation codon for the Trek2b isoform spans two exons, with the adenosine found at the 3' exon-intron boundary of exon 1b, and the thymidine and guanosine found at the 5' intron-exon boundary of exon 2. As

such, Trek2b is slightly shorter (520 amino acids) than the two other N-terminal splice variants Trek2a (535 amino acids) and Trek2c (538 amino acids).

Trek2a, Trek2b, and Trek2c share coding sequence contributed by exons 2, 3, 4, 6, 7, and 8, and differ only at their N-termini (**Fig. 3C**).

Table 3. Murine Trek2-related cDNAs identified in the GenBank® database.

cDNA entries identified from a BLAST search with sequence corresponding to the first pore-domain of Trek2 (taken from NM_029911). Exon assembly, nomenclature and protein size (in number of amino acids, AA) are outlined in the table above. *The AK031904 database entry lacks a thymidine in Exon 2 found in all other Trek2-related cDNAs and the mouse *Trek2* gene. The primary amplicon generated by RT-PCR from mouse brain total RNA using Trek2b isoform-specific oligonucleotides contained also this thymidine; as such, the predicted Trek2b protein is corrected to be 520 amino acids.

Two	Exon Assembly	Nomenclature	Protein size (AA)
NM_029911	1a, 2, 3, 4, 6, 7, 8	Trek2a	535
BC137869	1a, 2, 3, 4, 6, 7, 8	Trek2a	535
BC132487	1a, 2, 3, 4, 6, 7, 8	Trek2a	535
AK082153	1a, 2, 3, 4, 6, 7, 8	Trek2a	535
AK036066	1a, 2, 3, 4, 6, 7, 8	Trek2a	535
AK031904	1b, 2, 3, 4, 6, 7, 8	Trek2b	520 *
DQ185134	1c, 2, 3, 4, 6, 7, 8	Trek2c	538
AK019376	1c, 2, 3, 4, 5	Trek2c-1p	241

Table 3

Figure 3. Structure and splicing of the mouse *Trek2* gene.

A) *Trek2* intron-exon structure and nomenclature. Exons 1b and 5 are previously-unreported exons. Note the different scales on the left and right side of the gene depiction. **B)** Linear alignments of *Trek2*-1p mRNA and protein. Numbers above the mRNA refer to the corresponding *Trek2* gene exons. M1 and M2 denote the location of the two transmembrane segments, whereas P1 denotes the location of the pore domain. Scale bar = 35 amino acids (A.A.). **C)** Sequence alignment of the unique N-terminal domains in *Trek2a*, *Trek2b*, and *Trek2c*. The thin vertical line denotes the boundary between corresponding coding sequence in exon 1(a/b/c) and exon 2. **D)** Linear alignments of *Trek2b* mRNA and protein. Numbers above the mRNA refer to the corresponding *Trek2* gene exons. M1-M4 denote the locations of the four transmembrane segments, and P1-2 denote the location of the 2 pore domains. The scale is the same as that used in panel **B**.

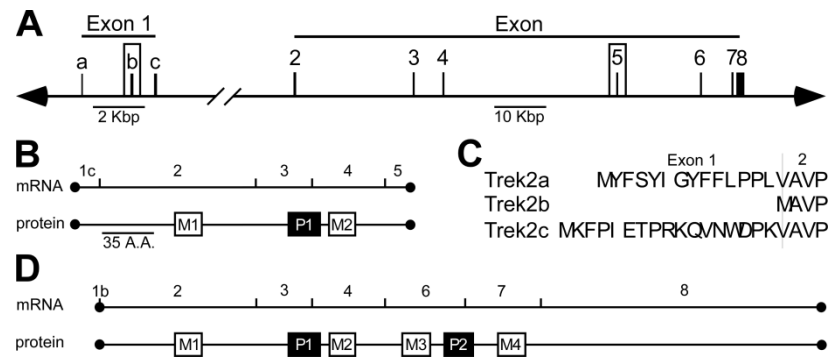


Figure 3

Distribution of *Trek2* splice variants

We next examined the tissue distribution of *Trek2*-1p and *Trek2b*, along with *Trek2a* and *Trek2c*, using a multi-tissue mouse cDNA panel and a PCR strategy involving intron-spanning, isoform-specific oligonucleotides (**Fig. 4A,B**). *Trek2*-1p expression was detected in the mouse brain, spleen and testis (**Fig. 4B**), with lower levels observed in heart, lung, and muscle; no expression of *Trek2*-1p was detected in liver or kidney. *Trek2a*, *Trek2b*, and *Trek2c* were detected in brain, with lower levels observed in heart, spleen, and lung. Little or no expression of *Trek2a*, *Trek2b*, or *Trek2c* was detected in muscle, kidney, liver or testis.

We next sought insight into the regional distribution of the *Trek2* splice variants in the CNS. Expression of the four *Trek2* splice variants was evaluated in a cDNA panel containing 15 different CNS structures (**Fig. 4A,C**). While all four variants showed broad distribution in the CNS, *Trek2*-1p exhibited the most restricted expression pattern of the splice variants tested. Robust signals corresponding to *Trek2*-1p were observed in brainstem, cerebellum, posterior cortex, cerebrum, hippocampus, medulla, olfactory bulb and pons. Lower intensity signals were observed in entorhinal cortex and striatum, whereas little or no expression was detected in frontal cortex, hypothalamus, midbrain, spinal cord, and thalamus. *Trek2a*, *Trek2b*, and *Trek2c* were broadly expressed in the CNS, with the most robust signals observed in the brainstem and cerebellum. None of the 3 N-terminal *Trek2* variants was detected in the thalamus, despite the clear presence of the positive control transcript (GAPDH). While the

regional expression patterns for Trek2 splice variants were largely overlapping, some isoform-dependent differences were observed. For example, Trek2b and Trek2c were detected in the cerebellum, while Trek2a expression was not. Similarly, expression of Trek2a and Trek2c, but not Trek2b, was observed in the midbrain.

Figure 4. Expression patterns of mouse *Trek2* splice variants.

A) Schematic depiction of mouse *Trek2* splice variant mRNAs, showing intron-exon boundaries and locations of isoform-specific oligonucleotides used for analysis of *Trek2* variant expression in mouse tissues. Black circles denote the boundaries of *Trek2* coding sequence. **B)** Representative ethidium bromide-stained DNA gel segments showing *Trek2* isoform-specific and intron-spanning amplicons in several mouse tissues (n=3 separate experiments per *Trek2* isoform). The size and DNA sequence of the primary amplicon corresponded to the intended *Trek2* isoform in all cases. Lower intensity bands located near the primary amplicons were seen in some lanes (e.g., *Trek2a* in spleen). Water was used as a negative control for each unique PCR reaction. A comparable level of GAPDH expression was observed in all mouse tissues. **C)** Representative ethidium bromide-stained DNA gel segments showing *Trek2* splice variant expression in 15 different CNS sub-regions (n=3 separate experiments per isoform). Lanes on the right side of the gel contain results of RT-PCR experiments using isoform-specific PCR primers and total brain mRNA; mRNA samples were treated with (+RT) or without (-RT) reverse-transcriptase. A comparable level of GAPDH expression was observed in all CNS sub-regions.

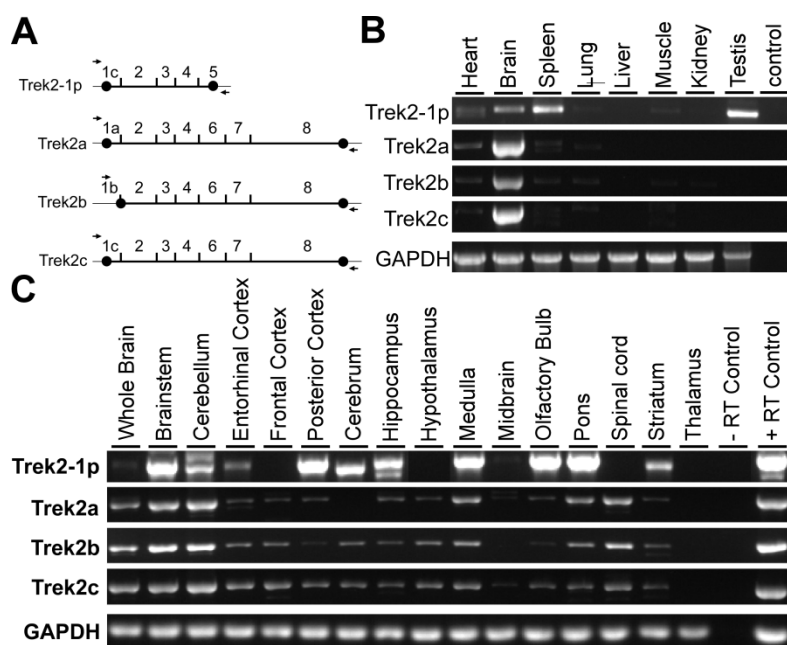


Figure 4

Functional characterization of Trek2 splice variants

To probe the impact of alternative splicing on Trek2 channel function, we next measured whole-cell currents in HEK 293 cells expressing individual Trek2 splice variants. Expression constructs for each variant were generated with sequence for the myc epitope tag engineered into the C-terminus. All three N-terminal Trek2 splice variants yielded novel currents exhibiting outward rectification (under conditions of physiological internal and external K^+ concentrations) that were distinct from currents measured in mock-transfected control cells (**Fig. 5A,D**). While considerable cell-to-cell variability in whole-cell current amplitudes was observed, clear group differences were found in cells transfected with Trek2a, Trek2b, and Trek2c. Cells expressing Trek2b exhibited large currents (3-20 nA at +60 mV), whereas currents measured in cells expressing Trek2a and Trek2c were markedly smaller (0.5-5 nA at 60 mV) (**Fig. 5A,D**).

Reversal potentials measured for cells expressing Trek2a (-60 ± 6 mV; $n=18$), Trek2b (-70 ± 2 mV; $n=21$), and Trek2c (-62 ± 3 mV; $n=27$) were comparable, and significantly more negative than those measured in mock-transfected control cells (-24 ± 4 mV; $n=12$, $P < 0.001$). These observations are expected for cells over-expressing K^+ -selective ion channels. Indeed, when K^+ concentrations in the bath were increased from 4 mM to either 20 or 40 mM, the reversal potential of the whole-cell current measured in cells expressing the novel Trek2b variant shifted toward more depolarized membrane potentials, consistent with expectations for a K^+ -selective ion channel (**Fig. 5B,C**). Moreover, the slope of

the line fitting the plot of whole-cell current reversal potential versus the natural log of $[K^+]_o/[K^+]_i$ was 20 ± 1 mV, close to the predicted value of 25.3 mV for a perfectly-selective K^+ channel measured at room temperature.

Cells transfected with Trek2-1p showed no novel currents (**Fig. 5D**), despite the appearance of recombinant protein (not shown). As a truncated C-terminal splice variant of Trek1 has been reported and shown to exert a dominant negative influence on the functional expression of Trek1 [39, 44], we asked whether Trek2-1p acts as a dominant negative influence on Trek2. Cells were co-transfected with 1:1 mixtures of Trek2b and either empty vector or Trek2-1p. We did not detect any difference in current amplitudes between cells expressing Trek2b in the absence or presence of Trek2-1p (**Fig. 5E**).

Figure 5. Functional characterization of Trek2 splice variants.

A) Sample traces showing whole-cell currents evoked by a voltage step protocol (-100 to +60 mV, in 20 mV increments; 500 ms step durations) in HEK 293 cells expressing myc-tagged Trek2a, Trek2b, or Trek2c variants. Currents observed in mock-transfected cells were negligible. Scale bars = 1 nA, 100 ms.

B) Sample traces showing the effect of external K^+ concentration ($[K^+]_o$; 4, 20, 40 mM) on the whole-cell current evoked by a ramp protocol (-100 to 60 mV in 1 s) in a cell expressing Trek2b. Note the rightward shift in reversal potential accompanying the increase in $[K^+]_o$, and the increased inward current flow at higher $[K^+]_o$, consistent with previous analyses of the Trek2 rectification profile.

C) Summary plot of current reversal potentials in Trek2b-expressing cells as a function of $[K^+]_o$ (n=5). **D)** Summary of outward currents (measured at 60 mV) in cells expressing Trek2a, Trek2b, Trek2C, and Trek2-1p, as well as mock-transfected controls. The results of a Kruskal-Wallis test were significant (H=55.3, 4 df, $P<0.0001$), indicating that mean current amplitudes were significantly different across groups. Symbols: **,*** $P<0.01$ and 0.001, respectively, vs. mock-transfected; #,### $P<0.05$ and 0.01, respectively, vs. Trek2b. **E)** Summary of outward currents (measured at 60 mV) in cells expressing Trek2b in the absence or presence of Trek2-1p (n=7). The results of a Mann-Whitney test were not significant (U=11.0, $P=0.1$), indicating that mean current amplitudes were not significantly different between the 2 groups.

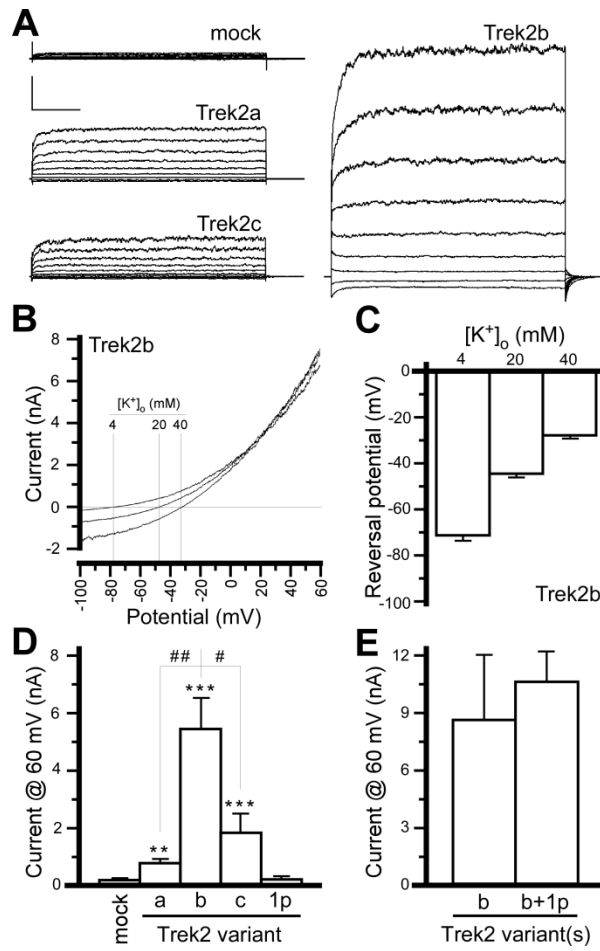


Figure 5

Surface expression of Trek2 splice variants

Previous comparative functional assessments of recombinant human TREK2A and TREK2C splice variants revealed no isoform-dependent differences in channel selectivity, single channel conductance, or mean open time, arguing that the short unique N-terminal domains do not influence fundamental biophysical properties of Trek2 channels [41, 43]. Indeed, a mutant version of rat Trek2c lacking the first 21 amino acids (*i.e.*, a mutant with a N-terminus virtually identical to the murine Trek2b variant described herein) exhibited functional properties indistinguishable from full-length Trek2c [43]. Accordingly, we surmised that the elevated whole-cell currents seen in cells expressing Trek2b reflected isoform-dependent differences in channel expression and/or distribution on the membrane surface. Indeed, levels of total Trek2b protein were significantly greater than levels of either Trek2a or Trek2c in whole-cell extracts from transfected HEK 293 cells (**Fig. 6A,C**).

Plasma membrane levels of the N-terminal Trek2 splice variants were determined using a surface biotinylation approach (**Experimental Procedures**). In brief, membrane proteins were tagged with a membrane-impermeable biotin reagent, and biotinylated proteins were then enriched using streptavidin precipitation, followed by quantitative immunoblotting for the myc-tagged Trek2 variants. The level of Trek2b at the plasma membrane of transfected cells was significantly greater than surface levels of either Trek2a or Trek2c (**Fig. 6B, D**). Moreover, the ratio of surface-to-total Trek2b protein was significantly higher than that measured for either Trek2a or Trek2c (**Fig. 6D**, right plot).

Figure 6. Whole-cell and plasma membrane expression levels of Trek2 splice variants.

A) Representative immunoblot of total Trek2 protein from HEK 293 cells expressing Trek2a, Trek2b, or Trek2c. Three separate transfections per Trek2 variant were performed, and the levels of both the Trek2 variant and β -actin were determined in each sample. **B)** Representative immunoblot of Trek2 splice variants found in samples of biotinylated surface proteins. **C)** Summary plot depicting the level of total Trek2 protein expressed in HEK293 cells, normalized to the level of β -actin (n=10). ANOVA revealed a statistically greater amount of Trek2b total protein compared to both Trek2a and Trek2c ($F_{(2,27)}=21.45$, $P<0.001$). **D)** Summary graph depicting total Trek2 protein (Input), total Trek2 biotinylated protein (Eluate), and surface-to-total protein ratio (S:T). Three independent experiments are summarized. Isoform-dependent differences in the levels of Trek2 in input ($F_{(2,7)}=18.7$, $P<0.05$) and eluate ($F_{(2,7)}=131.964$, $P<0.001$) samples were observed, as well as in the S-T ratio ($F_{(2,7)}=9.5$, $P<0.05$). Symbols: *, *** $P<0.05$ and 0.001, respectively, vs. Trek2a and Trek2c.

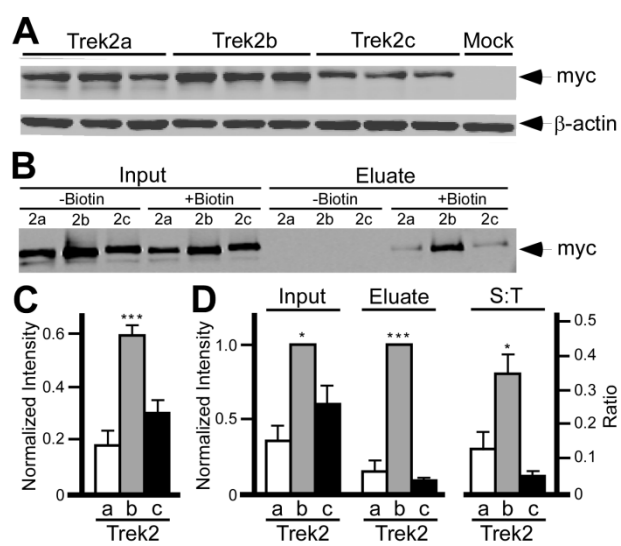


Figure 6

Discussion

Most previous studies involving rodent Trek2 expression patterns or function have not differentiated between the Trek2a and Trek2c variants, or have involved only a specific (often un-specified) Trek2 isoform [14, 16, 18, 20, 42, 45, 80, 138]. In addition, most effort to understand the structural influences on Trek channel function have centered on the intracellular C-terminus, which has been implicated in channel modulation by phosphorylation, temperature, arachidonic acid, and volatile anesthetics, and on protein-protein interactions involving the A kinase anchoring protein (AKAP-150) and microtubule associated protein-2 (Map2) [45, 47, 80, 81]. Accordingly, one goal of the present study was to evaluate possible distinctions in the expression patterns or function of the known N-terminal splice variants of Trek2, Trek2a and Trek2c. In addition, we describe two novel variants of the mouse *Trek2* gene, including a third N-terminal splice variant (Trek2b).

While tissue and CNS distributions of the three N-terminal splice variants were comparable, whole-cell currents seen in cells expressing Trek2b were significantly larger than those measured in cells expressing Trek2a or Trek2c. Previous work has ruled out a contribution of the extreme N-terminus to mean open time, single channel conductance, and ion selectivity, as a truncated mutant of rat Trek2c lacking the first 37 N-terminal amino acids behaved identically to the full length protein [43]. While the different current amplitudes observed in cells expressing Trek2a, Trek2b, and Trek2c could be explained by differences in the activation properties of these channels, the correlation

between current and surface protein levels suggests a simpler explanation. As Trek2b lacks the unique and short N-terminal domains found on Trek2a and Trek2c, we infer that the Trek2 N-terminus regulates channel trafficking and/or stability. Indeed, the ratio of surface-to-total Trek2b was greater than that determined for Trek2a or Trek2c, arguing that Trek2b is either more efficiently targeted to the plasma membrane, or is less efficiently internalized or degraded, or both. Interestingly, the N-terminus has been implicated in the regulation of surface trafficking for Trek1 through an interaction with β -COP [50].

N-terminal Trek2 splice variants in humans and rats corresponding to mouse Trek2a (human: NM_021161; rat: EDL81687) and Trek2c (human: NM_138317; rat: NM_023096) have been reported [41]. Interestingly, sequence homology is relatively low for the unique N-terminal domain in the Trek2a variant across the three species (not shown). As key functional domains are typically conserved across species, this could argue that the unique N-terminus of Trek2a serves no important role in channel function or regulation. Alternatively, given the relative hydrophobicity of this domain, it may serve as a signal or leader sequence that targets Trek2a to a particular cellular sub-domain. In contrast to Trek2a, the unique N-terminal domain in Trek2c is perfectly conserved across mice, rats, and humans, and it possesses some intriguing elements. For example, the lysine residue found at the N-terminus of Trek2c is predicted to be a destabilizing influence on protein stability, as per the N-end rule [139]. Moreover, the Trek2c N-terminal domain consists of a combination of hydrophobic and hydrophilic residues, a signature of proteins that undergo

Hsc70-mediated degradation [140]. The lack of specific targeting sequences and/or trafficking signals in Trek2b may explain the robust expression levels observed for this isoform in transfected cells.

There is currently no homolog of Trek2b reported in either human or rat. Alignment of mouse exon 1b with the human *TREK2* gene suggests a possible human homolog. In rat, however, we were unable to detect a possible Trek2b variant. As coding sequence in exon 1b is restricted to a single adenosine at the intron-exon boundary, the only sequence that can be used for alignment purposes is 5'UTR, which may be less conserved across species. Mouse Trek2b was so-named as its first exon is located between the exons that are utilized to generate Trek2a and Trek2c. While a human TREK2B variant has been reported (NP_612191; [41]) it is clearly distinct from the mouse Trek2b variant characterized herein. The human TREK2B variant exhibits a unique 18 amino-acid N-terminal domain and is expressed in pancreas and kidney, but not brain [25]. Moreover, the first exon of human TREK2B is located downstream of human exon 1c. Alignment of human exon 1b with the mouse *Trek2* gene yielded no obvious homology. Thus, species differences exist with respect to *Trek2* gene structure and alternative splicing, producing multiple distinct and species-specific Trek2 variants.

The Trek2-1p variant evaluated in this study, which utilizes exon 1c and exon 5, resembles an inwardly-rectifying K⁺ (K_{IR}) channel in terms of predicted membrane topology, and is expressed in multiple tissues and brain regions. We have also detected expression of Trek2-1p variants utilizing exons 1a and

1b in the mouse CNS (not shown). To date, we have been unable to detect novel currents resulting from heterologous over-expression of Trek2a/b/c-1p. While a C-terminal splice variant of Trek1 exhibiting only a single transmembrane segment was shown recently to act as a dominant negative modulator of Trek1 by limiting its surface delivery [39] (Veale et al., 2010), we observed no impact of Trek2-1p expression on current amplitudes in cells expressing Trek2b. It is possible that Trek2-1p variants require heteroassembly with another channel subunit, or a binding partner, to form functional channels. Alternatively, these might be regulated in a distinct manner, such that our recording conditions were not suitable to observe substantial channel activity. Finally, these variants may be subject to nonsense-mediated decay, where the splicing event serves to down regulate Trek2 activity.

In summary, we identified two novel alternative splice variants of the mouse *Trek2* gene that exhibit widespread distribution in the mouse CNS. Our findings demonstrate that N-terminal variation can influence current amplitude and surface level of Trek2 channels. Accordingly, differential and dynamic regulation of Trek2 isoform expression may mediate changes in the intrinsic excitability of neurons.

Chapter 3

A ROLE FOR TREK CHANNELS DURING CELL CYCLE PROGRESSION

Introduction

Dividing cells undergo cellular replication via a common cell cycle process termed mitosis, which is an important aspect in many physiological processes. For instance, wound healing involves the generation of new cells to repair damaged tissue [141]. During fetal development, pluripotent stem cells undergo mitosis in order to create new cells, which may then terminally differentiate into non-diving cells, such as neurons [142]; this process is also very important during adult neurogenesis [143]. Disregulation of cell division may lead to uncontrolled growth, which is a critical feature of all cancers. Thus, understanding the mechanisms that contribute to the regulation of the cell cycle and processes surrounding cell division are critical to human health.

Terminally differentiated cells are maintained in the G0 phase, which is considered to be outside of the cell cycle. Many dividing cells may also spend time in this G0 or quiescent phase, where they may enter or exit the cell cycle in response to different signals. Upon entrance into the cell cycle, all cells will travel through a series of identical phases. The first phase, interphase, is comprised of G1, S-phase and G2. During G1, cells increase production of amino acids in preparation for DNA replication, which is rapidly completed during S-phase. This is followed by G2, where a cell begins to replicate organelles and other cellular components that will be divided between the two daughter cells. After the completion of interphase, cells enter the mitotic phase, also called mitosis. During this phase, chromosomes, cytoplasm and cellular

organelles are divided, and the process of active division results in the formation of two identical daughter cells.

Progression of the cell cycle is under strict regulation; this involves a number of oscillating cyclins that drive the cycle forward, and a series of checkpoints, which ensure proper cycle progression. In addition to these well documented cell cycle modulators, a number of other factors have been shown to have an influence on cell cycle progression, including membrane voltage [144], cytosolic pH [145], and cell volume [146].

Ion channels are found in all cell types and contribute to cell function in many ways including regulating and directing cell cycle entry and progression [147]. Included in this category are members of the K^+ channel family. Indeed, all K^+ channel subfamilies include members which have roles related to cell cycle regulation or progression [147].

Much of what is known about cell cycle regulation has been established through studies investigating the dysregulation of cell proliferation. Here, the presence of many K^+ channels has been documented. Many K^+ channels have been observed in many solid tumors including breast, colon, prostate, as well as in immortal cell lines [147, 148]. Furthermore, pharmacological or genetic blockers of many K^+ channels have been shown to alter cell proliferation [148].

The importance of K^+ channels has been further emphasized, as a clear correlation has been made between membrane potential and mitotic activity [149]. Actively dividing tumor cells have been shown to be very depolarized, in contrast to differentiated cells in G_0 , which are more hyperpolarized [149, 150].

This dependence on membrane potential highlights a potential role for two-pore domain K^+ channels, which have a well-documented role in maintaining the background leak current that contributes greatly to a cell's resting membrane potential [81].

Indeed Task3 (Kcnk9), another member of the two-pore domain K^+ channel family, has been shown to be highly expressed in many solid tumors, including breast, lung, colorectal, prostate, melanoma, and glioblastoma [80, 151-153]. Furthermore, the presence of Task3 promotes tumor progression and resistance to oxygen and serum deprivation [151, 153, 154]. In contrast to this proposed role as tumor promoting, upregulation of Task3 has also been shown to reduce tumor cell migration [155]. Additionally, Task3 has been shown to play a role in neuronal cell apoptosis [156]. These inconsistencies highlight the need for further studies aimed at understanding how such K^+ channels contribute to cell cycle regulation.

As membrane potential, intracellular pH, cell volume, and oxygen sensitivity all have well documented roles in cell cycle regulation [144-146, 149, 157], members of the Trek family are obvious candidates for cell cycle regulation as they have been shown to be involved in all of these processes [81]. All Trek family members have been identified in both adult neural progenitor cells [136] and neural stem cells [137], where pharmacological blockade of Trek1 resulted in a reduction in cell proliferation [137]. Furthermore, Trek1 and Trek2 display very high levels of mRNA expression during embryogenesis, where they are especially high in the ventricular and subventricular zones, consistent with a

role in cell division [120]. Trek1 has also been shown to be upregulated in prostate cancer and prostate cancer cell lines, where the expression of a dominant negative variant of Trek1 will slow cell proliferation [134]. Given the therapeutic potential for regulating cell division, understanding a potential role for Trek1 and Trek2 in cell cycle regulation is critical.

Experimental Procedures

Generation of stable cell lines. Epitope-tagged (myc) Trek1 (NM_010607) and Trek2 (DQ185134) constructs were generated as described [33]. Trek1 and Trek2 were transfected into HEK293 cells (ATCC; Manassas, VA) using the calcium phosphate method and cultured according to manufacturer recommendations. Transfected cells were selected for by incubation in the presence of 400ug/ml G418 (Sigma-Aldrich Corporation; St. Louis, MO) for 3-4 weeks. Individual clones were collected and amplified. The presence of Trek protein was validated by immunoblotting and immunocytochemistry (**Fig. 7**).

Cell-cycle synchronization. Cells were arrested in G0 by incubating cells in serum free media for 24-48h. Cells were arrested at G1/S by incubating cells with 2.5mM thymidine (Sigma-Aldrich Corporation; St. Louis, MO) for 16h, followed by 10h in standard media, followed by 16-24h with 2.5 mM thymidine. Cells were arrested in M phase through a 30 hour serum starvation followed by

16-24h incubation with 800 nM nocodazole (Sigma-Aldrich Corporation; St. Louis, MO)

Immunoblotting. Cells were collected in 1 mL cold PBS then centrifuged for 1 min at 10,000 rpm. The pellet was resuspended in 250 μ L 2X LDS loading buffer (Life Technologies; Grand Island, NY) and sonicated briefly. Samples were run on a 12% bis-tris gel and transferred onto a nitrocellulose membrane (Thermo Fisher Scientific Inc.; Rockford, IL). Membranes were incubated with mouse anti-c-myc (1:1000 dilution; Hoffman-La Roche Ltd; Basel, Switzerland), mouse anti- β -actin (1:10000 dilution, Abcam PLC ab6276; Cambridge, MA), mouse anti-cyclin B1 clone GNS3 (1:500 dilution, EMD Millipore; Billerica, MA), or mouse anti-cyclin E clone HE12 (1:500 dilution, EMD Millipore; Billerica, MA) antibodies. Membranes were incubated with donkey anti mouse IRDye 800CW (1:7000 dilution, LiCor Biosciences; Lincoln, NE), and visualized using the Odyssey Image System (LiCor Biosciences; Lincoln, NE). Intensities of Trek and cyclin bands were normalized to the corresponding β -actin band.

Immunocytochemistry. Cells were grown and/or drug treated after adherence on poly-l-lysine coated (Sigma-Aldrich Corporation; St. Louis, MO) glass coverslips (Warner Instruments LLC; Hamden, CT). Cells were rinsed with Tris-Buffered Saline solution (TBS: 3 mM KCL, 135 mM NaCl, 25 mM Tris-base, pH7.4) and fixed by a 5 min incubation in 50% Lana's Buffer (water, 8% paraformaldehyde, 14% picrate, 0.16M PO_4) followed by 5 min in full strength

Lana's buffer. Cells were washed 3x over 5 min with TBS, and permeabilized using TBS + 0.2% Triton-X100 + 0.2% Tween-20 for 10 minutes. Cells were then incubated for 1h with mouse anti-c-myc (1:500 dilution, Hoffman-La Roche Ltd; Basel, Switzerland), in blocking buffer (TBS + 0.2% Tween-20 + 0.2% casein). Cells were washed 3x over 5 min with TBS, and incubated for 30 min with and CY3- conjugated donkey anti-mouse IgG (Jackson ImmunoResearch Laboratories Inc; West Grove, PA) and Sybr Green II (1:30000 dilution, Life Technologies; Grand Island, NY) in blocking buffer. Coverslips were then rinsed 3x over 5 min with TBS, dehydrated in graded alcohols (50%-100%) and cleared in xylene. Coverslips were mounted on slides using DPX (Sigma-Aldrich Corporation; St. Louis, MO). Images were collected using a conventional fluorescence microscope (Olympus BH-50; Tokyo, Japan). Digital images were collected using a Scion 1396 digital camera (Scion Corp. Frederick, MD) and adjusted for publication with the public domain software ImageJ (Rasband, 1997-2006).

Electrophysiology. Cells were plated onto poly-L-lysine (Sigma-Aldrich Corporation; St. Louis, MO) coated coverslips (Warner Instruments LLC; Hamden, CT) at a density of 35,000 cells per coverslip and recorded from 24h later (stable cell line validation) or treated as specified. Recordings were done using the equipment and solutions described [33]. Upon achieving whole-cell access, cells were held at -80mV for 1 min before being subjected to a voltage

ramp (-100mV to +60mV in 1 s). Only experiments with low R_A (<15 m Ω) and stable baselines (>-100 pA) were included in the final dataset.

Flow Cytometry. 1.0×10^6 cells were collected and re-suspended in 200 μ l PBS + 0.05% FBS solution. Cells were fixed and permeabilized by the dropwise addition of 70% ice cold ethanol and incubated overnight at 4° C. Fixed cells were pelleted and resuspended in 1 ml of 40 μ g/ml propidium iodide (Sigma-Aldrich Corporation; St. Louis, MO) + 100 μ g/ml RNaseA (Invitrogen Life Sciences; Carlsbad, CA) and incubated for 1h at 37°C. Flow cytometry analysis was carried out with FACSCalibur (Becton, Dickinson, and Company; Franklin Lakes, NJ) data was captured with CellQuest Pro v. 5.2.1 (Becton, Dickinson, and Company; Franklin Lakes, NJ) and analyzed using Flo Jo 8.8.6 (Treestar inc; Ashland, OR). Each analysis was carried out with at least 10,000 events.

qRT-PCR. Cells were synchronized in 6-well plates and collected using 0.05% Trypsin/EDTA (Invitrogen Life Sciences; Carlsbad, CA). Poly(A) mRNA was isolated using the RNeasy Plus Micro Kit (Qiagen; Valencia, CA) following manufacturers recommendations. 5 μ l of isolated RNA was reverse transcribed using the iScript cDNA synthesis kit (Bio-Rad; Hercules, CA) following manufacturer's recommendations and diluted to a final volume of 100 μ l. Real-time PCR was performed using the LightCycler 480 DNA SYBR Green I Master kit according to manufacturer's recommendations (Roche Diagnostics

Corporation; Indianapolis, IN), and run using the LightCycler 480 real-time PCR system (Roche Diagnostics Corporation; Indianapolis, IN). The following LightCycler amplification program was used: a pre-incubation of 95 °C for 5 min, followed by 45 cycles of 95 °C for 10s, 60 °C for 30s and 72 °C for 10s. A final oligonucleotide concentration of 1 μM was used for Trek1 and Trek2 primer pairs, and 1.5 μM for β-actin. An amplicon of 102 bp was amplified targeting Trek1 (NM_010607) using the following primers Fw (position 969-990): 5' ttgccaagtgaagacacat 3' and Rv (position 1050-1071): 5' tgtttggctctctcctctttg 3'. An amplicon of 108 bp was amplified targeting Trek2 (DQ185134) using the following primers Fw (position 379-401): 5' ctgattcagcatgcactcgat 3' and Rv (position 466-487): 5' agtgccttcttctttgctggg 3'. β -Actin was used as a reference target using the following primers Fw 5' atcatgtttgagccttcaacac 3' and Rv 5' tctgcgcaagttaggtttgc 3''. A single product was amplified from each primer pair, as indicated by a single peak obtained during a melting curve (65 °C to 97 °C). Data was analyzed using the $2^{-\Delta\Delta Ct}$ method as described [158].

Data analysis. All data are expressed as mean ± SEM and were analyzed using Graph Pad Prism 5 (GraphPad Software; La Jolla, CA) by ANOVA, followed by Newman-Keuls (NK) *post hoc* test when a significant interaction was identified.

Results

Characterization of Trek1 and Trek2 expressing stable cell lines

While characterizing K⁺ currents from HEK293 cells transiently transfected with Trek2, we observed significant variability in whole-cell currents [33]. Some cells displayed current profiles and amplitudes which were only marginally over baseline, whereas others displayed very large whole cell currents (data not shown). We hypothesized this was the result of inconsistencies in the number of DNA copies transfected into each individual cell. In order to obtain more consistent levels of Trek protein, we generated HEK293 cells stably expressing epitope (myc) tagged versions of Trek1 and Trek2. We first verified the presence of Trek1 and Trek2 protein using immunocytochemistry (**Fig. 7A**). Trek1 and Trek2 protein was detected via fluorescence in all cells observed within the visualization field at fluorescent levels significantly over baseline. The presence of Trek1 and Trek2 protein was also verified via immunoblotting, where Trek1 and Trek2 protein was detected at their expected molecular weights (**Fig. 7B**).

The presence of functional Trek1 and Trek2 protein was evaluated using a voltage ramp (-100- +60mV, 1s) from cells patched in whole-cell configuration. Both Trek1 and Trek2 expressing cells displayed resting membrane potentials significantly more negative than mock transfected cells (**Fig. 8A**), consistent with the overexpression of a K⁺ channel. Furthermore, the reversal potentials obtained from the voltage ramp were significantly more negative than those

observed from mock transfected cells, (**Fig. 8B**), also consistent with the overexpression of a K^+ selective channel.

In contrast to our earlier hypothesis, whole cell currents measured at +60 mV displayed significant variability similar to that observed previously from transiently transfected cells [33]. Current densities at +60 mV are displayed in a scatterplot (**Fig. 8C**). Significant variability is observed in currents from cells expression either Trek1 or Trek2, which appear to cover a similar span although overall Trek1 currents are generally larger. Sample traces from low (**Fig. 8D**) and high (**Fig. 8E**) current densities displayed outwardly-rectifying currents from all cells expressing Trek1, consistent with that of a Trek1 channel [21]. This is in contrast to cells expressing Trek2, where a population of cells displays current densities which are similar or only slightly larger than mock transfected cells (**Fig. 8C**). In these cells, the rectification profile resembles that of mock transfected cells (**Fig. 8D**), where current rectifies outward but displays a plateau at higher voltages. In addition to this profile, a small subset of cells displayed a hybrid of these, which resembled that of a linear rectifying channel at higher voltages, likely the combination of endogenous K^+ channels and low levels of active Trek2 (data not shown). High current densities from Trek2 expressing cells displayed outward rectification consistent with that of a Trek2 channel (**Fig. 8E**) [14, 16].

Figure 7. Biochemical characterization of Trek1 and Trek2 stable cell lines.

A) Representative images of Trek1, Trek2, and mock transfected cell lines after immunocytochemical staining using an anti-myc antibody. SYBR green staining highlights cells in the visual field. **B)** Immunoblot from Trek1, Trek2, and mock transfected stable cell lines, indicating the presence of Trek1 (44 kDa) and Trek2 (60 kDa) in their corresponding cell lines.

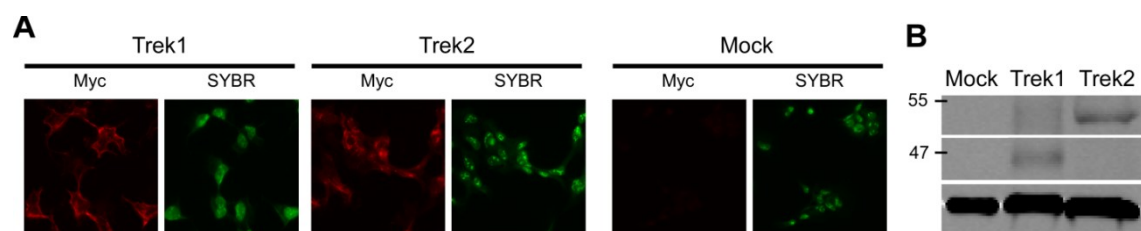


Figure 7

Figure 8. Electrophysiological characterization of Trek1 and Trek2 stable cell lines.

Whole-cell parameters were measured from Trek1, Trek2, and mock transfected cell lines (n=12-18). Current amplitudes were determined using a voltage ramp from -100 mV to +60 mV over 1s. **A)** A scatter plot displays current densities measured at +60 mV from Trek1, Trek2, and mock transfected cell lines. **B)** Reversal potentials measured from Trek1 and Trek2 stable cell lines are significantly more negative than those measured from mock transfected cell lines ($F_{(2,43)}=48.50$, $P<0.001$), indicative of a K^+ channel. **C)** Resting membrane potentials measured from Trek1 and Trek2 stable cell lines are significantly more negative than those measured from mock transfected cell lines ($F_{(2,43)}=21.35$, $P<0.001$), consistent with the expression of a K^+ channel. **D/E)** Representative traces from cells displaying “low” (**D**) or “high” (**E**) current densities from Trek1, Trek2 and mock-transfected cell lines. The corresponding current densities are represented by grey (Low) and white (High) dots in **C**. Symbols: *** $P<0.001$ vs. mock transfected

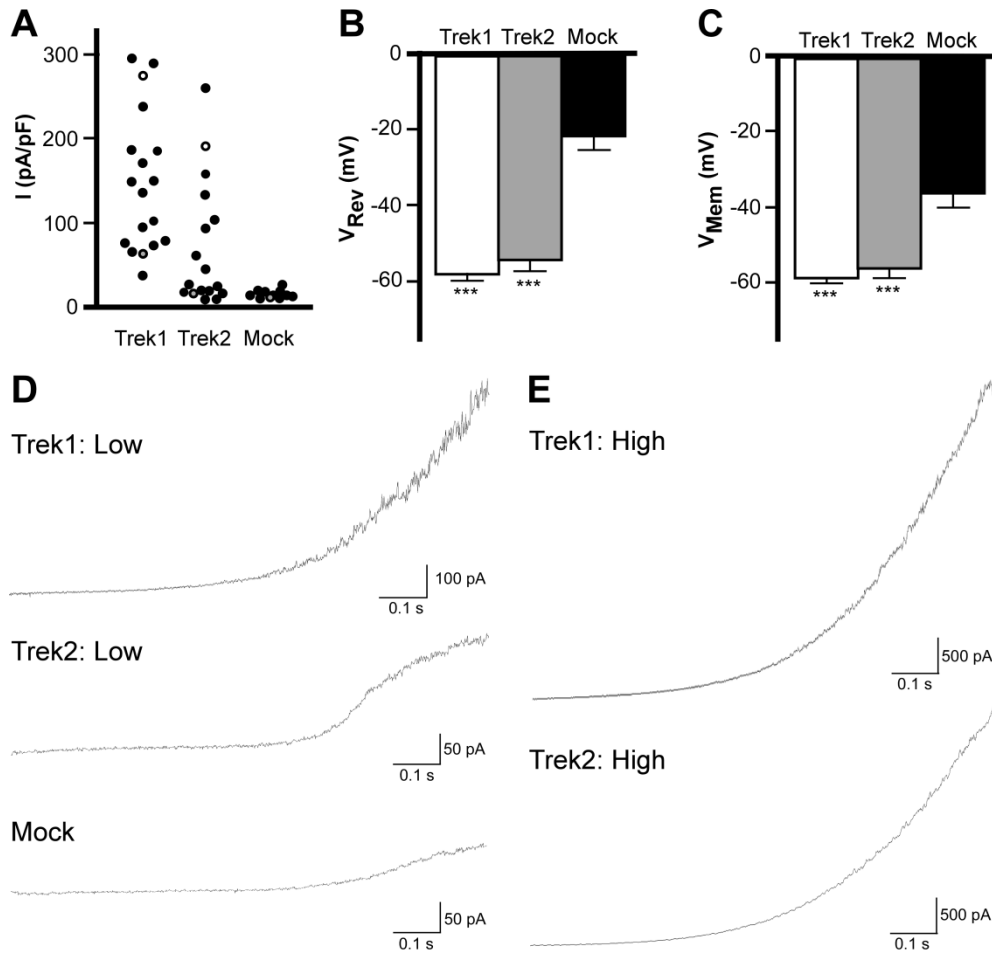


Figure 8

Validation of cell cycle arrest

As significant differences in whole-cell current amplitudes were still present in cells stably expressing Trek1 and Trek2, we hypothesized this variability correlated with differences in the cell cycle stage of a particular cell when electrophysiological recordings were conducted. In order to test this, we utilized previously documented pharmacological treatments to arrest cells in three stages of the cell cycle. Serum starvation was used to arrest cells in G0 [159], a double thymidine block was used to arrest cells at the G1/S boundary [160], and nocodazole treatment after 24h serum starvation was used to arrest cells in the early phases of mitosis [160]. To validate these treatment methods, we subjected Trek1, Trek2 and mock cells to each drug treatment and used flow cytometry to evaluate DNA content in treated cells (**Fig. 9A**). Serum starved cells (ss) displayed a sharp 1x peak, indicating that a vast majority of cells contained only a single set of DNA, consistent with a G0 arrest. A majority of thymidine treated cells also display 1x peak, with the broader base representing the start of S phase in many cells. This profile is consistent with a treatment that would arrest cells at the G1/S boundary. Nocodazole treated cells display high numbers in the 2x peak consistent with cells that contain two sets of DNA, and thus have completed S-phase, as expected after nocodazole treatment.

Fluctuations in cyclin levels are responsible for the progression of dividing cells through the cell cycle. In order to further validate our pharmacological treatments, we used quantitative immunoblotting to assess the levels of cyclin B and cyclin E in Trek1, Trek2 and mock transfected cell lines after cell cycle

arrest. A representative immunoblot from mock transfected cells is displayed in **Figure 9B**. The level of cyclin B increases as the cell cycle progresses through S- phase and G2, where they peak during mitosis. In all three cell lines, the levels of cyclin B levels were highest in nocodazole treated cells, consistent with cells arrested in M-phase (**Fig. 9B,C**). Cyclin E levels peak at the border of G1 and S- phase. In all three cell lines, the highest levels of cyclin E were observed in thymidine treated cells, consistent with cells arrested at the G1/S boundary (**Fig. 9B,D**). Taken together these results suggest our drug treatments are effective at enriching Trek1, Trek2 and mock transfected cells in the desired cell cycle stage.

Figure 9. Validation of cell-cycle synchronization.

Cells were arrested in G0 (serum starvation/ss), G1/S (thymidine/thy), and M phase (nocodazole/noc). **A)** Histogram of DNA vs cell number as obtained by flow cytometry. A peak at 400 represents a single copy of DNA (G0/G1 phase), whereas a peak at 800 represents two copies of DNA (G2/M). Cells between represent those obtained during DNA replication, in S phase. **B)**

Representative immunoblots displaying relative levels of cyclin B and cyclin E after cell synchronization of mock transfected cells. **C/D)** Relative levels of cyclin B (**C**) and cyclin E (**D**) in Trek1 (white), Trek2 (grey) and mock transfected (black) cell lines normalized to serum starved cells (n=6). As predicted, cyclin B is greatest in nocodazole treated cells and cyclin E is greatest in thymidine treated cells.

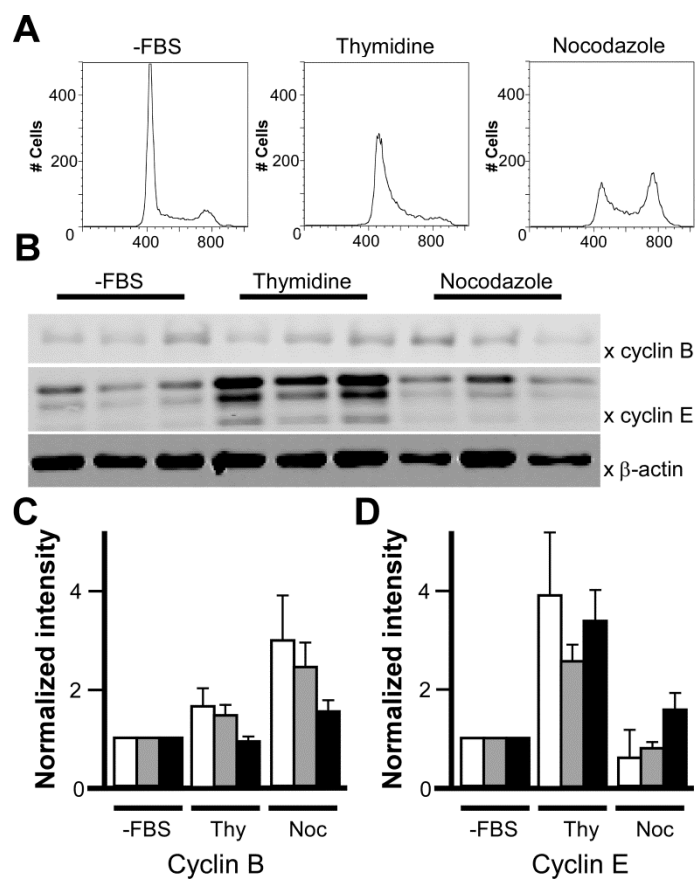


Figure 9

Trek channel currents through the cell cycle

To test the hypothesis that the variability in current amplitudes observed from Trek expressing cells corresponds with the position of a cell within the cell cycle, we arrested cells in either G₀, G₁/S, or M phase and conducted whole-cell electrophysiology on arrested cells. Trek1 expressing cells displayed outwardly-rectifying currents at all cell cycle stages (**Fig. 10A**). No difference in current amplitude at +60mV were observed between serum starved and thymidine treated cells, however nocodazole treated cells displayed a trend ($P=0.12$) toward increased current amplitudes (**Fig. 10D**). Trek2 expressing cells displayed significantly greater current amplitudes at +60 mV from cells arrested with nocodazole when compared to cells arrested through serum starvation or thymidine treatment (**Fig. 10E**). Interestingly, both serum starved and thymidine treated cells displayed rectification profiles similar to mock transfected cells (**Fig. 10B,C**) and likely make up the population of cells clustered at current densities similar to mock (**Fig. 8C**). Current densities at +60mV from Trek1 expressing cells were greater in all treatment groups compared with those from Trek2 expressing cells (**Fig. 10D,E**). Despite this difference, within group profiles were similar; relatively lower current densities were obtained from serum starved and thymidine treated cells compared with the relatively large currents obtained from nocodazole treated cells (**Fig. 10D,E**). Mock transfected cells displayed current profiles consistent throughout cell cycle (**Fig. 10C**). Interestingly, mock transfected cells displayed significantly greater current amplitudes at +60 mV after thymidine treatment

(Fig. 10F). Thus, HEK293 cells may endogenously express a K⁺ channel subject to cell cycle regulation. Together these data suggest an increase in current amplitudes from cells expressing Trek1 or Trek2 arrested in mitosis.

Figure 10. Effect of cell cycle synchronization on Trek whole-cell currents.

Whole-cell current amplitudes were measured from Trek1, Trek2, and mock transfected cell lines using a voltage ramp from -100 mV to +60 over 1s (n=10-20). **A-C)** Representative traces from Trek1 (**A**), Trek2 (**B**), and mock transfected (**C**) cell lines after arresting cells in G0 (ss), G1/S (thy), or M phase (noc). **D-F)** Current densities from Trek1 (**D**), Trek2 (**E**), and mock transfected (**F**) cell lines after cell cycle arrest. Nocodazole treated cells displayed higher current densities, albeit not-significant for Trek1 ($F_{(2,45)}=2.195$, $P=0.12$), and Trek2 (Trek2 ($F_{(2,50)}=9.97$, $P<0.001$). Interestingly, mock transfected cells treated with thymidine displayed significantly greater current densities compared with serum starved cells ($F_{(2,30)}=3.98$, $P<0.05$). Symbols: *, *** $P<0.05$ and 0.001, respectively, vs. serum starved. ###, $P<0.001$ vs. thymidine.

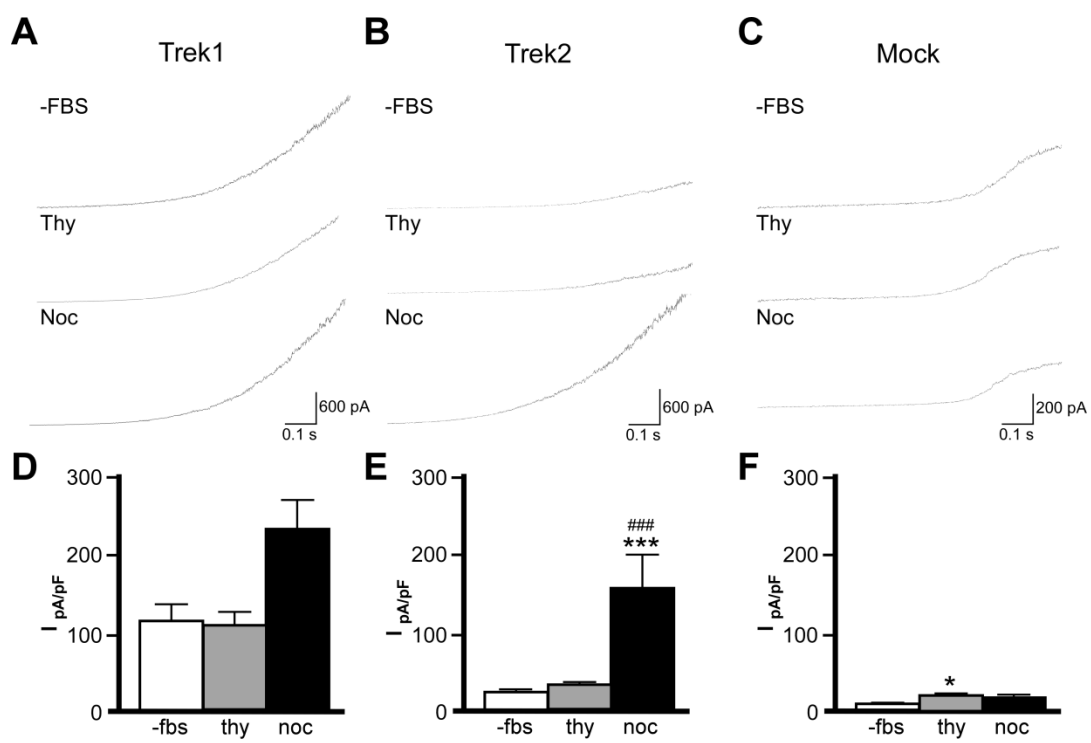


Figure 10

Trek channel protein and mRNA expression through the cell cycle

In order to identify the underlying cause of Trek1 and Trek2 current variability throughout the cell cycle, we arrested Trek1 and Trek2 stably expressing cell lines in G0, G1/S, and M phase and measured total whole cell protein. Trek1 and Trek2 band intensities were first normalized to β -actin, then to the serum starved cells as a standard of comparison. Representative immunoblots for Trek1 (**Fig. 11A**) and Trek2 (**Fig. 11B**) show increased Trek protein from nocodazole treated cells, quantified in **Figure 11C**. Comparatively low levels of Trek protein were present in serum starved and thymidine treated cells, whereas significantly more protein is measured from nocodazole treated cells. These data are consistent with the changes in current amplitude observed from nocodazole treated cells.

Changes in protein level are most easily explained as a downstream consequence of altered mRNA levels. To test this hypothesis, stably expressing Trek1 and Trek2 cell lines were arrested at various cell cycle stages and total mRNA was quantified. mRNA levels from thymidine and nocodazole treated cells were normalized to serum starved cells for relative comparisons. As observed for total whole cell protein, similar levels of mRNA were detected from serum starved and thymidine treated cells, whereas nocodazole treated cells displayed ~2-fold increase (**Fig. 11D**). This cell-cycle dependent variability in mRNA likely underlies the initial variability in current amplitudes from Trek1 and Trek2 expressing cells. As the CAG promoter was used to drive recombinant Trek expression, this is likely not a Trek dependent effect.

Figure 11. Effect of cell cycle synchronization on Trek protein and mRNA expression.

A/B) Representative immunoblots of Trek1 (**A**) and Trek2 (**B**) expression levels after arresting cells in G0 (serum starved/ss), G1/S (thymidine/thy), or M phase (nocodazole/noc). **C)** Quantification of Trek1 and Trek2 protein after cell cycle synchronization, normalized to serum starved levels (n=9). Nocodazole treated cells display significantly greater Trek1 ($F_{(2,24)}=9.39$, $P<0.001$) and Trek2 ($F_{(2,24)}=16.38$, $P<0.001$) protein levels than serum starved or thymidine treated cells. **D)** Fold increase in *Trek1* and *Trek2* mRNA after treatment with nocodazole (n=9). Both *Trek1* ($F_{(2,24)}=8.70$, $P<0.01$) and *Trek2* ($F_{(2,24)}=30.98$, $P<0.001$) display significantly greater mRNA levels after nocodazole treatment. Symbols: **, *** $P<0.01$ and 0.001 , respectively, vs. serum starved. ##, ###, $P<0.01$ and 0.001 , respectively, vs. thymidine.

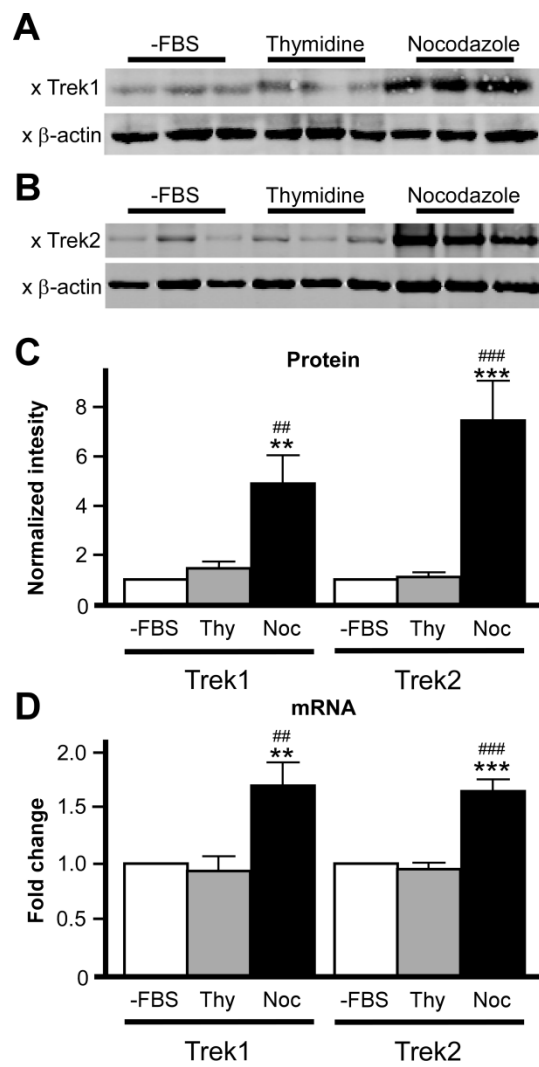


Figure 11

Discussion

The initial variability in whole cell current amplitudes from transfected HEK293 cells expressing either Trek1 or Trek2 lead us to hypothesize that channel activity may be a result of cell cycle dependent changes. Indeed, enrichment of cells undergoing mitosis displayed significantly greater current amplitudes when compared to cells arrested in G0 or G1. The functional difference was mimicked by whole cell protein levels, which displayed a similar increase during mitosis. This was ultimately determined to result from increased levels of Trek1 and Trek2 mRNA during mitosis, likely a Trek-independent consequence of cell cycle on the promoter used to drive recombinant expression.

The coding sequences of Trek1 and Trek2 were cloned into the commercially available mammalian expression vector pcDNA3.1 (Life Technologies; Grand Island, NY), where the cytomegalovirus immediate-early promoter (CMV) was replaced with the chicken β -Actin promoter coupled with the CMV early enhancer (CAG). Both the CMV and CAG promoters have been shown to drive high levels of recombinant protein expression in a variety of cell lines [161-163]. While CMV remains the most common promoter present in most commercially available plasmids, the CAG promoter has been shown to produce greater levels of recombinant expression in some cases [161, 162], which rationalized its use in this study. While some labs have observed greater recombinant protein expression using CAG, others report the opposite results

[164, 165]. Ultimately, it is difficult to draw overriding conclusions, as cell line, method of transfection, and encoded protein all likely affect expression levels.

The changes in mRNA levels during mitosis found in our study are in direct contradiction to other published data, which displays no change in protein levels of green fluorescent protein (EGFP) in a transgenic mouse expressing their protein of interest co-translated with EGFP under the control of the CAG promoter [166]. Their results suggest continued and unchanging expression of EGFP in cultured mouse embryonic fibroblast (MEF) cells throughout the cell cycle [166]. The methodological factors we utilized are very different from those used previously, and represent the most likely explanation for the differences in results. Indeed, each individual cell type will express an overlapping, but distinct set of endogenous proteins that may influence cellular behaviors including division.

While the rationale behind this study involved the observation that Trek currents display significant variability when expressed in HEK293 cells, which we can attribute to an interaction between the CAG promoter and cellular division, there is still the possibility that Trek channels exert an influence over the cell cycle. The presence of Trek channels have been detected in a number of immortal cell lines including the epithelial cell lines MLE-12 [131], Calu3 [167], and H441 [168], as well as the human adrenocortical cell line (H295R) [169], the human keratinocyte cell line (HaCaT) [170], and the mouse pancreatic b cell line (MIN6) [135]. Trek expression within such cell lines, would be driven by their endogenous promoters, and include potentially

important regulatory information encoded in the 3' or 5' untranslated regions. A more physiologically relevant study could also be conducted on neural stem cells or neural progenitor cells, as Trek channels have been found in both cell types [136, 137]. Of course the difficulty in obtaining these cells and the low numbers available for harvest may present additional complications.

While the conclusions to this study provide little insight into Trek channel regulation or activity, they do highlight many important considerations that must be remembered while conducting basic scientific research. The use of cell lines to study the effect of recombinant expressed proteins has been, and continues to be, an important method used to generate new and important discoveries. The ability to isolate particular components of a signaling pathway in a controlled environment is critical to enhancing our understanding of many physiological conditions. However, the use of endogenous systems, such as primary cultured cells, remains a superior method to study the physiological behaviors of cellular proteins.

Chapter 4

BEHAVIORAL CHARACTERIZATION OF MICE LACKING TREK CHANNELS

**Mirkovic, K., J. Palmersheim, F. Lesage, and K. Wickman,
Behavioral characterization of mice lacking Trek channels.
Front Behav Neurosci 2012; 6:1-9.**

Introduction

In situ hybridization revealed a broad distribution of *Trek1* in the rat CNS [30, 41], and genetic ablation of *Trek1* correlates with multiple neurophysiological and neurobehavioral phenotypes. *Trek1*^{-/-} mice are more sensitive to ischemia and epilepsy, show lower sensitivity to the effects of inhaled anesthetics, and display an increased sensitivity to thermal and mechanical pain [25-27]. *Trek1*^{-/-} mice also exhibit a depression-resistant phenotype, suggesting that *Trek1*-containing channels are a potential downstream target of selective serotonin reuptake inhibitors (SSRIs). Indeed, these drugs had no effect on *Trek1*^{-/-} mice [28]. Accordingly, *Trek1* represents a potential target for novel therapeutic strategies to combat depression [88-91, 171].

Compared with *Trek1*, relatively little is known about the neurobiological relevance of *Trek2*. An early study described a limited CNS distribution of *Trek2* [30]. Other evidence, however, including results from human tissue PCR, *in situ* hybridization from zebrafish, and rat *in situ* hybridization data suggest that *Trek2* is expressed broadly throughout the CNS [29, 41, 172]. Moreover, we reported recently using a cDNA panel that *Trek2* mRNA is expressed in most regions of the mouse brain [33]. These observations suggest that *Trek2* may make a broad and significant contribution to neurophysiology and behavior.

While RNAi-dependent knockdown of *Trek2* in the entorhinal cortex was shown to disrupt spatial memory [73], data concerning the neurobehavioral

relevance of *Trek2* are scant. The recent development of mice lacking *Trek2* (*Trek2*^{-/-}) and all three members of the *Trek* channel family (*Trek1/2/Traak*^{-/-}), however, permit rigorous testing of the role of *Trek* channels, and *Trek2*-containing channels in particular, in behavior [27, 82]. In this study, we probe the consequences of constitutive *Trek* gene ablation in mice, in paradigms that assess motor activity, coordination, anxiety-related behavior, learning and memory, and drug-induced reward-related behavior.

Experimental Procedures

Experimental subjects. All animal use was approved by the University of Minnesota Institutional Animal Care and Use Committee and carried out in accordance with National Institutes of Health guidelines. All mice used in this study were bred on-site, housed in same-sex groups of 2-5 after weaning, and provided with food and water *ad libitum*. Mice were kept on a 12 h light/dark cycle, with lights on between 0700 and 1900. All tests were performed between 0900 and 1600. Mice lacking *Trek2* (*Trek2*^{-/-}) and mice lacking *Trek1*, *Trek2*, and *Traak* (*Trek1/2/Traak*^{-/-}) were generated as described [27, 82]. Null mutations were backcrossed against the C57BL/6J inbred strain for 10+ generations prior to establishing the breeding cages used to generate subjects for this study. Both male and female mice (5-10 wks) were evaluated in all behavioral tests. No more than three distinct behavioral tests were performed on any single animal, and in no instance were animals evaluated in any test

after completing the morphine-induced motor activity, conditioned place preference studies, or the contextual fear conditioning test.

Locomotor activity. One day prior to locomotor activity assessments, mice were habituated to handling (5 min) and testing room (60 min). On the first day of testing, mice were placed in open-field activity chambers (ENV-515; Med Associates, Inc.; St. Albans, VT), housed within sound-attenuating cubicles for 60 min. The open-field was illuminated with 28 V DC/100 mA house lights (ENV-215M; Med Associates, Inc.) during testing. Total distance traveled, thigmotaxis, and time/entries into the central area of the open-field were recorded using Open Field Activity Software package v. 4.0 (Med Associates, Inc.). For the morphine-induced motor activity study, total distance traveled was measured for 60 min, beginning 10 min after an intraperitoneal (i.p.) injection of morphine (Sigma; St Louis, MO). Each mouse received all morphine doses, with 3 rest days between injections.

Rotarod. Motor coordination was assessed using an accelerating rotarod (IITC Life Sciences; Woodland Hills, CA), as described [173]. Briefly, mice were acclimated to the testing room 1 h prior to evaluation. Each subject was given two trials to acclimate to the task, followed by 6-test trial. Animals were allowed a minimum of 15 min to rest between trials, followed by a 2 h break after trial 4. After placement of the subject on the rod, the rod was accelerated from 4 to 27

rpm over a 5 min period. Latency to fall was recorded when a subject fell from the rod, or made 2 full revolutions while clinging to the drum.

Elevated plus maze. Anxiety-related behavior was measured using the elevated plus maze, as described [174]. In brief, mice were acclimated to the testing room 1 h prior to evaluation. The maze consisted of two open and two closed arms, as well as an exposed center panel, elevated 52 cm off the floor of the testing room (Columbus Instruments, Inc.; Columbus, OH). Testing was conducted under standard room lighting conditions. Each trial began with the placement of the mouse in the maze center, facing a closed arm; subsequent activity was recorded by video camera for 5 min. The time spent by each mouse in the open and closed arms was scored manually by two investigators blind to subject genotype. Time spent in the EPM center was not included as time in either open or closed arms.

Light/Dark box. The light/dark test was performed in a modified two-compartment mouse CPP chamber (Env-3013-2; Med Associates, Inc.) housed in a sound-attenuating cubicle. Flooring was normalized in both compartments using plexiglass inserts. The overhead light was turned off in the black chamber (dark), while the white (light) chamber was illuminated by a 28 V DC/100 mA light bulb (ENV-221M; Med Associates, Inc.) connected to a 3-channel light control unit (ENV-226B; Med Associates, Inc.) set at intensity level 10. Mice were acclimated to the testing room for 30 min before testing. The

mouse was placed in the center of the black chamber and allowed full access to both compartments after a 5 s delay. Time spent and distance traveled in both compartments was recorded during a 10 min trial using Med-PC software (Med Associates, Inc.).

Contextual fear conditioning. Contextual fear conditioning was conducted in 30.5 x 24.1 x 21.0 cm conditioning chambers (VFC_008; Med Associates, Inc.), housed in a sound-attenuating cubicle, utilizing steel bar flooring connected to a shock generator. The chamber was illuminated using a combination infrared and visual overhead light box (NIR-100; Med Associates, Inc.). Mice were allowed to acclimate to the testing room for 30 min prior to testing. Training consisted of 120 s baseline exposure followed by three conditioning trials. Each conditioning trial consisted of a 20 s light cue (ENV-229M; Med Associates, Inc.), a 20 s latency period, and a 2 s shock (0.7 mA), with an inter-trial interval of 60 s. A 5 min test session was conducted 24 h later, where time spent freezing and number of freezing episodes were recorded using “Video freeze” software (Med Associates, Inc.).

Novel object recognition. The novel object recognition study was performed using open-field environments (ENV-022MD; Med Associates, Inc.), housed within sound-attenuating cubicles, and illuminated with 28 V DC/100 mA house lights (ENV-215M; Med Associates, Inc.). On Day 1, mice were handled and habituated to the open field environment for 60 min. On Day 2, mice were

evaluated over 4 sessions, separated by 10 min breaks, during which subjects were returned to their home cages. In Session 1, animals were allowed to explore the open-field environment for 30 min. In Sessions 2 and 3, mice were re-introduced to the open-field environment for 10 min, and in both sessions the environments contained two identical objects (familiar). In Session 4, mice were re-introduced to the open-field environment for 5 min, now containing one familiar and one novel object. Session 4 was videotaped and the time subjects spent interacting with each object was recorded manually. A subject was considered to be interacting with an object if its nose was directed toward (and within 2 cm of) the object. Objects used in this study were a single red Duplo (The LEGO Group; Enfield, CT) and a blue cap from a 50 mL conical tube. Objects were counter-balanced to account for any object preference effects.

Conditioned place preference. Conditioned place preference was performed in two-compartment mouse conditioned place preference (CPP) chambers (Env-3013-2; Med Associates, Inc.), housed within sound-attenuating cubicles. One compartment contained white walls and a mesh floor, and the other contained black walls and a rod floor. The overhead light was identical in both chambers: a 28 V DC/100 mA light (ENV-221M; Med Associates, Inc.) connected to a 3-channel light control unit (ENV-226B; Med Associates, Inc.) set at intensity level 8. All subjects were acclimated to handling (5 min) and the testing room (1 h) for 2-3 d prior to beginning the 5-day test. On Day 1, mice were placed in the chamber for 15 min with the door separating compartments

open; time spent in each compartment was recorded. Subjects spending more than 65% of their time in either compartment on Day 1 were excluded from the study. On Days 2-4, mice were subjected to two 20-min conditioning sessions, one in the morning (0900-1100) and one in the afternoon (1400-1600). In the morning session, mice were given an subcutaneous (s.c.) saline injection and confined to the compartment that was preferred on Day 1. In the afternoon sessions, mice were given s.c. morphine and confined to the opposite compartment. On Day 5, mice were placed in the chamber for 15 min with the door separating the compartments open; time spent in each compartment was then recorded during a 15 min test session using Med-PC software. The change in time spent on the drug-paired side as measured on Day 1 and Day 5 (Day 5 - Day 1) was taken as the measure of morphine-induced conditioned place preference.

Data analysis. Data are expressed throughout as mean \pm SEM and were analyzed using Sigma Plot 11.0 (Systat Software Inc.; Chicago, IL) or Prism v. 11 (GraphPad Software Inc.; La Jolla, CA). The potential impact of gender on performance in each task was assessed with two-way ANOVA for all tasks except rotarod, morphine-induced locomotor activation, and conditioned place preference, where a 3-way ANOVA was used. If the results of statistical analysis revealed no significant impact of gender on task performance, data from male and female subjects were pooled to increase the power of the analysis. Open field activity, elevated plus maze, light/dark box, contextual fear

conditioning, and novel object recognition data were analyzed using one-way ANOVA; the Newman Keuls *post hoc* test was used when a significant interaction was found. For rotarod and morphine-induced motor activity data, a two-way ANOVA with repeated measures was used. Data from the morphine-induced conditioned place preference study was analyzed using a standard two-way ANOVA. Differences were considered significant if $P < 0.05$.

Results

The main goal of this study was to evaluate wild-type C57BL/6J and congenic *Trek2*^{-/-} mice in tests of motor activity, coordination, anxiety, learning and memory, and reward-related behavior. Congenic mice lacking all three members of the Trek subfamily (*Trek1/2/Traak*^{-/-} mice) were evaluated in parallel, as up-regulation of *Trek1* and/or *Traak* might compensate for the loss of *Trek2* and suppress neurobehavioral phenotypes. Prior to testing, we profiled *Trek2*^{-/-} and *Trek1/2/Traak*^{-/-} mice for gross deficiencies in sensory perception that might influence performance in the chosen behavioral tests. *Trek2*^{-/-} and *Trek1/2/Traak*^{-/-} mice were indistinguishable from wild-type counterparts by all visual criteria, and they responded normally, without excessive vocalization, to gentle prodding and handling. No genotype-dependent differences in body weight were observed (not shown). Following acclimation to a dark room, *Trek2*^{-/-} and *Trek1/2/Traak*^{-/-} mice exhibited a normal pupil response (constriction) to a bright light. *Trek2*^{-/-} and *Trek1/2/Traak*^{-/-} mice also exhibited normal forepaw extension upon lowering to

their home cage or benchtop, indicative of intact vision and normal depth perception. *Trek2^{-/-}* and *Trek1/2/Traak^{-/-}* mice exhibited normal responses to sudden sounds (clapping), arguing against gross deficits in hearing. Thus, no obvious developmental abnormalities, or deficits in touch, vision, or hearing, were evident in *Trek2^{-/-}* and *Trek1/2/Traak^{-/-}* mice.

Motor activity and coordination

Wild-type, *Trek2^{-/-}* and *Trek1/2/Traak^{-/-}* mice were monitored for 60 min in open-field activity chambers for distance traveled and position within the field. Because we observed an influence of gender on time spent in and entries into the center of the open-field, all open-field activity data for male and female subjects were analyzed separately. No genotype-dependent differences were observed in male or female mice with respect to total distance traveled (**Fig. 12A**) or velocity (**Fig. 12B**). In male mice, no genotype-dependent differences were detected with respect to thigmotaxis (calculated as the ratio of distance traveled in the field periphery to total distance traveled), time spent in the center of the open-field, or number of entries into the center of the open-field (**Fig. 12C,D,E**). In female mice, however, both *Trek2^{-/-}* and *Trek1/2/Traak^{-/-}* mice showed less thigmotaxis (**Fig. 12C**). Female *Trek2^{-/-}* and *Trek1/2/Traak^{-/-}* mice also spent more time than wild-type controls in the field center (**Fig. 12D**), and exhibited significantly more entries into the center as compared to wild-type female controls (**Fig. 12E**), behaviors consistent with lower anxiety-related behavior [175].

Motor coordination was evaluated in wild-type, *Trek2*^{-/-}, and *Trek1/2/Traak*^{-/-} mice using an accelerating rotarod test as described [173]. No effect of gender was observed in this task ($F_{(1,263)}=2.9$, $P=0.09$); as such male and female data were pooled. No genotype-dependent differences were observed with respect to ability of the mice to learn the task, learning rate, or peak performance (**Fig. 12F**).

Figure 12. Motor activity and coordination in mice lacking *Trek* channels.

Open-field activity was measured in wild-type (WT, white), *Trek2*^{-/-} (T2, gray), and *Trek1/2/Traak*^{-/-} (TTT, black) mice during a 60-min test session (n=8-12 per group). **A)** Total distance traveled during the 60-min session. No genotype-dependent differences were observed between male ($F_{(2,29)}=2.3$, $P=0.12$) or female ($F_{(2,30)}=1.9$, $P=0.17$) *Trek2*^{-/-}, *Trek1/2/Traak*^{-/-}, and wild-type mice. **B)** Velocity during open-field activity; no genotype-dependent differences were observed between male ($F_{(2,29)}=2.1$, $P=0.14$) or female ($F_{(2,30)}=0.3$, $P=0.78$) *Trek2*^{-/-}, *Trek1/2/Traak*^{-/-}, and wild-type mice. **C)** Thigmotaxis scores (distance traveled in periphery/total distance traveled); no genotype-dependent differences were observed in male animals ($F_{(2,29)}=2.2$, $P=0.13$), whereas both *Trek2*^{-/-} and *Trek1/2/Traak*^{-/-} females traveled less distance in the field periphery than wild-type controls ($F_{(2,30)}=11.0$, $P<0.001$). **D)** Time spent in the center of the open-field; a mild genotype-dependent difference was observed for male animals ($F_{(2,29)}=3.4$, $P<0.05$), though *post hoc* pairwise comparisons did not reveal a difference between *Trek2*^{-/-}, *Trek1/2/Traak*^{-/-}, and wild-type controls. *Trek2*^{-/-} and *Trek1/2/Traak*^{-/-} females spent significantly more time in the center than wild-type controls ($F_{(2,30)}=18.7$, $P<0.0001$). **E)** Number of entries into center of the open-field; no genotype-dependent differences were observed in male animals ($F_{(2,29)}=2.1$, $P=0.14$), whereas both *Trek2*^{-/-} and *Trek1/2/Traak*^{-/-} females made more entries into the center than wild-type controls ($F_{(2,30)}=7.7$, $P<0.01$). **F)** Rotarod performance of wild-type, *Trek2*^{-/-}, and *Trek1/2/Traak*^{-/-} mice, measured over 6 separate trials (n=11-18 per

group). A main effect of trial number was observed ($F_{(5,228)}=8.80$, $P<0.001$); within-genotype, pair-wise comparisons are not shown on the plot. A main effect of genotype was not detected ($F_{(2,228)}=3.0$, $P=0.06$), nor was there a significant interaction between trial and genotype ($F_{(10,228)}=0.8$, $P=0.62$).

Symbols: *, **, *** $P<0.05$, 0.01, and 0.001, respectively, vs. wild-type.

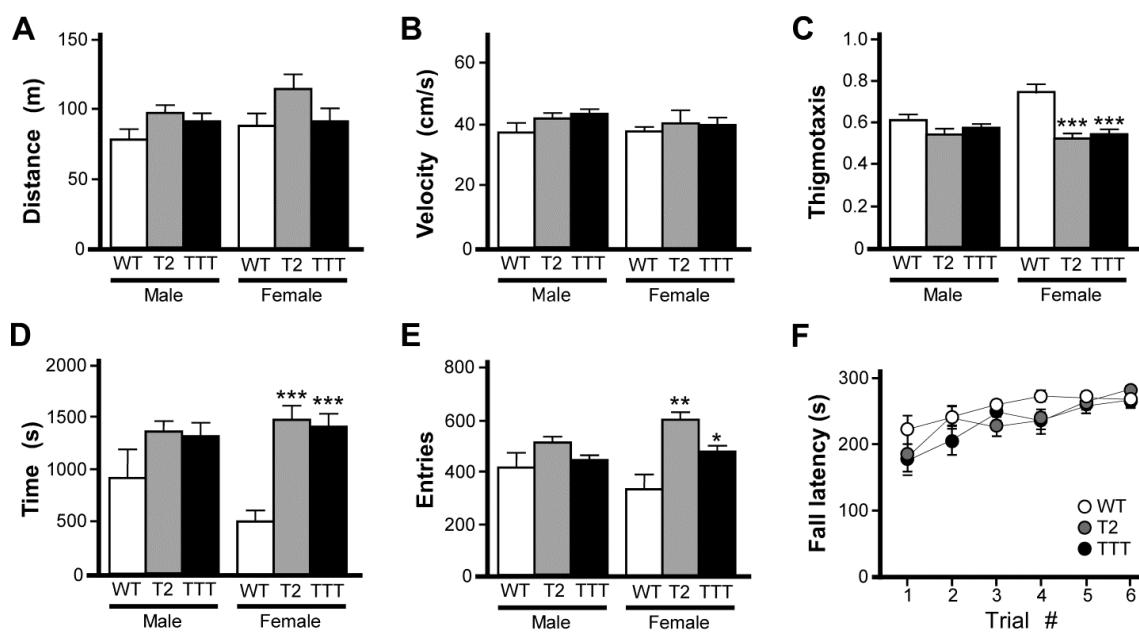


Figure 12

Anxiety-related behavior

While rotarod and open-field activity data indicated that *Trek2*^{-/-} and *Trek1/2/Traak*^{-/-} mice do not exhibit gross deficiencies in motor activity or coordination, the reduced thigmotaxis observed in female *Trek2*^{-/-} and *Trek1/2/Traak*^{-/-} mice argued that Trek channels may influence anxiety-related behavior. To gain additional insight into anxiety-related behavior in *Trek2*^{-/-} and *Trek1/2/Traak*^{-/-} mice, we next examined performance in an elevated plus maze, an established measure of anxiety-related behavior [176]. While *Trek2*^{-/-} and *Trek1/2/Traak*^{-/-} mice tended to spend more time in the open arms (**Fig. 13A**), and made more entries into the open arms of the maze (**Fig. 13B**), differences were not significant, for either gender. Similarly, no genotype-dependent differences were observed in either male or female mice in terms of the time spent in closed arms (**Fig. 13C**) or number of entries into the closed arms (**Fig. 13D**).

We also tested animals in the light/dark box, an alternative measure of anxiety-related behavior [177]. In this task, animals are placed in a two-compartment chamber, one dark and the other brightly illuminated. Increased time spent in the light chamber is consistent with reduced anxiety-related behavior [178]. As an influence of gender was previously observed in the open-field test, we again analyzed data from male and female subjects separately. Total time spent in the light compartment did not differ between genotypes in male or female mice (**Fig. 14A**). Moreover, no gender or genotype differences

were observed with respect to total distance traveled during the 10-min trial (not shown) or distance traveled in the light compartment (**Fig. 14B**).

Figure 13. Elevated plus maze performance in mice lacking *Trek* channels.

Wild-type (WT, white), *Trek2*^{-/-} (T2, gray), and *Trek1/2/Traak*^{-/-} (TTT, black) mice were evaluated in a 5 min (300 s) EPM test (n=8-19 per group). No genotype-dependent differences were observed with respect to male or female mice in time spent in (**A**; male: $F_{(2,40)}=0.8$, $P=0.46$; female: $F_{(2,49)}=1.4$, $P=0.25$) or number of entries into (**B**; male: $F_{(2,40)}=1.9$, $P=0.16$; female: $F_{(2,49)}=0.9$, $P=0.41$) the open arms. Likewise, no significant differences were observed with respect to genotype in time spent in (**C**; male: $F_{(2,40)}=0.5$, $P=0.59$; female: $F_{(2,49)}=0.1$, $P=0.93$) or number of entries into (**D**; male: $F_{(2,40)}=0.03$, $P=0.97$; female: $F_{(2,48)}=0.3$, $P=0.77$) the closed arms.

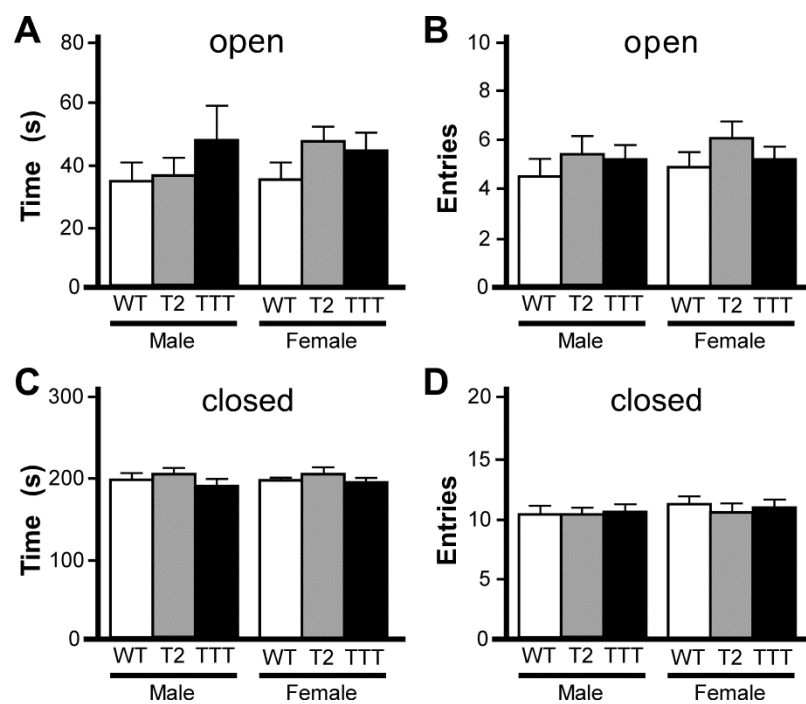


Figure 13

Figure 14. Light/dark box behavior in mice lacking Trek channels.

Wild-type (WT, white), *Trek2*^{-/-} (T2, gray), and *Trek1/2/Traak*^{-/-} (TTT, black) mice were evaluated in a 10 min (600 s) light/dark box test (n=5-12 per group).

A) Time spent in the light compartment; no genotype-dependent differences were observed for male ($F_{(2,22)}=2.7$, $P=0.09$) or female ($F_{(2,25)}=1.0$, $P=0.38$) mice. **B)** Distance traveled in the light compartment; no genotype-dependent differences were observed in male ($F_{(2,22)}=1.7$, $P=0.21$) or female ($F_{(2,25)}=0.2$, $P=0.82$) mice.

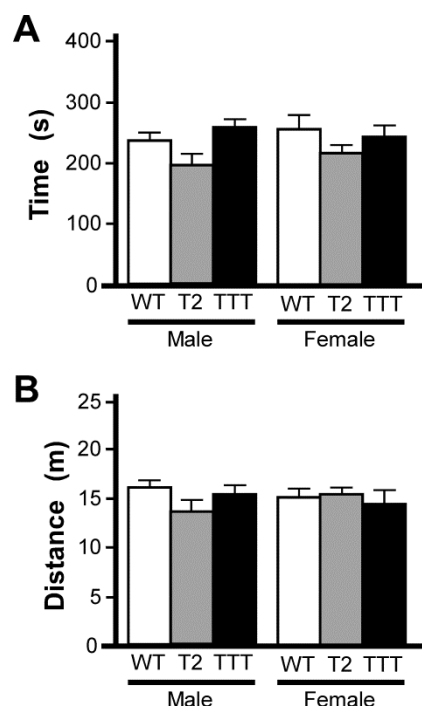


Figure 14

Learning and memory

To assess the learning and memory ability of *Trek2^{-/-}* and *Trek1/2/Traak^{-/-}* mice, we first tested animals in a contextual fear conditioning task. This 2 d test of Pavlovian learning involves the association of a painful stimulus (foot shock) with an environment [179]. The first session included three conditioning trials separate by 60 s, each consisting of a 2 s (0.7 mA) shock delivered after presentation of a 20 s light cue. The test day consisted of a 5 min re-exposure to the training environment and evaluation of freezing behavior. No effect of gender was observed in total time spent freezing ($F_{(1,29)}=2.8$, $P=0.11$) or in the number of freezing episodes ($F_{(1,29)}=0.1$, $P=0.72$); as such, data from male and female subjects were pooled. No genotype-dependent differences were observed in total time spent freezing (**Fig. 15A**) or in the number of freezing episodes (**Fig. 15B**).

We next tested the effect of *Trek* ablation in the novel object recognition task, which has been used to assess working memory, anxiety, and preference for novelty in rodents [180]. The task requires an animal to recognize and recall prior experience with a familiar object, and discriminate that object from a novel object. In our paradigm, mice were exposed to the open-field chamber for 60 min on the day prior to testing. On test day, mice were re-introduced to the open-field chamber for 30 min, then again in two consecutive 10 min sessions incorporating an object (familiar), and finally in a 5-min test session where both the familiar object and a novel object were present in the field. The time spent exploring both objects was recorded during the test session. No effect of

gender was observed for any parameter analyzed (time exploring novel object, $F_{(1,19)}=0.4$, $P=0.55$; time exploring familiar object, $F_{(1,19)}=0.8$, $P=0.39$; total time exploring objects, $F_{(1,19)}=0.1$, $P=0.78$; discrimination ratio, $F_{(1,19)}=2.3$, $P=0.14$), and as such, data from male and female subjects were pooled. The total time spent exploring both the familiar (**Fig. 16A**) and novel (**Fig. 16B**) objects during the test session were not different across genotypes, nor was the total time spent exploring both objects (**Fig. 16C**). And, while all genotypes showed a preference for the novel object over the familiar, no differences were observed with respect to genotype in this regard (**Fig. 16D**).

Figure 15. Contextual fear conditioning in mice lacking Trek channels.

Wild-type (WT, white), *Trek2*^{-/-} (T2, gray), and *Trek1/2/Traak*^{-/-} (TTT, black) mice were evaluated in 5 min (300 s) contextual fear conditioning test (n=9-14 per group). **A)** Time spent freezing; no genotype-dependent differences were observed with respect to time spent freezing ($F_{(2,34)}=2.4$, $P=0.11$). **B)** Freezing episodes; no genotype-dependent differences were observed with respect to number of freezing episodes ($F_{(2,34)}=1.4$, $P=0.25$).

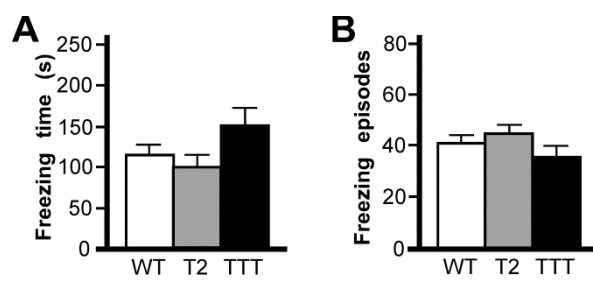


Figure 15

Figure 16. Novel object recognition in mice lacking Trek channels.

Wild-type (WT, white), *Trek2*^{-/-} (T2, gray), and *Trek1/2/Traak*^{-/-} (TTT, black) mice were evaluated in a novel object recognition task (n=7-9 per group). No genotype-dependent differences were observed in terms of the amount of time spent during a 5 min (300 s) test session interacting with the familiar object (**A**; $F_{(2,22)}=1.7$, $P=0.21$), time spent interacting with the novel object (**B**; $F_{(2,22)}=1.0$, $P=0.39$), total time interacting with the familiar and novel object (**C**; $F_{(2,22)}=1.2$, $P=0.31$), or in object discrimination ratio (**D**; $F_{(2,22)}=0.1$, $P=0.87$), defined as the ratio of time spent exploring the novel object to the total time spent exploring both objects [$\text{time}_{\text{novel}}/(\text{time}_{\text{familiar}}+\text{time}_{\text{novel}})$].

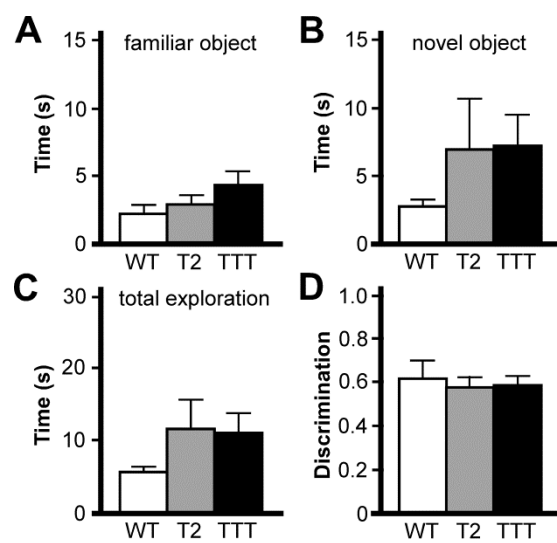


Figure 16

Reward-related behavior

Normal opioid-induced motor stimulation and conditioned place preference require activation of mu opioid receptors in midbrain structures, including ventral tegmental area [181-184]. Mu opioid receptors are metabotropic (G protein-coupled) receptors linked to the $G_{i/o}$ subclass of G proteins. Previous studies have indicated that both *Trek1* and *Trek2* can be activated by GPCRs linked to $G_{i/o}$ G proteins [14, 15, 21, 24, 73, 74], and both channels are expressed in the mouse midbrain [185]. Accordingly, we evaluated the impact of *Trek* ablation on the motor-stimulatory and rewarding effect of morphine, the prototypical mu opioid receptor agonist. Morphine doses higher than 30 mg/kg yielded elevated stereotypic movements and reduced overall activity levels in wild-type mice (not shown), and thus, 30 mg/kg morphine was selected as the maximal dose in this study. No effect of gender was observed in this task ($F_{(1,114)} < 0.001$, $P = 0.98$); as such, data from male and female subjects were pooled. Systemic morphine administration stimulated motor activity in a dose-dependent manner in all genotypes (**Fig. 17A**). While no difference between genotypes was observed at the lowest morphine doses evaluated (3 and 10 mg/kg), *Trek1/2/Traak*^{-/-} mice exhibited less morphine-induced motor activity at the 30 mg/kg dose.

Morphine-induced conditioned place preference was analyzed in wild-type, *Trek2*^{-/-} and *Trek1/2/Traak*^{-/-} mice using a two-compartment chamber. On Day 1, mice were allowed to explore both sides of the chamber during a 15 min session, and time spent on each side of the chamber was recorded. Over the

next 3 days, animals were subjected to conditioning sessions where saline (AM session) or morphine (1, 3, or 10 mg/kg; PM session) was administered systemically prior to confinement in a defined (counterbalanced) side of the chamber. In a pilot study involving wild-type mice, no difference in the magnitude of the morphine-induced conditioned place preference was observed for 10 and 30 mg/kg morphine doses ($t_{22}=0.2$, $P=0.9$). Accordingly, wild-type and *Trek*^{-/-} mice were challenged with 10 mg/kg morphine as the highest dose in this test. No effect of gender was observed ($F_{(1,64)}=0.1$, $P=0.81$); as such, male and female data was pooled. A dose-dependent increase in time spent in the drug-paired side was observed for all genotypes, and the magnitude of the morphine-induced CPP measured in *Trek2*^{-/-} and *Trek1/2/Traak*^{-/-} mice was no different from wild-type controls at any dose tested (**Fig. 17B**).

Figure 17. Opioid-induced motor activity and reward in mice lacking *Trek* channels.

A) Morphine-induced locomotor activity was measured during a 60 min session in wild-type (WT, white), *Trek2*^{-/-} (T2, gray), and *Trek1/2/Traak*^{-/-} (TTT, black) mice (n=12-16 per group). Significant main effects of morphine dose ($F_{(3,144)}=250.6$, $P<0.0001$) and genotype ($F_{(2,144)}=4.6$, $P<0.05$) were observed, as well as a dose x genotype interaction ($F_{(6,114)}=2.5$, $P<0.05$). While no significant differences were observed between genotypes at either the 3 mg/kg or 10 mg/kg doses, *Trek1/2/Traak*^{-/-} showed a slightly blunted response to 30 mg/kg morphine as compared to wild-type controls. **B)** Morphine-induced CPP was measured in wild-type (n=10-15/dose), *Trek2*^{-/-} (n=7-9/dose), and *Trek1/2/Traak*^{-/-} (n=6-7/dose) mice using a standard CPP test. While a significant main effect of morphine dose was observed ($F_{(2,73)}=9.0$, $P<0.001$), there was no main effect of genotype ($F_{(2,73)}=0.5$, $P=0.59$) or dose x genotype interaction ($F_{(4,73)}=0.32$, $P=0.86$). No genotype-dependent differences were observed in morphine-induced CPP, as measured by calculating the change in time spent (Δ time spent) in the drug-paired side from Day 1 to Day 5. In panels **A** and **B**, only within-dose pair-wise comparisons are highlighted. Symbols: *** $P<0.01$, vs. wild-type.

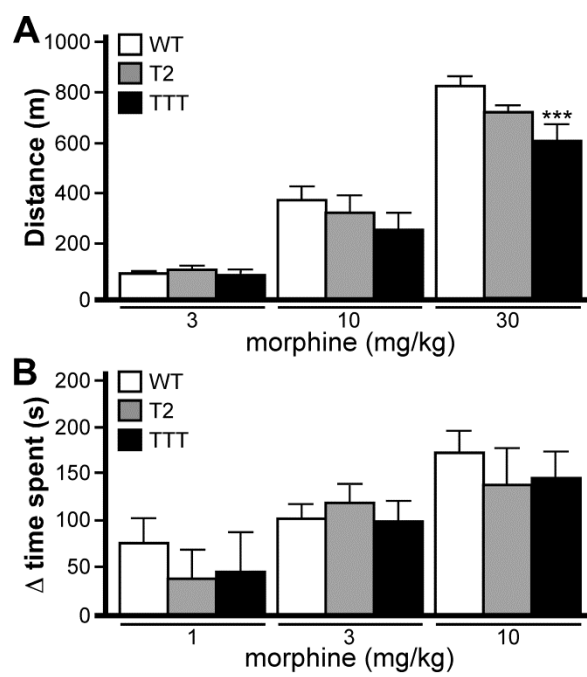


Figure 17

Discussion

Recent work by our laboratory, as well as *in situ* hybridization data collected by the Allen Institute for Brain Research [185], suggests a widespread distribution of *Trek2* mRNA in the mouse CNS. Accordingly, and given the well-documented and broad expression of *Trek1* and *Traak* in the rodent CNS [29, 30, 41], one might predict that Trek channel activity influences neurophysiology and behavior in a broad manner. The primary goal of this study was to begin assessing the impact of *Trek* ablation on mouse behavior, using a representative battery of behavioral paradigms.

Trek gene ablation exerted little influence on motor activity or coordination. A significant difference, and clear interaction between genotype and gender, was observed in anxiety-related behavior in the open-field. Female *Trek2*^{-/-} and *Trek1/2/Traak*^{-/-} mice exhibited significantly reduced thigmotaxis and increased time spent in the center of the open-field. While many brain regions have been linked to anxiety, the hippocampus and amygdala are key anatomic loci for anxiety-related behavior [186, 187]. In this regard, the relatively high level of *Trek2* mRNA observed in both structures in the mouse and human may be relevant [29, 33, 185]. However, *Trek2*^{-/-} and *Trek1/2/Traak*^{-/-} mice performed similar to wild-type controls in the elevated plus maze and light/dark box tests, other established tests of anxiety-related behavior. Such discrepancies within anxiety-related behavioral paradigms have been reported for other mutant mouse strains [188-190], and argue that any influence of Trek channels on anxiety-related behavior is modest and/or not uniform.

Recent work has shown that *Trek* channels mediate, in part, the inhibitory effect of GABA_B receptor stimulation on neurons in the hippocampus and entorhinal cortex [73, 76], and have suggested a role for *Trek* channels in learning and memory [73]. We, however, observed no influence of *Trek* ablation on learning and memory, as assessed using novel object recognition and contextual fear conditioning tasks. One concern in studies involving these and other standard paradigms is whether underlying abnormalities in sensory perception influence behavioral outcomes. And while our experience did not reveal gross deficiencies in vision, hearing, or touch in *Trek*^{-/-} mice, we cannot exclude the possibility that subtle differences exist that impacted their performance in some of the chosen tasks. For example, previous studies have revealed decreased pain thresholds with *Trek1*^{-/-} and *Traak*^{-/-} mice [25, 26]. As such, the behavior of *Trek*^{-/-} mice in paradigms that involve an aversive stimulus, such as a foot shock (e.g., contextual fear conditioning), could reflect altered sensitivity to the aversive stimulus, altered associative learning processes and/or memory recall, or a mixture of influences. Nevertheless, the simplest interpretation of our fear conditioning and novel object recognition data is that *Trek* channels exert little if any significant influence over associative learning processes.

Trek channels are activated by receptors linked to G_{i/o} G proteins in a process thought to involve inhibition of cAMP production and a decrease in PKA-dependent phosphorylation [14, 15, 24, 73, 74]. Opioids such as morphine bind to G_{i/o} coupled receptors expressed in the midbrain, leading to

increased motor activity and conditioned place preference [181-184]. As Trek channels are expressed in the mouse midbrain [185], we probed for a contribution of Trek channels to opioid-induced reward-related behavior. Interestingly, *Trek1/2/Traak*^{-/-} mice did display a blunted motor-stimulatory response to the highest dose of morphine tested. As *Trek2*^{-/-} mice behaved normally in this task, the phenotype is most likely attributable to the loss of Trek1, since Traak channels are not modulated by G protein signaling [20, 22, 44]. In contrast, we found no impact of Trek channel ablation on morphine-induced conditioned place preference. Thus, consistent with our assessment of anxiety-related behavior in *Trek*^{-/-} mice, any contribution of Trek channels to opioid-induced reward-related behavior appear to be modest and paradigm-dependent.

While the broad CNS distribution of Trek channels suggests that this channel family makes significant contributions to many behaviors, we found few robust neurobehavioral phenotypes in *Trek*^{-/-} mice in this study. This may be due to compensation by a non-Trek K_{2P} channel and/or the selection of behaviors and paradigms where Trek channel influence is not striking. Alternatively, Trek channel activity may be low under normal conditions, becoming evident and impactful only under certain circumstances, such as ischemia [27, 112, 119, 191]. Indeed, Trek channels are activated by polyunsaturated fatty acids [14, 15, 22], intracellular acidification [14, 19, 20], and membrane stretch [14-16], and all three of these influences are triggered by cerebral ischemia. Moreover, *Trek1*^{-/-} mice show enhanced sensitivity to

ischemia [27], and *Trek1* is up-regulated after focal ischemia [112]. Recently, *Trek2* expression was shown to increase after exposure to ischemic conditions [113]. Thus, future studies exploring the neurophysiological relevance of *Trek2*-containing channels under ischemic conditions will be important.

Chapter 5

DISCUSSION

Challenges in studying Trek channels

Pharmacological and regulatory modulation of Trek channels

Despite the fact that Trek1 and Trek2 were identified only a few years apart, significantly more research has focused on Trek1. Trek1/*Kcnk2* was the second member of the K_{2P} family to be identified [21], thus the gene name *Kcnk2*. In contrast Trek2/*Kcnk10* was the 9th member identified [14, 16]. The abundance of Trek1-related research was furthered by the generation of the *Trek1*^{-/-} mouse in 2004 [27], which displayed very clinically relevant phenotypes, and led to more focused research on this Trek family member when compared to the others.

The indication that Trek channels, specifically Trek1, may be involved in neuroprotection inspired a number of groups to conduct research related to Trek1 in neuroprotection after ischemia. This, followed by work which identified an anti-depressant phenotype in the *Trek1*^{-/-} mouse [28], opened up another major field of study into potential pharmaceuticals that target Trek1 for the treatment of depression, and into human polymorphisms in the *KCNK2* gene that may predict patients responses to current therapeutics.

One reason knockout mice have been such a valuable tool to study Trek family members, is that there are no selective pharmacological blockers for any of the three family members. There are a vast number of pharmacological agents that can affect (either activate or inhibit) Trek channels (**Table 1,2**). However, these agents generally activate/inhibit many channels, making results obtained from their use difficult to interpret. For example, if one were to use a

pharmacological agent to verify the contribution of a Trek channel to a given current, but that pharmacological agent also blocked a different channel which was also involved in the production of that current, it would not be possible to identify which drug target (the Trek channel or other channel) was responsible if a reduction in current were seen. The use of a *Trek^{-/-}* mouse would be critical to validate possible Trek involvement. To do so, one would look for changes from the specified current; if a difference was observed from the *Trek^{-/-}* mouse it would almost certainly be the result of *Trek* channel ablation. This is likely one reason why more research has been focused on Trek1 compared with Trek2. The recent generation of the *Trek2^{-/-}* mouse [82] should ignite more research into this important Trek family member as well.

Trek1 and Trek2 display similar, if not identical, modulation, which makes identifying which Trek family member may be responsible for a specific Trek-related observation difficult. To date, only a single difference has been identified with respect to modulation of Trek1 and Trek2. This work suggested that, while intracellular acidification activates both Trek1 and Trek2, extracellular acidification results in the inhibition of Trek1 and activation of Trek2 [71]. However, another group reports no effect of extracellular acidification on Trek2 [14], thus additional work is needed to validate this single observed difference. Another potential difference in channel modulation may involve the activation by PKG. While both channels display identical responses to kinase modulation by PKA, PKC and AMPK [14, 15, 21, 24, 35, 41, 70, 73-75, 78, 80], only Trek1 has been shown to be activated by PKG phosphorylation

[35]. Interestingly, the serine identified as the target of PKG in the c-terminus of Trek1 is not conserved in Trek2; however no studies have investigated a role for PKG in regulation of Trek2.

Few differences have been identified with respect to pharmacological manipulations of Trek1 and Trek2 as well. While more pharmacological studies have been conducted with Trek1 as the target, all pharmacological agents that have also been applied to Trek2 have displayed the identical response as that seen for Trek1. A single difference in pharmacological modulation has been documented. The pharmacological agent, 2-nitrobenzoic acid, has been shown to directly inhibit Trek2, whereas Trek1 displays no sensitivity to this agent [192]. Thus, this blocker may be one way to isolate endogenous Trek2 currents from other Trek family members in future experiments.

GPCR activation of Trek channels

Our initial interests in the Trek channel family, specifically in Trek1 and Trek2, stemmed from the observations that channel activity was modulated by G protein-dependent signaling [14, 15, 21, 24]. Our lab has had a long-standing interest in how G proteins modulate K⁺ channels, specifically K⁺ channels which are activated downstream of G_{i/o} GPCRs. The G-protein gated inwardly rectifying K⁺ channels (Girks) have been well documented in contributing to the K⁺ current after activation of G_{i/o} GPCRs. While Girk channels are important contributors to G_{i/o} GPCR-activated K⁺ currents, many groups have observed residual K⁺ current after pharmacological blockade or

genetic ablation of Girk channels [193, 194]. We hypothesized that Trek channels may also contribute to the K^+ current generated after $G_{i/o}$ GPCR activation.

Despite a well-established role for Trek channel modulation by PKA using pharmacological manipulations of the PKA signaling pathway [14, 15, 24, 35, 41, 73, 74], and a number of studies which utilized a more physiologically-relevant model through co-expression of Trek channels with G_s or $G_{i/o}$ GPCRs, we encountered numerous challenges when re-constituting these signaling pathways in HEK293 cells [14, 24, 73-75].

Trek channels display a “run-up” phenomenon when over-expressed in mammalian cells and recorded in whole-cell configuration. Indeed we observed current amplitudes at +60 (voltage-ramp -100 to +60 mV, 1s) increase 20-30 fold over the course of 5 minutes (data not shown). We are not the only lab to report this “run-up” phenomenon; one other group reported difficulty with this issue in their studies [24]. Through a series of point mutations to the consensus PKA and PKC phosphorylation sites on the C-terminus of Trek1, this group determined that at rest, there is a basal level of PKA and PKC phosphorylation of Trek channels, which render a portion of the channels inactive. Indeed, mutation to the PKA and PKC phosphorylation sites eliminated the run-up observed [24]. This group concluded that after obtaining whole-cell access, an unknown member of the phosphatase family, dephosphorylates the PKA and PKC phosphorylation sites on Trek1 rendering the channel active [24]. As more PKA and PKC phosphorylation sites are de-phosphorylated, more Trek

channels become active, resulting in a progressive increase in Trek currents, which we observe as “run-up”. This group showed that inclusion of okadaic acid, to block intracellular phosphatases, in the pipette solution significantly reduced the run-up observed [24].

We were most interested in studying the potential $G_{i/o}$ GPCR activation of Trek channels, where the proposed mechanism involved a basal level of active PKA, thus Trek channel phosphorylation (i.e channels in the closed state). Upon activation of a $G_{i/o}$ GPCR, one would predict a reduction in cAMP, a reduction in active PKA, and presumably a de-phosphorylation event, which would then activate the Trek channel. This is the model that has been proposed for Trek2 activation by α_2 adrenergic receptor and the $GABA_B$ receptor in the entorhinal cortex [73, 74].

A major challenge we faced in our experiments was determining when to apply the GPCR agonist, such that receptor-induced activation could be measured. The increase in current amplitudes, or “run-up”, occurred over a prolonged period of time, and made it difficult to determine when “a new baseline” was achieved. The currents would appear to normalize, only to begin increasing again. There always remained the concern, that any increase in Trek current observed was not the result of receptor induced activation, but a result of “run-up” that would have also occurred in the absence of receptor activation. Another concern was that “run-up” would result in the opening of all Trek channels present at the surface, such that no further activation could be

accomplished after receptor activation. These two concerns made data interpretation difficult.

One way to validate that an increase in channel activity is the result of receptor-induced activation, is to remove the receptor agonist (or apply an antagonist) at the end of the experiment, where one would expect to observe a reversal in channel activation (i.e channel inhibition). In the literature, the inhibition of Trek channels after activation of G_s and G_q GPCRs co-expressed with Trek channels has been repeatedly demonstrated to be reversible [14, 24, 70, 78]. In contrast, Trek channel activation by $G_{i/o}$ GPCRs has always been reported as irreversible [14, 73, 74]. The irreversibility of an activated Trek channel would be consistent with “run-up” that was mistaken for channel activation, as current that results from channel “run-up” generally remains elevated. More work is needed to validate that Trek channels can be activated downstream of $G_{i/o}$ GPCR activation, and the mechanism involved.

Summary of major findings

Trek2 channel diversity

Our study, identifying and characterizing the splice variants of Trek2 in the mouse, stemmed from the observation that multiple murine Trek2 isoforms existed and were being published under the same name “Trek2”. These include the isoforms we now call Trek2a and Trek2c. We identified three different exons, which could be alternatively utilized as the first exon, to generate three N-terminal splice variants. Two had been previously

documented and utilized for *in vitro* studies. The start codon for the third splice variant is generated from the 'AU' present in what we termed exon 1b, and the 'G' encoded in the exon 2, that is shared by all isoforms. This generates an N-terminal truncated variant that contains no unique sequence from that of the other splice variants.

We also identified a previously unreported exon (exon 8), which when utilized, results in C-terminal truncated variants. The C-terminal truncated variants each contain two transmembrane domains, as well as a single pore-domain, resembling those of the inwardly rectifying K⁺ channel family. While these are structurally very different from K_{2P} family members, they could presumably generate functional channels through a tetrameric multimerization of subunits. In our hands, we did not observe functional currents from these variants when heterologously expressed, nor did they appear to alter the function of full-length Trek2, whether they may function endogenously remains unknown.

All three full-length Trek2 isoforms are highly expressed in the CNS, where they exhibit broad expression profiles. When heterologously expressed, the novel Trek2b isoform displayed significantly greater whole-cell current amplitudes than either Trek2a or Trek2c, a phenomenon that correlated with an increase in cell surface expression.

How the three Trek2 isoforms contribute to cell excitability remains unknown. The overlapping and broad expression of *Trek2* mRNA suggests little specificity in terms of isoform localization. Furthermore, single channel

properties do not differ between isoforms [43], thus the physiological rationale for the redundancy remains unknown. A complete Trek channel is formed through the dimerization of two individual subunits. As Trek2b displays greater surface levels, heteromeric channels containing Trek2b may serve to increase Trek channel levels at the surface, and thus serve as a means of titrating neuronal excitability. This scenario could also explain the significant overlap in distribution.

Another possible explanation for multiple Trek2 isoforms may involve unique protein-protein interactions that involve one Trek2 isoform and not the others. It is unlikely that AKAP150 or Map2 displays differential binding specificity among isoforms, as the C-terminal region responsible for these interactions is conserved among isoforms [45, 47], however unknown interactions may exist for this channel. The potential for heteromultimerization of two Trek2 isoforms, differences in binding partners, and alterations in surface expression may represent a way to fine-tune Trek2 channel activity through the alternative splicing of *Trek2*.

Trek channel activity during cell cycle progression

Whether Trek channel activity may influence, or be influenced by, progression of the cell cycle remains unknown. While our study sought to address this, we ultimately concluded that the CAG promoter is influenced by cell cycle progression; however no conclusions could be made about whether Trek channels influence cell cycle progression.

While we were unable to validate an influence of Trek channel expression on cell cycle progression, nor an influence of cell cycle progression on Trek channel expression/function, there is a body of evidence that connect Trek channels with the cell cycle. To begin, Trek channels are present in neuronal stem cells [137] and neuronal progenitor cells [136], and the expression levels and localization patterns of *Trek1* and *Trek2* mRNA change during embryonic development. Most notably, *Trek2* mRNA levels have been shown to reduce during the early post-natal period [120].

Furthermore, *Trek1* has been implicated in prostate cancer, as *Trek1* expression is present in the prostate only when cancerous cells have also been detected [134]. Interestingly, the level of *Trek1* expression also correlates with the grade and staging of the disease [134]. Furthermore, the heterologous expression of *Trek1* in cell lines increases the proliferation rate, and pharmacological blockade in cells endogenously expressing *Trek1* slows the proliferation rate [134]. Thus *Trek1* may represent a novel target for the treatment of prostate cancer. Trek channels are also present in a number of other immortal cell lines where their role in cell proliferation has not been established. The presence of Trek channels have not yet been documented in any other tumors. However, as solid tumors often experience conditions of ischemia, the presence of channels shown to provide protective effects during ischemia, such as Trek channels, may provide benefits to tumor cells.

Trek channel contributions to behavior

We were the first lab to behaviorally characterize the *Trek2*^{-/-} mouse, and despite the broad localization of *Trek2* in the CNS, we observed very little difference between *Trek2*^{-/-} and wild-type mice in the behavioral tasks employed. Furthermore, ablation of the entire family (*Trek1/2/Traak*^{-/-} mouse) also produced little in terms of phenotype. One interpretation of these results is that under normal conditions, Trek channels contribute little to neurophysiology and, only under specific conditions, such as during ischemia, may Trek channels exert a biophysical contribution.

There is a substantial amount of research that supports a role for Trek channels in neuroprotection after ischemia. First of all, Trek channels are activated by intracellular acidification [14, 19, 20], membrane stretch [14-16], and PUFAs [14, 15, 19], all present during ischemia [93]. Trek channels are also activated by a number of neuroprotective drugs (**Table 1**), including riluzole [14, 102-104], which is clinically used in the treatment of amyotrophic lateral sclerosis (ALS). Furthermore, the *Trek1*^{-/-} mouse is more susceptible to kainic acid- and pentylenetetrazole-induced seizures, where greater mortality rates are observed [27]. Greater damage has also been documented from *Trek1*^{-/-} knockout mice after being subjected to a number of ischemia producing models, including global ischemia, focal ischemia, spinal cord ischemia, and decompression sickness [27, 114], which was discussed in greater detail in the introduction. As PUFAs display neuroprotective effects that are lost in *Trek1*^{-/-} mice, it is likely at least one mechanism through which protection is provided in through these channels [27].

Future directions

Trek2 in neuroprotection after ischemia

The lack of any major behavioral phenotype in *Trek2*^{-/-} mice argues, that despite widespread distribution, Trek2 channels provide little in terms of neurophysiology and behavior. One possible explanation is that Trek2 contributes little under basal conditions, but becomes impactful under certain conditions, such as during ischemia. A neuroprotective role for Trek1 has been shown by subjecting *Trek1*^{-/-} mice to number of *in vivo* models of ischemia. Intracellular acidification, membrane stretch, and PUFA's are all present during ischemia [93], and display no differences with respect to their ability to activate both Trek1 and Trek2. Furthermore, the neuroprotective agent, riluzole, and the neuroprotective flavonoids baicalein and wogonin also activate Trek2 channels [14, 104]. Thus, Trek2 may also play a role in neuroprotection during ischemia.

Other studies have also been conducted which support a role for Trek2 in neuroprotection. Indeed, Trek2 protein levels have been shown to increase in cultured astrocytes after subjecting cells to glutamate excitotoxicity, an *in vitro* model used to mimic cellular excitability [113]. Moreover, *Trek2* mRNA and protein levels have been shown to increase in the hippocampus and cortex after inducing cerebral ischemia in the rat [110].

The recent generation of the *Trek2*^{-/-} mouse will be invaluable to test a role for Trek2 in neuroprotection after ischemia [82]. Subjecting *Trek2*^{-/-} mice to an *in vivo* model of global ischemia should be conducted. One way to accomplish

this is to induce a transient bilateral occlusion of the common carotid arteries during systemic hypotension for 30 min. After reversal, recovery would be monitored for seizures and/or death. If Trek2 provided a neuroprotective effect after ischemia, *Trek2*^{-/-} mice would be expected to display increased seizure activity and death compared to wild-type controls.

Another *in vivo* model of ischemia commonly applied to rodents, which mimics human stroke, is the middle cerebral artery occlusion. In this model, a monofilament is inserted into the common carotid artery to occlude the middle cerebral artery. The monofilament is left in place for 1 hour after which reperfusion is allowed. Mice are then monitored for neurological deficits and tissue can be examined post mortem for infarct size. In this model, *Trek2*^{-/-} mice would be expected to display more severe neurological deficits and show greater infarct size than wild-type controls, if Trek2 provided a neuroprotective effect.

Additional experiments could be conducted to determine whether neuroprotective drugs, such as riluzole, provide their beneficial effect through activation of Trek channels. To answer this question, riluzole would be given to wild-type and *Trek*^{-/-} mice before the induction of global or focal ischemia. If riluzole was acting, in part, through its actions on Trek channels, *Trek*^{-/-} mice would display less protective effects after treatment with riluzole. The same experimental model could be used to test other neuroprotective agents such as baicalein, wogonin, linolenic acid, and/or lysophosphatidylcholine.

G_{i/o} GPCR-dependent activation of Trek channels

Relatively little is known with respect to the contribution of Trek1 and/or Trek2 channels to G_{i/o} GPCR-dependent K⁺ currents in native cells. Resolving this issue has been difficult as no selective pharmacological inhibitors exist for either of these two channels. Two studies propose Trek2 is a downstream effect of α 2 adrenergic receptors and GABA_B receptors in the entorhinal cortex, however this observation was based upon characterizations of the K⁺ current resembling those of the Trek family (insensitive to 4-AP, TEA, etc.) [73, 74]. The major piece of evidence supporting the role for Trek2 came from the inclusion of function blocking Trek2 antibodies in the recording pipette, which reduced the GPCR-induced K⁺ current [73, 74].

A recent paper described the use of a photoswitchable conditional subunit, to show that Trek1 channels contribute to the native GABA_B receptor-induced K⁺ current observed in hippocampal neurons [76]. This group capitalizes on a technology that incorporates a photoswitchable pore blocker into the Trek1 channel. In the presence of a 380 nm light wave, the channel will be tethered in a conformation that permits the blocking of the pore by a quaternary ammonium pore blocker, rendering the channel inactive. In the dark, the channel is unblocked and can function normally.

Girk channels are known to contribute to a majority of the GABA_B receptor induced K⁺ current in hippocampal neurons, however ~30% of the K⁺ current remains after pharmacological blockade of Girk channels [195]. To test whether Trek1 contributed to the remainder of the GABA_B receptor-induced K⁺

current, the mutant channel was transfected into hippocampal neurons. The GABA_B receptor was activated in the presence of Girk channel blockers in the dark (native conformation) and under illumination with 380 nm light (blocked conformation). The residual GABA_B receptor-induced current present in the dark was abolished under illumination conditions indicating that Trek1 did contribute to the GABA_B receptor-induced K⁺ current.

The photoswitchable conditional subunit strategy could be used to test the contribution of Trek1 and/or Trek2 to other GABA_B receptor-induced K⁺ currents in other native cell types, such as stellate neurons in the entorhinal cortex or GABA neurons in the ventral tegmental area. Moreover, the photoswitchable conditional subunit strategy could also be used to test the contribution of Trek1 and/or Trek2 to other G_{i/o} GPCR-induced currents, such as those produced by activation of the mu opioid receptor or members of groups II or III metabotropic glutamate receptors. Identifying how Trek channels contribute endogenously is important to further our understanding of this channel family.

Conclusion

Despite their identification over one decade ago, there is still much to be learned in terms of Trek channel contributions at the both the cellular level and whole animal level. The use of *Trek*^{-/-} mice and new technology that may serve in lieu of selective pharmacological blockers are only two way to aid in the advancement of the field. Future studies will be able to provide new insights into the neurobehavioral and physiological relevance of Trek channels.

Chapter 6

BIBLIOGRAPHY

1. Hille, B., *Ion Channels of Excitable Membranes*. Third ed 2001, Sunderland: Sinauer Associates, Inc.
2. Bear, M.F., B.W. Connors, and M.A. Paradiso, *Neuroscience Exploring the Brain*. Third ed 2007, Baltimore: Lippincott, Williams, and Wilkins.
3. Katzung, B.G., S.B. Masters, and A.J. Trevor, *Basic and Clinical Pharmacology*. Eleventh ed 2009: The McGraw-Hill Companies, Inc.
4. Kurachi, Y., L.Y. Jan, and M. Lazdunski, eds. *Potassium Ion Channels*. Current Topics in Membranes. Vol. 46. 1999, Academic Press: San Diego
5. Shieh, C.C., M. Coghlan, J.P. Sullivan, and M. Gopalakrishnan, Potassium channels: molecular defects, diseases, and therapeutic opportunities. *Pharmacol Rev* 2000; 52:557-94.
6. Molnar, P. and J.J. Hickman, eds. *Patch-Clamp Methods and Protocols*. 2007, Humana Press.
7. Hodgkin, A.L. and A.F. Huxley, A quantitative description of membrane current and its application to conduction and excitation in nerve. *J Physiol* 1952; 117:500-44.
8. Lesage, F., E. Guillemare, M. Fink, F. Duprat, M. Lazdunski, G. Romey, and J. Barhanin, TWIK-1, a ubiquitous human weakly inward rectifying K⁺ channel with a novel structure. *EMBO J* 1996; 15:1004-11.
9. Goldstein, S.A., L.A. Price, D.N. Rosenthal, and M.H. Pausch, ORK1, a potassium-selective leak channel with two pore domains cloned from *Drosophila melanogaster* by expression in *Saccharomyces cerevisiae*. *Proc Natl Acad Sci U S A* 1996; 93:13256-61.
10. Czempinski, K., S. Zimmermann, T. Ehrhardt, and B. Muller-Rober, New structure and function in plant K⁺ channels: KCO1, an outward rectifier with a steep Ca²⁺ dependency. *EMBO J* 1997; 16:2565-75.
11. Moshelion, M., D. Becker, K. Czempinski, B. Mueller-Roeber, B. Attali, R. Hedrich, and N. Moran, Diurnal and circadian regulation of putative potassium channels in a leaf moving organ. *Plant Physiol* 2002; 128:634-42.

12. Kunkel, M.T., D.B. Johnstone, J.H. Thomas, and L. Salkoff, Mutants of a temperature-sensitive two-P domain potassium channel. *J Neurosci* 2000; 20:7517-24.
13. de la Cruz, I.P., J.Z. Levin, C. Cummins, P. Anderson, and H.R. Horvitz, sup-9, sup-10, and unc-93 may encode components of a two-pore K⁺ channel that coordinates muscle contraction in *Caenorhabditis elegans*. *J Neurosci* 2003; 23:9133-45.
14. Lesage, F., C. Terrenoire, G. Romey, and M. Lazdunski, Human TREK2, a 2P domain mechano-sensitive K⁺ channel with multiple regulations by polyunsaturated fatty acids, lysophospholipids, and G_s, G_i, and G_q protein-coupled receptors. *J Biol Chem* 2000; 275:28398-405.
15. Patel, A.J., E. Honore, F. Maingret, F. Lesage, M. Fink, F. Duprat, and M. Lazdunski, A mammalian two pore domain mechano-gated S-like K⁺ channel. *EMBO J* 1998; 17:4283-90.
16. Bang, H., Y. Kim, and D. Kim, TREK-2, a new member of the mechanosensitive tandem-pore K⁺ channel family. *J Biol Chem* 2000; 275:17412-9.
17. Maingret, F., I. Lauritzen, A.J. Patel, C. Heurteaux, R. Reyes, F. Lesage, M. Lazdunski, and E. Honore, TREK-1 is a heat-activated background K⁺ channel. *EMBO J* 2000; 19:2483-91.
18. Kang, D., C. Choe, and D. Kim, Thermosensitivity of the two-pore domain K⁺ channels TREK-2 and TRAAK. *J Physiol* 2005; 564:103-16.
19. Maingret, F., A.J. Patel, F. Lesage, M. Lazdunski, and E. Honore, Mechano- or acid stimulation, two interactive modes of activation of the TREK-1 potassium channel. *J Biol Chem* 1999; 274:26691-6.
20. Kim, Y., C. Gnatenco, H. Bang, and D. Kim, Localization of TREK-2 K⁺ channel domains that regulate channel kinetics and sensitivity to pressure, fatty acids and pHi. *Pflugers Arch* 2001; 442:952-60.
21. Fink, M., F. Duprat, F. Lesage, R. Reyes, G. Romey, C. Heurteaux, and M. Lazdunski, Cloning, functional expression and brain localization of a novel unconventional outward rectifier K⁺ channel. *EMBO J* 1996; 15:6854-62.
22. Maingret, F., A.J. Patel, F. Lesage, M. Lazdunski, and E. Honore, Lysophospholipids open the two-pore domain mechano-gated K⁺ channels TREK-1 and TRAAK. *J Biol Chem* 2000; 275:10128-33.

23. Bockenhauer, D., N. Zilberberg, and S.A. Goldstein, KCNK2: reversible conversion of a hippocampal potassium leak into a voltage-dependent channel. *Nat Neurosci* 2001; 4:486-91.
24. Murbartian, J., Q. Lei, J.J. Sando, and D.A. Bayliss, Sequential phosphorylation mediates receptor- and kinase-induced inhibition of TREK-1 background potassium channels. *J Biol Chem* 2005; 280:30175-84.
25. Alloui, A., K. Zimmermann, J. Mamet, F. Duprat, J. Noel, J. Chemin, N. Guy, N. Blondeau, N. Voilley, C. Rubat-Coudert, M. Borsotto, G. Romey, C. Heurteaux, P. Reeh, A. Eschalier, and M. Lazdunski, TREK-1, a K⁺ channel involved in polymodal pain perception. *EMBO J* 2006; 25:2368-76.
26. Noel, J., K. Zimmermann, J. Busserolles, E. Deval, A. Alloui, S. Diochot, N. Guy, M. Borsotto, P. Reeh, A. Eschalier, and M. Lazdunski, The mechano-activated K⁺ channels TRAAK and TREK-1 control both warm and cold perception. *EMBO J* 2009; 28:1308-18.
27. Heurteaux, C., N. Guy, C. Laigle, N. Blondeau, F. Duprat, M. Mazzuca, L. Lang-Lazdunski, C. Widmann, M. Zanzouri, G. Romey, and M. Lazdunski, TREK-1, a K⁺ channel involved in neuroprotection and general anesthesia. *EMBO J* 2004; 23:2684-95.
28. Heurteaux, C., G. Lucas, N. Guy, M. El Yacoubi, S. Thummler, X.D. Peng, F. Noble, N. Blondeau, C. Widmann, M. Borsotto, G. Gobbi, J.M. Vaugeois, G. Debonnel, and M. Lazdunski, Deletion of the background potassium channel TREK-1 results in a depression-resistant phenotype. *Nat Neurosci* 2006; 9:1134-41.
29. Medhurst, A.D., G. Rennie, C.G. Chapman, H. Meadows, M.D. Duckworth, R.E. Kelsell, Gloger, II, and M.N. Pangalos, Distribution analysis of human two pore domain potassium channels in tissues of the central nervous system and periphery. *Brain Res Mol Brain Res* 2001; 86:101-14.
30. Talley, E.M., G. Solorzano, Q. Lei, D. Kim, and D.A. Bayliss, Cns distribution of members of the two-pore-domain (KCNK) potassium channel family. *J Neurosci* 2001; 21:7491-505.
31. Hervieu, G.J., J.E. Cluderay, C.W. Gray, P.J. Green, J.L. Ranson, A.D. Randall, and H.J. Meadows, Distribution and expression of TREK-1, a

- two-pore-domain potassium channel, in the adult rat CNS. *Neuroscience* 2001; 103:899-919.
32. Meadows, H.J., C.D. Benham, W. Cairns, I. Gloger, C. Jennings, A.D. Medhurst, P. Murdock, and C.G. Chapman, Cloning, localisation and functional expression of the human orthologue of the TREK-1 potassium channel. *Pflugers Arch* 2000; 439:714-22.
 33. Mirkovic, K. and K. Wickman, Identification and characterization of alternative splice variants of the mouse *Trek2/Kcnk10* gene. *Neuroscience* 2011; 194:11-8.
 34. Xian Tao, L., V. Dyachenko, M. Zuzarte, C. Putzke, R. Preisig-Muller, G. Isenberg, and J. Daut, The stretch-activated potassium channel TREK-1 in rat cardiac ventricular muscle. *Cardiovasc Res* 2006; 69:86-97.
 35. Koh, S.D., K. Monaghan, G.P. Sergeant, S. Ro, R.L. Walker, K.M. Sanders, and B. Horowitz, TREK-1 regulation by nitric oxide and cGMP-dependent protein kinase. An essential role in smooth muscle inhibitory neurotransmission. *J Biol Chem* 2001; 276:44338-46.
 36. Honore, E., F. Maingret, M. Lazdunski, and A.J. Patel, An intracellular proton sensor commands lipid- and mechano-gating of the K⁺ channel TREK-1. *EMBO J* 2002; 21:2968-76.
 37. Kim, Y., H. Bang, C. Gnatenco, and D. Kim, Synergistic interaction and the role of C-terminus in the activation of TRAAK K⁺ channels by pressure, free fatty acids and alkali. *Pflugers Arch* 2001; 442:64-72.
 38. Bearzatto, B., F. Lesage, R. Reyes, M. Lazdunski, and P.M. Laduron, Axonal transport of TREK and TRAAK potassium channels in rat sciatic nerves. *Neuroreport* 2000; 11:927-30.
 39. Veale, E.L., K.A. Rees, A. Mathie, and S. Trapp, Dominant negative effects of a non-conducting TREK1 splice variant expressed in brain. *J Biol Chem* 2010; 285:29295-304.
 40. Thomas, D., L.D. Plant, C.M. Wilkens, Z.A. McCrossan, and S.A. Goldstein, Alternative translation initiation in rat brain yields K_{2P}2.1 potassium channels permeable to sodium. *Neuron* 2008; 58:859-70.
 41. Gu, W., G. Schlichthorl, J.R. Hirsch, H. Engels, C. Karschin, A. Karschin, C. Derst, O.K. Steinlein, and J. Daut, Expression pattern and functional characteristics of two novel splice variants of the two-pore-domain potassium channel TREK-2. *J Physiol* 2002; 539:657-68.

42. Kang, D., C. Choe, E. Cavanaugh, and D. Kim, Properties of single two-pore domain TREK-2 channels expressed in mammalian cells. *J Physiol* 2007; 583:57-69.
43. Simkin, D., E.J. Cavanaugh, and D. Kim, Control of the single channel conductance of $K_{2P}10.1$ (TREK-2) by the amino-terminus: role of alternative translation initiation. *J Physiol* 2008; 586:5651-63.
44. Fink, M., F. Lesage, F. Duprat, C. Heurteaux, R. Reyes, M. Fosset, and M. Lazdunski, A neuronal two P domain K^+ channel stimulated by arachidonic acid and polyunsaturated fatty acids. *EMBO J* 1998; 17:3297-308.
45. Sandoz, G., S. Thummler, F. Duprat, S. Feliciangeli, J. Vinh, P. Escoubas, N. Guy, M. Lazdunski, and F. Lesage, AKAP150, a switch to convert mechano-, pH- and arachidonic acid-sensitive TREK K^+ channels into open leak channels. *EMBO J* 2006; 25:5864-72.
46. Colledge, M., R.A. Dean, G.K. Scott, L.K. Langeberg, R.L. Huganir, and J.D. Scott, Targeting of PKA to glutamate receptors through a MAGUK-AKAP complex. *Neuron* 2000; 27:107-19.
47. Sandoz, G., M.P. Tardy, S. Thummler, S. Feliciangeli, M. Lazdunski, and F. Lesage, Mtap2 is a constituent of the protein network that regulates twik-related K^+ channel expression and trafficking. *J Neurosci* 2008; 28:8545-52.
48. Dehmelt, L. and S. Halpain, The MAP2/Tau family of microtubule-associated proteins. *Genome Biol* 2005; 6:204.
49. Obar, R.A., J. Dingus, H. Bayley, and R.B. Vallee, The RII subunit of cAMP-dependent protein kinase binds to a common amino-terminal domain in microtubule-associated proteins 2A, 2B, and 2C. *Neuron* 1989; 3:639-45.
50. Kim, E., E.M. Hwang, O. Yarishkin, J.C. Yoo, D. Kim, N. Park, M. Cho, Y.S. Lee, C.H. Sun, G.S. Yi, J. Yoo, D. Kang, J. Han, S.G. Hong, and J.Y. Park, Enhancement of TREK1 channel surface expression by protein-protein interaction with β -COP. *Biochem Biophys Res Commun* 2010; 395:244-50.
51. Klein, M., J. Camardo, and E.R. Kandel, Serotonin modulates a specific potassium current in the sensory neurons that show presynaptic facilitation in *Aplysia*. *Proc Natl Acad Sci U S A* 1982; 79:5713-7.

52. Shuster, M.J. and S.A. Siegelbaum, Pharmacological characterization of the serotonin-sensitive potassium channel of *Aplysia* sensory neurons. *J Gen Physiol* 1987; 90:587-608.
53. Siegelbaum, S.A., J.S. Camardo, and E.R. Kandel, Serotonin and cyclic AMP close single K⁺ channels in *Aplysia* sensory neurones. *Nature* 1982; 299:413-7.
54. Klein, M. and E.R. Kandel, Mechanism of calcium current modulation underlying presynaptic facilitation and behavioral sensitization in *Aplysia*. *Proc Natl Acad Sci U S A* 1980; 77:6912-6.
55. Castellucci, V. and E.R. Kandel, Presynaptic facilitation as a mechanism for behavioral sensitization in *Aplysia*. *Science* 1976; 194:1176-8.
56. Vanderpe, D.H. and C.E. Morris, Stretch activation of the *Aplysia* S-channel. *J Membr Biol* 1992; 127:205-14.
57. Buttner, N., S.A. Siegelbaum, and A. Volterra, Direct modulation of *Aplysia* S-K⁺ channels by a 12-lipoxygenase metabolite of arachidonic acid. *Nature* 1989; 342:553-5.
58. Winegar, B.D., D.F. Owen, C.S. Yost, J.R. Forsayeth, and E. Mayeri, Volatile general anesthetics produce hyperpolarization of *Aplysia* neurons by activation of a discrete population of baseline potassium channels. *Anesthesiology* 1996; 85:889-900.
59. Maingret, F., M. Fosset, F. Lesage, M. Lazdunski, and E. Honore, TRAAK is a mammalian neuronal mechano-gated K⁺ channel. *J Biol Chem* 1999; 274:1381-7.
60. Lauritzen, I., J. Chemin, E. Honore, M. Jodar, N. Guy, M. Lazdunski, and A. Jane Patel, Cross-talk between the mechano-gated K_{2P} channel TREK-1 and the actin cytoskeleton. *EMBO Rep* 2005; 6:642-8.
61. Danthi, S., J.A. Enyeart, and J.J. Enyeart, Modulation of native TREK-1 and Kv1.4 K⁺ channels by polyunsaturated fatty acids and lysophospholipids. *J Membr Biol* 2003; 195:147-64.
62. Uauy, R., D.R. Hoffman, P. Peirano, D.G. Birch, and E.E. Birch, Essential fatty acids in visual and brain development. *Lipids* 2001; 36:885-95.

63. Balboa, M.A. and J. Balsinde, Oxidative stress and arachidonic acid mobilization. *Biochim Biophys Acta* 2006; 1761:385-91.
64. Khan, W.A., G.C. Blobe, and Y.A. Hannun, Arachidonic acid and free fatty acids as second messengers and the role of protein kinase C. *Cell Signal* 1995; 7:171-84.
65. Harizi, H., J.B. Corcuff, and N. Gualde, Arachidonic-acid-derived eicosanoids: roles in biology and immunopathology. *Trends Mol Med* 2008; 14:461-9.
66. Chemin, J., A. Patel, F. Duprat, M. Zanzouri, M. Lazdunski, and E. Honore, Lysophosphatidic acid-operated K^+ channels. *J Biol Chem* 2005; 280:4415-21.
67. Chemin, J., A.J. Patel, F. Duprat, I. Lauritzen, M. Lazdunski, and E. Honore, A phospholipid sensor controls mechanogating of the K^+ channel TREK-1. *EMBO J* 2005; 24:44-53.
68. Lopes, C.M., T. Rohacs, G. Czirjak, T. Balla, P. Enyedi, and D.E. Logothetis, PIP_2 hydrolysis underlies agonist-induced inhibition and regulates voltage gating of two-pore domain K^+ channels. *J Physiol* 2005; 564:117-29.
69. Chemin, J., C. Girard, F. Duprat, F. Lesage, G. Romey, and M. Lazdunski, Mechanisms underlying excitatory effects of group I metabotropic glutamate receptors via inhibition of 2P domain K^+ channels. *EMBO J* 2003; 22:5403-11.
70. Kang, D., J. Han, and D. Kim, Mechanism of inhibition of TREK-2 ($K_{2P}10.1$) by the G_q -coupled M3 muscarinic receptor. *Am J Physiol Cell Physiol* 2006; 291:C649-56.
71. Sandoz, G., D. Douguet, F. Chatelain, M. Lazdunski, and F. Lesage, Extracellular acidification exerts opposite actions on TREK1 and TREK2 potassium channels via a single conserved histidine residue. *Proc Natl Acad Sci U S A* 2009; 106:14628-33.
72. Cohen, A., Y. Ben-Abu, S. Hen, and N. Zilberberg, A novel mechanism for human $K_{2P}2.1$ channel gating. Facilitation of C-type gating by protonation of extracellular histidine residues. *J Biol Chem* 2008; 283:19448-55.
73. Deng, P.Y., Z. Xiao, C. Yang, L. Rojanathammanee, L. Grisanti, J. Watt, J.D. Geiger, R. Liu, J.E. Porter, and S. Lei, GABA_B receptor activation

inhibits neuronal excitability and spatial learning in the entorhinal cortex by activating TREK-2 K⁺ channels. *Neuron* 2009; 63:230-43.

74. Xiao, Z., P.Y. Deng, L. Rojanathammanee, C. Yang, L. Grisanti, K. Permpoonputtana, D. Weinshenker, V.A. Doze, J.E. Porter, and S. Lei, Noradrenergic depression of neuronal excitability in the entorhinal cortex via activation of TREK-2 K⁺ channels. *J Biol Chem* 2009; 284:10980-91.
75. Cain, S.M., H.J. Meadows, J. Dunlop, and T.J. Bushell, mGlu4 potentiation of K_{2P}2.1 is dependant on C-terminal dephosphorylation. *Mol Cell Neurosci* 2008; 37:32-9.
76. Sandoz, G., J. Levitz, R.H. Kramer, and E.Y. Isacoff, Optical Control of Endogenous Proteins with a Photoswitchable Conditional Subunit Reveals a Role for TREK1 in GABA_B Signaling. *Neuron* 2012; 74:1005-14.
77. Liu, H., J.A. Enyeart, and J.J. Enyeart, Potent inhibition of native TREK-1 K⁺ channels by selected dihydropyridine Ca²⁺ channel antagonists. *J Pharmacol Exp Ther* 2007; 323:39-48.
78. Yamamoto, S., T. Kanno, K. Yamada, Y. Yasuda, and T. Nishizaki, Dual regulation of heat-activated K⁺ channel in rat DRG neurons via α_1 and β adrenergic receptors. *Life Sci* 2009; 85:167-71.
79. Lesage, F., F. Maingret, and M. Lazdunski, Cloning and expression of human TRAAK, a polyunsaturated fatty acids-activated and mechano-sensitive K⁺ channel. *FEBS Lett* 2000; 471:137-40.
80. Kreneisz, O., J.P. Benoit, D.A. Bayliss, and D.K. Mulkey, AMP-activated protein kinase inhibits TREK channels. *J Physiol* 2009; 587:5819-30.
81. Enyedi, P. and G. Czirjak, Molecular background of leak K⁺ currents: two-pore domain potassium channels. *Physiol Rev* 2010; 90:559-605.
82. Guyon, A., M.P. Tardy, C. Rovere, J.L. Nahon, J. Barhanin, and F. Lesage, Glucose inhibition persists in hypothalamic neurons lacking tandem-pore K⁺ channels. *J Neurosci* 2009; 29:2528-33.
83. Franks, N.P. and W.R. Lieb, Volatile general anaesthetics activate a novel neuronal K⁺ current. *Nature* 1988; 333:662-4.
84. Gruss, M., T.J. Bushell, D.P. Bright, W.R. Lieb, A. Mathie, and N.P. Franks, Two-pore-domain K⁺ channels are a novel target for the

- anesthetic gases xenon, nitrous oxide, and cyclopropane. *Mol Pharmacol* 2004; 65:443-52.
85. Harinath, S. and S.K. Sikdar, Trichloroethanol enhances the activity of recombinant human TREK-1 and TRAAK channels. *Neuropharmacology* 2004; 46:750-60.
 86. Kennard, L.E., J.R. Chumbley, K.M. Ranatunga, S.J. Armstrong, E.L. Veale, and A. Mathie, Inhibition of the human two-pore domain potassium channel, TREK-1, by fluoxetine and its metabolite norfluoxetine. *Br J Pharmacol* 2005; 144:821-9.
 87. Eckert, M., B. Egenberger, F. Doring, and E. Wischmeyer, TREK-1 isoforms generated by alternative translation initiation display different susceptibility to the antidepressant fluoxetine. *Neuropharmacology* 2011; 61:918-23
 88. Mazella, J., O. Petrault, G. Lucas, E. Deval, S. Beraud-Dufour, C. Gandin, M. El-Yacoubi, C. Widmann, A. Guyon, E. Chevet, S. Taouji, G. Conductier, A. Corinus, T. Coppola, G. Gobbi, J.L. Nahon, C. Heurteaux, and M. Borsotto, Spadin, a sortilin-derived peptide, targeting rodent TREK-1 channels: a new concept in the antidepressant drug design. *PLoS Biol* 2010; 8:e1000355.
 89. Moha Ou Maati, H., J. Veysiere, F. Labbal, T. Coppola, C. Gandin, C. Widmann, J. Mazella, C. Heurteaux, and M. Borsotto, Spadin as a new antidepressant: absence of TREK-1-related side effects. *Neuropharmacology* 2012; 62:278-88.
 90. Liou, Y.J., T.J. Chen, S.J. Tsai, Y.W. Yu, C.Y. Cheng, and C.J. Hong, Support for the involvement of the KCNK2 gene in major depressive disorder and response to antidepressant treatment. *Pharmacogenet Genomics* 2009; 19:735-41.
 91. Perlis, R.H., P. Moorfani, J. Fagerness, S. Purcell, M.H. Trivedi, M. Fava, A.J. Rush, and J.W. Smoller, Pharmacogenetic analysis of genes implicated in rodent models of antidepressant response: association of TREK1 and treatment resistance in the STAR*D study. *Neuropsychopharmacology* 2008; 33:2810-9.
 92. Dillon, D.G., R. Bogdan, J. Fagerness, A.J. Holmes, R.H. Perlis, and D.A. Pizzagalli, Variation in TREK1 gene linked to depression-resistant phenotype is associated with potentiated neural responses to rewards in humans. *Hum Brain Mapp* 2010; 31:210-21.

93. White, B.C., J.M. Sullivan, D.J. DeGracia, B.J. O'Neil, R.W. Neumar, L.I. Grossman, J.A. Rafols, and G.S. Krause, Brain ischemia and reperfusion: molecular mechanisms of neuronal injury. *J Neurol Sci* 2000; 179:1-33.
94. World Health Organization Department of Health Statistics and Informatics in the Information, E.a.R.C., *The global burden of disease 2004 update*, 2004, WHO: Geneva.
95. Yavin, E., B. Kunievsky, N.G. Bazan, and S. Harel, Regulation of arachidonic acid metabolism in the perinatal brain during development and under ischemic stress. *Adv Exp Med Biol* 1992; 318:315-23.
96. Xiao, Y. and X. Li, Polyunsaturated fatty acids modify mouse hippocampal neuronal excitability during excitotoxic or convulsant stimulation. *Brain Res* 1999; 846:112-21.
97. Lauritzen, I., N. Blondeau, C. Heurteaux, C. Widmann, G. Romey, and M. Lazdunski, Polyunsaturated fatty acids are potent neuroprotectors. *EMBO J* 2000; 19:1784-93.
98. Blondeau, N., C. Widmann, M. Lazdunski, and C. Heurteaux, Polyunsaturated fatty acids induce ischemic and epileptic tolerance. *Neuroscience* 2002; 109:231-41.
99. Lang-Lazdunski, L., N. Blondeau, G. Jarretou, M. Lazdunski, and C. Heurteaux, Linolenic acid prevents neuronal cell death and paraplegia after transient spinal cord ischemia in rats. *J Vasc Surg* 2003; 38:564-75.
100. Heurteaux, C., C. Laigle, N. Blondeau, G. Jarretou, and M. Lazdunski, Alpha-linolenic acid and riluzole treatment confer cerebral protection and improve survival after focal brain ischemia. *Neuroscience* 2006; 137:241-51.
101. Blondeau, N., I. Lauritzen, C. Widmann, M. Lazdunski, and C. Heurteaux, A potent protective role of lysophospholipids against global cerebral ischemia and glutamate excitotoxicity in neuronal cultures. *J Cereb Blood Flow Metab* 2002; 22:821-34.
102. Cadaveira-Mosquera, A., S.J. Ribeiro, A. Reboreda, M. Perez, and J.A. Lamas, Activation of TREK currents by the neuroprotective agent riluzole in mouse sympathetic neurons. *J Neurosci* 2011; 31:1375-85.

103. Duprat, F., F. Lesage, A.J. Patel, M. Fink, G. Romey, and M. Lazdunski, The neuroprotective agent riluzole activates the two P domain K⁺ channels TREK-1 and TRAAK. *Mol Pharmacol* 2000; 57:906-12.
104. Kim, E.J., D. Kang, and J. Han, Baicalein and wogonin are activators of rat TREK-2 two-pore domain K⁺ channel. *Acta Physiol (Oxf)* 2011; 202:185-92.
105. Lips, J., P. de Haan, P. Bodewits, I. Vanicky, M. Dzoljic, M.J. Jacobs, and C.J. Kalkman, Neuroprotective effects of riluzole and ketamine during transient spinal cord ischemia in the rabbit. *Anesthesiology* 2000; 93:1303-11.
106. Son, D., P. Lee, J. Lee, H. Kim, and S.Y. Kim, Neuroprotective effect of wogonin in hippocampal slice culture exposed to oxygen and glucose deprivation. *Eur J Pharmacol* 2004; 493:99-102.
107. Gao, Z., K. Huang, and H. Xu, Protective effects of flavonoids in the roots of *Scutellaria baicalensis* Georgi against hydrogen peroxide-induced oxidative stress in HS-SY5Y cells. *Pharmacol Res* 2001; 43:173-8.
108. Schmitt-Schillig, S., S. Schaffer, C.C. Weber, G.P. Eckert, and W.E. Muller, Flavonoids and the aging brain. *J Physiol Pharmacol* 2005; 56 Suppl 1:23-36.
109. Xu, X., Y. Pan, and X. Wang, Alterations in the expression of lipid and mechano-gated two-pore domain potassium channel genes in rat brain following chronic cerebral ischemia. *Brain Res Mol Brain Res* 2004; 120:205-9.
110. Li, Z.B., H.X. Zhang, L.L. Li, and X.L. Wang, Enhanced expressions of arachidonic acid-sensitive tandem-pore domain potassium channels in rat experimental acute cerebral ischemia. *Biochem Biophys Res Commun* 2005; 327:1163-9.
111. Sun, L.N., L.L. Li, Z.B. Li, L. Wang, and X.L. Wang, Protective effects of TREK-1 against oxidative injury induced by SNP and H₂O₂. *Acta Pharmacol Sin* 2008; 29:1150-6.
112. Wang, M., J. Song, W. Xiao, L. Yang, J. Yuan, W. Wang, Z. Yu, and M. Xie, Changes in lipid-sensitive two-pore domain potassium channel TREK-1 expression and its involvement in astrogliosis following cerebral ischemia in rats. *J Mol Neurosci* 2012; 46:384-92.

113. Kucheryavykh, L.Y., Y.V. Kucheryavykh, M. Inyushin, Y.M. Shuba, P. Sanabria, L.A. Cubano, S.N. Skatchkov, and M.J. Eaton, Ischemia increases TREK-2 channel expression in astrocytes: relevance to glutamate clearance. *Open Neurosci J* 2009; 3:40-47.
114. Vallee, N., C. Meckler, J.J. Risso, and J.E. Blatteau, Neuroprotective role of the TREK-1 channel in decompression sickness. *J Appl Physiol* 2012; 112:1191-6.
115. Namiranian, K., C.D. Brink, J.C. Goodman, C.S. Robertson, and R.M. Bryan, Jr., Traumatic brain injury in mice lacking the K⁺ channel, TREK-1. *J Cereb Blood Flow Metab* 2011; 31:e1-6.
116. Miller, P., P.J. Kemp, A. Lewis, C.G. Chapman, H.J. Meadows, and C. Peers, Acute hypoxia occludes hTREK-1 modulation: re-evaluation of the potential role of tandem P domain K⁺ channels in central neuroprotection. *J Physiol* 2003; 548:31-7.
117. Miller, P., C. Peers, and P.J. Kemp, Polymodal regulation of hTREK1 by pH, arachidonic acid, and hypoxia: physiological impact in acidosis and alkalosis. *Am J Physiol Cell Physiol* 2004; 286:C272-82.
118. Miller, P., P.J. Kemp, and C. Peers, Structural requirements for O₂ sensing by the human tandem-P domain channel, hTREK1. *Biochem Biophys Res Commun* 2005; 331:1253-6.
119. Caley, A.J., M. Gruss, and N.P. Franks, The effects of hypoxia on the modulation of human TREK-1 potassium channels. *J Physiol* 2005; 562:205-12.
120. Aller, M.I. and W. Wisden, Changes in expression of some two-pore domain potassium channel genes (KCNK) in selected brain regions of developing mice. *Neuroscience* 2008; 151:1154-72.
121. Brazel, C.Y., M.J. Romanko, R.P. Rothstein, and S.W. Levison, Roles of the mammalian subventricular zone in brain development. *Prog Neurobiol* 2003; 69:49-69.
122. Ming, G.L. and H. Song, Adult neurogenesis in the mammalian brain: significant answers and significant questions. *Neuron* 2011; 70:687-702.
123. Kanjhan, R., A.M. Anselme, P.G. Noakes, and M.C. Bellingham, Postnatal changes in TASK-1 and TREK-1 expression in rat brain stem and cerebellum. *Neuroreport* 2004; 15:1321-4.

124. Goonetilleke, L. and J. Quayle, TREK-1 K⁺ channels in the cardiovascular system: their significance and potential as a therapeutic target. *Cardiovasc Ther* 2012; 30:e23-9.
125. Aimond, F., J.M. Rauzier, C. Bony, and G. Vassort, Simultaneous activation of p38 MAPK and p42/44 MAPK by ATP stimulates the K⁺ current ITREK in cardiomyocytes. *J Biol Chem* 2000; 275:39110-6.
126. Kelly, D., L. Mackenzie, P. Hunter, B. Smaill, and D.A. Saint, Gene expression of stretch-activated channels and mechanoelectric feedback in the heart. *Clin Exp Pharmacol Physiol* 2006; 33:642-8.
127. Tan, J.H., W. Liu, and D.A. Saint, Differential expression of the mechanosensitive potassium channel TREK-1 in epicardial and endocardial myocytes in rat ventricle. *Exp Physiol* 2004; 89:237-42.
128. Enyeart, J.A., H. Liu, and J.J. Enyeart, Curcumin inhibits bTREK-1 K⁺ channels and stimulates cortisol secretion from adrenocortical cells. *Biochem Biophys Res Commun* 2008; 370:623-8.
129. Baker, S.A., W.J. Hatton, J. Han, G.W. Hennig, F.C. Britton, and S.D. Koh, Role of TREK-1 potassium channel in bladder overactivity after partial bladder outlet obstruction in mouse. *J Urol* 2010; 183:793-800.
130. Baker, S.A., G.W. Hennig, J. Han, F.C. Britton, T.K. Smith, and S.D. Koh, Methionine and its derivatives increase bladder excitability by inhibiting stretch-dependent K⁺ channels. *Br J Pharmacol* 2008; 153:1259-71.
131. Schwingshackl, A., B. Teng, M. Ghosh, A.N. West, P. Makena, V. Gorantla, S.E. Sinclair, and C.M. Waters, Regulation and function of the two-pore-domain (K_{2P}) potassium channel Trek-1 in alveolar epithelial cells. *Am J Physiol Lung Cell Mol Physiol* 2012; 302:L93-L102.
132. Buxton, I.L., C.A. Singer, and J.N. Tichenor, Expression of stretch-activated two-pore potassium channels in human myometrium in pregnancy and labor. *PLoS One* 2010; 5:e12372.
133. Monaghan, K., S.A. Baker, L. Dwyer, W.C. Hatton, K. Sik Park, K.M. Sanders, and S.D. Koh, The stretch-dependent potassium channel TREK-1 and its function in murine myometrium. *J Physiol* 2011; 589:1221-33.
134. Voloshyna, I., A. Besana, M. Castillo, T. Matos, I.B. Weinstein, M. Mansukhani, R.B. Robinson, C. Cordon-Cardo, and S.J. Feinmark,

- TREK-1 is a novel molecular target in prostate cancer. *Cancer Res* 2008; 68:1197-203.
135. Kang, D., C. Choe, and D. Kim, Functional expression of TREK-2 in insulin-secreting MIN6 cells. *Biochem Biophys Res Commun* 2004; 323:323-31.
 136. Pruss, H., M. Dewes, C. Derst, F. Fernandez-Klett, R.W. Veh, and J. Priller, Potassium channel expression in adult murine neural progenitor cells. *Neuroscience* 2011; 180:19-29.
 137. Xi, G., X. Zhang, L. Zhang, Y. Sui, J. Hui, S. Liu, Y. Wang, L. Li, and Z. Zhang, Fluoxetine attenuates the inhibitory effect of glucocorticoid hormones on neurogenesis in vitro via a two-pore domain potassium channel, TREK-1. *Psychopharmacology (Berl)* 2011; 214:747-59.
 138. Kim, J.S., J.Y. Park, H.W. Kang, E.J. Lee, H. Bang, and J.H. Lee, Zinc activates TREK-2 potassium channel activity. *J Pharmacol Exp Ther* 2005; 314:618-25.
 139. Bachmair, A., D. Finley, and A. Varshavsky, In vivo half-life of a protein is a function of its amino-terminal residue. *Science* 1986; 234:179-86.
 140. Majeski, A.E. and J.F. Dice, Mechanisms of chaperone-mediated autophagy. *Int J Biochem Cell Biol* 2004; 36:2435-44.
 141. Gurtner, G.C., S. Werner, Y. Barrandon, and M.T. Longaker, Wound repair and regeneration. *Nature* 2008; 453:314-21.
 142. Gotz, M. and W.B. Huttner, The cell biology of neurogenesis. *Nat Rev Mol Cell Biol* 2005; 6:777-88.
 143. Beukelaers, P., R. Vandenbosch, N. Caron, L. Nguyen, G. Moonen, and B. Malgrange, Cycling or not cycling: cell cycle regulatory molecules and adult neurogenesis. *Cell Mol Life Sci* 2012; 69:1493-503.
 144. Blackiston, D.J., K.A. McLaughlin, and M. Levin, Bioelectric controls of cell proliferation: ion channels, membrane voltage and the cell cycle. *Cell Cycle* 2009; 8:3519-28.
 145. Morrill, G.A. and E. Robbins, Changes in intracellular cations during the cell cycle in HeLa cells. *Physiol Chem Phys Med NMR* 1984; 16:209-19.
 146. Dubois, J.M. and B. Rouzair-Dubois, The influence of cell volume changes on tumour cell proliferation. *Eur Biophys J* 2004; 33:227-32.

147. Kunzelmann, K., Ion channels and cancer. *J Membr Biol* 2005; 205:159-73.
148. Wang, Z., Roles of K⁺ channels in regulating tumour cell proliferation and apoptosis. *Pflugers Arch* 2004; 448:274-86.
149. Binggeli, R. and R.C. Weinstein, Membrane potentials and sodium channels: hypotheses for growth regulation and cancer formation based on changes in sodium channels and gap junctions. *J Theor Biol* 1986; 123:377-401.
150. Wang, L., P. Zhou, R.W. Craig, and L. Lu, Protection from cell death by mcl-1 is mediated by membrane hyperpolarization induced by K⁺ channel activation. *J Membr Biol* 1999; 172:113-20.
151. Mu, D., L. Chen, X. Zhang, L.H. See, C.M. Koch, C. Yen, J.J. Tong, L. Spiegel, K.C. Nguyen, A. Servoss, Y. Peng, L. Pei, J.R. Marks, S. Lowe, T. Hoey, L.Y. Jan, W.R. McCombie, M.H. Wigler, and S. Powers, Genomic amplification and oncogenic properties of the KCNK9 potassium channel gene. *Cancer Cell* 2003; 3:297-302.
152. Kim, C.J., Y.G. Cho, S.W. Jeong, Y.S. Kim, S.Y. Kim, S.W. Nam, S.H. Lee, N.J. Yoo, J.Y. Lee, and W.S. Park, Altered expression of KCNK9 in colorectal cancers. *Apmis* 2004; 112:588-94.
153. Meuth, S.G., A.M. Herrmann, C.W. Ip, T. Kanyshkova, S. Bittner, A. Weishaupt, T. Budde, and H. Wiendl, The two-pore domain potassium channel TASK3 functionally impacts glioma cell death. *J Neurooncol* 2008; 87:263-70.
154. Pei, L., O. Wisner, A. Slavin, D. Mu, S. Powers, L.Y. Jan, and T. Hoey, Oncogenic potential of TASK3 (Kcnk9) depends on K⁺ channel function. *Proc Natl Acad Sci U S A* 2003; 100:7803-7.
155. Lee, G.W., H.S. Park, E.J. Kim, Y.W. Cho, G.T. Kim, Y.J. Mun, E.J. Choi, J.S. Lee, J. Han, and D. Kang, Reduction of breast cancer cell migration via up-regulation of TASK-3 two-pore domain K⁺ channel. *Acta Physiol (Oxf)* 2012; 204:513-24.
156. Patel, A.J. and M. Lazdunski, The 2P-domain K⁺ channels: role in apoptosis and tumorigenesis. *Pflugers Arch* 2004; 448:261-73.
157. Semenza, G.L., Hypoxia. Cross talk between oxygen sensing and the cell cycle machinery. *Am J Physiol Cell Physiol* 2011; 301:C550-2.

158. Schmittgen, T.D. and K.J. Livak, Analyzing real-time PCR data by the comparative C(T) method. *Nat Protoc* 2008; 3:1101-8.
159. Langan, T.J. and R.C. Chou, Synchronization of mammalian cell cultures by serum deprivation. *Methods Mol Biol* 2011; 761:75-83.
160. Ma, H.T. and R.Y. Poon, Synchronization of HeLa cells. *Methods Mol Biol* 2011; 761:151-61.
161. Chen, C.M., J. Krohn, S. Bhattacharya, and B. Davies, A comparison of exogenous promoter activity at the ROSA26 locus using a PhiC31 integrase mediated cassette exchange approach in mouse ES cells. *PLoS One* 2011; 6:e23376.
162. Alexopoulou, A.N., J.R. Couchman, and J.R. Whiteford, The CMV early enhancer/chicken beta actin (CAG) promoter can be used to drive transgene expression during the differentiation of murine embryonic stem cells into vascular progenitors. *BMC Cell Biol* 2008; 9:2.
163. Xia, X., Y. Zhang, C.R. Zieth, and S.C. Zhang, Transgenes delivered by lentiviral vector are suppressed in human embryonic stem cells in a promoter-dependent manner. *Stem Cells Dev* 2007; 16:167-76.
164. Qin, J.Y., L. Zhang, K.L. Clift, I. Hukur, A.P. Xiang, B.Z. Ren, and B.T. Lahn, Systematic comparison of constitutive promoters and the doxycycline-inducible promoter. *PLoS One* 2010; 5:e10611.
165. Nguyen, A.T., A.C. Dow, J. Kupiec-Weglinski, R.W. Busuttill, and G.S. Lipshutz, Evaluation of gene promoters for liver expression by hydrodynamic gene transfer. *J Surg Res* 2008; 148:60-6.
166. Fukuda, T., Y. Mishina, M.P. Walker, and R.P. DiAugustine, Conditional transgenic system for mouse aurora a kinase: degradation by the ubiquitin proteasome pathway controls the level of the transgenic protein. *Mol Cell Biol* 2005; 25:5270-81.
167. Davis, K.A. and E.A. Cowley, Two-pore-domain potassium channels support anion secretion from human airway Calu-3 epithelial cells. *Pflugers Arch* 2006; 451:631-41.
168. Inglis, S.K., S.G. Brown, M.J. Constable, N. McTavish, R.E. Olver, and S.M. Wilson, A Ba²⁺-resistant, acid-sensitive K⁺ conductance in Na⁺-absorbing H441 human airway epithelial cells. *Am J Physiol Lung Cell Mol Physiol* 2007; 292:L1304-12.

169. Brenner, T. and K.M. O'Shaughnessy, Both TASK-3 and TREK-1 two-pore loop K channels are expressed in H295R cells and modulate their membrane potential and aldosterone secretion. *Am J Physiol Endocrinol Metab* 2008; 295:E1480-6.
170. Kang, D., S.H. Kim, E.M. Hwang, O.S. Kwon, H.Y. Yang, E.S. Kim, T.H. Choi, J.Y. Park, S.G. Hong, and J. Han, Expression of thermosensitive two-pore domain K⁺ channels in human keratinocytes cell line HaCaT cells. *Exp Dermatol* 2007; 16:1016-22.
171. Moha ou Maati, H., R. Peyronnet, C. Devader, J. Veyssiere, F. Labbal, C. Gandin, J. Mazella, C. Heurteaux, and M. Borsotto, A human TREK-1/HEK cell line: a highly efficient screening tool for drug development in neurological diseases. *PLoS One* 2011; 6:e25602.
172. Gierten, J., D. Hassel, P.A. Schweizer, R. Becker, H.A. Katus, and D. Thomas, Identification and functional characterization of zebrafish K_{2P}10.1 (TREK2) two-pore-domain K⁺ channels. *Biochim Biophys Acta* 2012; 1818:33-41.
173. Anderson, G.R., Y. Cao, S. Davidson, H.V. Truong, M. Pravetoni, M.J. Thomas, K. Wickman, G.J. Giesler, Jr., and K.A. Martemyanov, R7BP complexes with RGS9-2 and RGS7 in the striatum differentially control motor learning and locomotor responses to cocaine. *Neuropsychopharmacology* 2010; 35:1040-50.
174. Pravetoni, M. and K. Wickman, Behavioral characterization of mice lacking GIRK/Kir3 channel subunits. *Genes Brain Behav* 2008; 7:523-31.
175. Simon, P., R. Dupuis, and J. Costentin, Thigmotaxis as an index of anxiety in mice. Influence of dopaminergic transmissions. *Behav Brain Res* 1994; 61:59-64.
176. Lister, R.G., The use of a plus-maze to measure anxiety in the mouse. *Psychopharmacology (Berl)* 1987; 92:180-5.
177. Bourin, M. and M. Hascoet, The mouse light/dark box test. *Eur J Pharmacol* 2003; 463:55-65.
178. Costall, B., B.J. Jones, M.E. Kelly, R.J. Naylor, and D.M. Tomkins, Exploration of mice in a black and white test box: validation as a model of anxiety. *Pharmacol Biochem Behav* 1989; 32:777-85.

179. Rudy, J.W., N.C. Huff, and P. Matus-Amat, Understanding contextual fear conditioning: insights from a two-process model. *Neurosci Biobehav Rev* 2004; 28:675-85.
180. Dere, E., J.P. Huston, and M.A. De Souza Silva, The pharmacology, neuroanatomy and neurogenetics of one-trial object recognition in rodents. *Neurosci Biobehav Rev* 2007; 31:673-704.
181. Latimer, L.G., P. Duffy, and P.W. Kalivas, Mu opioid receptor involvement in enkephalin activation of dopamine neurons in the ventral tegmental area. *J Pharmacol Exp Ther* 1987; 241:328-37.
182. Kalivas, P.W. and P. Duffy, Sensitization to repeated morphine injection in the rat: possible involvement of A10 dopamine neurons. *J Pharmacol Exp Ther* 1987; 241:204-12.
183. Bozarth, M.A., Neuroanatomical boundaries of the reward-relevant opiate-receptor field in the ventral tegmental area as mapped by the conditioned place preference method in rats. *Brain Res* 1987; 414:77-84.
184. Bozarth, M.A. and R.A. Wise, Involvement of the ventral tegmental dopamine system in opioid and psychomotor stimulant reinforcement. *NIDA Res Monogr* 1986; 67:190-6.
185. Lein, E.S., M.J. Hawrylycz, N. Ao, M. Ayres, A. Bensinger, A. Bernard, A.F. Boe, M.S. Boguski, K.S. Brockway, E.J. Byrnes, L. Chen, T.M. Chen, M.C. Chin, J. Chong, B.E. Crook, A. Czaplinska, C.N. Dang, S. Datta, N.R. Dee, A.L. Desaki, T. Desta, E. Diep, T.A. Dolbeare, M.J. Donelan, H.W. Dong, J.G. Dougherty, B.J. Duncan, A.J. Ebbert, G. Eichele, L.K. Estin, C. Faber, B.A. Facer, R. Fields, S.R. Fischer, T.P. Fliss, C. Frensley, S.N. Gates, K.J. Glattfelder, K.R. Halverson, M.R. Hart, J.G. Hohmann, M.P. Howell, D.P. Jeung, R.A. Johnson, P.T. Karr, R. Kawal, J.M. Kidney, R.H. Knapik, C.L. Kuan, J.H. Lake, A.R. Laramée, K.D. Larsen, C. Lau, T.A. Lemon, A.J. Liang, Y. Liu, L.T. Luong, J. Michaels, J.J. Morgan, R.J. Morgan, M.T. Mortrud, N.F. Mosqueda, L.L. Ng, R. Ng, G.J. Orta, C.C. Overly, T.H. Pak, S.E. Parry, S.D. Pathak, O.C. Pearson, R.B. Puchalski, Z.L. Riley, H.R. Rockett, S.A. Rowland, J.J. Royall, M.J. Ruiz, N.R. Sarno, K. Schaffnit, N.V. Shapovalova, T. Sivisay, C.R. Slaughterbeck, S.C. Smith, K.A. Smith, B.I. Smith, A.J. Sodt, N.N. Stewart, K.R. Stumpf, S.M. Sunkin, M. Sutram, A. Tam, C.D. Teemer, C. Thaller, C.L. Thompson, L.R. Varnam, A. Visel, R.M. Whitlock, P.E. Wohnoutka, C.K. Wolkey, V.Y. Wong, M. Wood, M.B. Yaylaoglu, R.C. Young, B.L. Youngstrom, X.F. Yuan, B. Zhang, T.A. Zwingman and A.R. Jones, Genome-wide atlas of gene expression in the adult mouse brain. *Nature* 2007; 445:168-76.

186. Canteras, N.S., L.B. Resstel, L.J. Bertoglio, P. Carobrez Ade, and F.S. Guimaraes, Neuroanatomy of anxiety. *Curr Top Behav Neurosci* 2010; 2:77-96.
187. Menard, J. and D. Treit, Effects of centrally administered anxiolytic compounds in animal models of anxiety. *Neurosci Biobehav Rev* 1999; 23:591-613.
188. Bhatnagar, S., L.M. Sun, J. Raber, S. Maren, D. Julius, and M.F. Dallman, Changes in anxiety-related behaviors and hypothalamic-pituitary-adrenal activity in mice lacking the 5-HT-3A receptor. *Physiol Behav* 2004; 81:545-55.
189. Salas, R., F. Pieri, B. Fung, J.A. Dani, and M. De Biasi, Altered anxiety-related responses in mutant mice lacking the beta4 subunit of the nicotinic receptor. *J Neurosci* 2003; 23:6255-63.
190. Lau, A.A., A.C. Crawley, J.J. Hopwood, and K.M. Hemsley, Open field locomotor activity and anxiety-related behaviors in mucopolysaccharidosis type IIIA mice. *Behav Brain Res* 2008; 191:130-6.
191. Buckler, K.J. and E. Honore, The lipid-activated two-pore domain K⁺ channel TREK-1 is resistant to hypoxia: implication for ischaemic neuroprotection. *J Physiol* 2005; 562:213-22.
192. Park, K.S., H. Bang, E.Y. Shin, C.H. Kim, and Y. Kim, The Inhibition of TREK2 Channel by an Oxidizing Agent, 5,5'-dithio-bis (2-nitrobenzoic acid), via Interaction with the C-terminus Distal to the 353rd Amino Acid. *Korean J Physiol Pharmacol* 2008; 12:211-6.
193. Arora, D., D.M. Haluk, S. Kourrich, M. Pravetoni, L. Fernandez-Alacid, J.C. Nicolau, R. Lujan, and K. Wickman, Altered neurotransmission in the mesolimbic reward system of Girk mice. *J Neurochem* 2010; 114:1487-97.
194. Labouebe, G., M. Lomazzi, H.G. Cruz, C. Creton, R. Lujan, M. Li, Y. Yanagawa, K. Obata, M. Watanabe, K. Wickman, S.B. Boyer, P.A. Slesinger, and C. Luscher, RGS2 modulates coupling between GABA_B receptors and GIRK channels in dopamine neurons of the ventral tegmental area. *Nat Neurosci* 2007; 10:1559-68.

195. Koyrakh, L., R. Lujan, J. Colon, C. Karschin, Y. Kurachi, A. Karschin, and K. Wickman, Molecular and cellular diversity of neuronal G-protein-gated potassium channels. *J Neurosci* 2005; 25:11468-78.
196. Dallas, M.L., J.L. Scragg, and C. Peers, Modulation of hTrek-1 by carbon monoxide. *Neuroreport* 2008; 19:345-8.
197. Takahira, M., M. Sakurai, N. Sakurada, and K. Sugiyama, Fenamates and diltiazem modulate lipid-sensitive mechano-gated 2P domain K⁺ channels. *Pflugers Arch* 2005; 451:474-8.
198. Ji, X.C., W.H. Zhao, D.X. Cao, Q.Q. Shi, and X.L Wang, Novel neuroprotectant chiral 3-n-butylphthalide inhibits tandem-pore-domain potassium channel TREK-1. *Acta Pharmacol Sin* 2011; 32:182-7.
199. Punke, M.A., T. Licher, O. Pongs, and P. Friederich, Inhibition of human TREK-1 channels by bupivacaine. *Anesth Analg* 2003; 96:1665-73.
200. Harinath, S., and S.K. Sikdar, Trichloroethanol enhances the activity of recombinant human TREK-1 and TRAAK channels. *Neuropharmacology* 2004; 46:750-60.
201. Thummler, S., F. Duprat, and M. Lazdunski, Antipsychotics inhibit TREK but not TRAAK channels. *Biochem Biophys Res Commun* 2007; 354:284-9.
202. Milosavljevic, N., C. Durantou, N. Djerbi, P.H Puech, P. Gounon, D. Lagadic-Gossmann, M.T. Dimanche-Boitrel, C. Rauch, M. Tauc, L. Counillon, and M. Poet, Nongenomic effects of cisplatin: acute inhibition of mechanosensitive transporters and channels without actin remodeling. *Cancer Res* 2010; 70:7514-22.
203. Hwang, S.J., N. O'Kane, C. Singer, S.M. Ward, K.M. Sanders, and S.D. Koh, Block of inhibitory junction potentials and TREK-1 channels in murine colon by Ca²⁺ store-active drugs. *J Physiol* 2008; 586:1169-84.
204. Meadows, H.J., C.G. Chapman, D.M. Duckworth, R.E. Kellsell, P.R. Murdock, S. Nasir, G. Rennie, and A.D. Randall, The neuroprotective agent sipatrigine (BW619C89) potently inhibits the human tandem pore-domain K⁺ channels TREK-1 and TRAAK. *Brain Res* 2001; 892:94-101.
205. Nayak, T.K., S. Harinath, S. Nama, K. Somasundaram, and S.K Sikdar, Inhibition of human two-pore domain K⁺ channel TREK1 by local anesthetic lidocaine: negative cooperativity and half-of-sites saturation kinetics. *Mol Pharmacol* 2009; 76:903-17.